UNIVERSITEIT VAN PRETORIA
UNIVERSITY OF PRETORIA
YUNIBESITHI YA PRETORIA

Development of transgenic *Plasmodium falciparum* parasites for K^+ channel functional investigation

by

Eunice Bitja Claassen
16313845

Supervisor: Dr Jandeli Niemand
Co-supervisor: Prof Lyn-Marie Birkholtz

Submitted in partial fulfilment of the requirements for the degree:

Magister Scientiae

(Specialisation in Biochemistry)

In the Faculty of Natural and Agricultural Sciences
Department of Biochemistry, Genetics and Microbiology
University of Pretoria

December 2022

UNIVERSITEIT VAN PRETORIA
UNIVERSITY OF PRETORIA
YUNIBESITHI YA PRETORIA

SUBMISSION DECLARATION

I, Eunice Claassen, declare that the dissertation, which I hereby submit for the degree *Magister Scientiae* in the Department of Biochemistry, Genetics and Microbiology at the University of Pretoria, is my own work and has not previously been submitted by me for a degree at this or any other tertiary institution.

SIGNATURE: 

DATE: 8 December 2022

UNIVERSITEIT VAN PRETORIA
UNIVERSITY OF PRETORIA
YUNIBESITHI YA PRETORIA

DECLARATION OF ORIGINALITY
University of Pretoria

The Department of Biochemistry, Genetics and Microbiology, University of Pretoria, places great emphasis upon integrity and ethical conduct in the preparation of all written work submitted for academic evaluation.

Full names of student: Eunice Bitja Claassen

Student number: 16313845

Declaration:

1. I understand what plagiarism is and am aware of the University's policy in this regard.
2. I declare that this assignment (e.g., essay, report, project, assignment, dissertation, thesis, etc) is my own original work. Where other people's work has been used (either from a printed source, Internet or any other source), this has been properly acknowledged and referenced in accordance with Departmental requirements.
3. I have not used work previously produced by another student or any other person to hand in as my own.
4. I have not allowed, and will not allow, anyone to copy my work with the intention of passing it off as his or her own work.

SIGNATURE: 

DATE: 8 December 2022

Acknowledgments

First and foremost, I would like to thank God for giving me everlasting strength throughout all of the challenging times of completing this research and dissertation.

Secondly, I would like to express my deepest appreciation for my supervisor, Dr Jandeli Niemand, for the patient guidance, continual encouragement, and valuable advice that she has provided, and for giving me the opportunity to do this degree. I would also like to thank Prof Lyn-Marie Birkholtz for her assistance and expertise as co-supervisor. Furthermore, I extend my gratitude to the Malaria Parasite Molecular Laboratory (M2PL) team for their input and willingness to assist whenever needed.

Additionally, I would like to thank my parents (Arno and Marianne Claassen) for their love, encouragement, and support, and for giving me so many opportunities that has enabled me to do this research. Furthermore, this endeavour could not have been undertaken without the care and support of my siblings (Adiël, Shalom, Didi, Ginomi, Donoven, Kahla, Hanani, and Andrew). I am also deeply indebted to my boyfriend (Stegmann), who has made countless sacrifices throughout this entire process, and who never stopped believing in me.

Lastly, I would like to acknowledge the financial assistance provided by the National Research Foundation (NRF) towards this research through an NRF-Grantholder linked bursary.

Summary

The elimination of the life-threatening malaria disease caused by *Plasmodium falciparum* parasites remains a global health challenge. It is imperative that novel biological targets are identified not only in the pathogenic asexual parasites, but also in the transmissible sexual gametocytes. However, the development of transmission-blocking interventions is difficult, as the biology behind important physiological processes during gametocyte development is not well understood. One such process is ion homeostasis, which is critical for *P. falciparum* parasites to maintain through the combined action of various ion transport pathways. A chemically diverse array of antiplasmodial compounds has been identified to disrupt ion homeostasis in *P. falciparum* parasites by disrupting the Na^+ gradient that is maintained by a cation ATPase, PfATP4. Similarly, interference of the K^+ gradient by ionophores, such as salinomycin, inhibits the proliferation of asexual parasites and the differentiation of gametocytes of parasites of *P. falciparum.* Two putative K^+ channels (PfK1 and PfK2) could be involved in maintaining the K^+ gradient in *P. falciparum* parasites. Of these, only PfK2 is expressed throughout gametocytogenesis, indicating that it is solely responsible for maintaining the K^+ gradient during these developmental stages. Since interference of the K^+ gradient prevents the development of gametocytes, PfK2 is believed to be associated with important biological processes during these stages. This study aimed to generate transgenic *P. falciparum pfk2* parasites for genetic disruption as well as conditional knockdown studies.

Pfk2 was targeted for genetic disruption to generate a truncated version of the protein. A 5' gene fragment was successfully cloned into a specialized gene disruption plasmid (pSLI-TGD), which included a selection-linked integration technique to select for genomic integration. Recombinant plasmids were transfected into asexual parasites twice, but for both attempts, parasites never recovered after drug pressure for episomal uptake. For the conditional knockdown approach, transgenic parasite lines were successfully generated, in which *pfk2* was modified with a *glmS* ribozyme to regulate the level of mRNA and ultimately the amount of gene product synthesized. Furthermore, *pfk2* was tagged with a green fluorescent protein for localization studies. This study has provided genetically modified parasites that will allow for future investigation of the functional relevance of PfK2 for *P. falciparum* parasites through a conditional knockdown system.

Table of Contents

List of Figures

List of Tables

List of Abbreviations

ACT	Artemisinin-based combination therapies
AmpR	Ampicillin resistance gene
BK	Big conductance
CaM	Calmodulin
CaMBD	Calmodulin binding domain
DDT	Dichlorodiphenyltrichloroethane
DHFR	Dihydrofolate reductase
EDC	Exoerythrocytic development cycle
E_m	Membrane potential
FACS	Fluorescence-activated cell sorting
G6PD	Glucose-6-phosphate dehydrogenase
gDNA	Genomic DNA
GFP	Green fluorescent protein
hDHFR	Human dihydrofolate reductase
HEPES	4-(2-hydroxyethyl)-1-piperazineethanesulfonic acid
hpi	Hours post invasion
IDC	Intraerythrocytic developmental cycle
IK	Intermediate conductance
IRS	Indoor residual spraying
LB	Luria Bertani
LLIN	Long-lasting insecticide-treated nets
NeoR	Neomycin resistance marker
NPP	New permeability pathways
Ori	Origin of replication
PCR	Polymerase chain reaction
PfATP4	P-type Na^+-ATPase
PfFNT	Lactate/H^+ symporter
PfPAT	H^+/pantothenate symporter
PfPiT	Na^+/phosphate symporter
pLDDT	Local-distance difference test
PSIPRED	PSI-blast secondary structure PREDiction
PV	Parasitophorous vacuole
PVM	Parasitophorous vacuolar membrane
RCK	Regulators of conductance of K^+
SK	Small conductance
SLI	Selection-linked integration
TGD	Targeted gene disruption

V-type	Vacuolar-type
WHO	World Health Organization
WT	Wild-type

Chapter 1: Literature review

1.1. Malaria as a life-threatening disease

Malaria is one of the most prevalent infectious diseases in the world. An estimated 241 million malaria cases occurred globally in 2020, where the World Health Organization (WHO) Africa region accounted for about 95 % of cases, followed by the WHO regions of South East Asia (2 %), Eastern Mediterranean (2 %), Western Pacific (0.7 %) and the Americas (0.3 %) (1). Pregnant women and children are high-risk populations for contracting malaria. About 77 % of the total 627 000 malaria deaths in 2020 were children younger than 5 years of age (1). Infection during pregnancy poses a significant problem, not only due to the increased risk of maternal death due to anaemia, but also due to the resulting premature births, miscarriages, or children with low birthweight, which in turn leads to impaired growth and cognitive development (2,3).

Malaria is caused by protozoan parasites of the genus *Plasmodium*. These single-celled eukaryotic parasites are transmitted to humans through the blood meal of infected female *Anopheles* mosquitoes (4). Of the more than 100 species of *Plasmodium,* six cause malaria in humans, namely: *Plasmodium falciparum, Plasmodium vivax, Plasmodium malariae, Plasmodium knowlesi, Plasmodium cynomolgi,* and *Plasmodium ovale*, with *Plasmodium ovale curtisi* and *Plasmodium ovale wallikeri* as subspecies (5,6). *P. falciparum* and *P. vivax* are the most predominant malaria parasites, with *P. falciparum* responsible for the majority of malaria cases and mortalities in Africa (1). Global efforts to eliminate malaria have prevented an estimated 1.7 billion malaria cases and 10.6 million malaria deaths in the period 2000 to 2020 (1). Despite the significant success in reducing the burden of malaria, global progress has begun to slow down (1). Additionally, the COVID-19 pandemic caused disruptions to essential malaria services, which resulted in an estimated 14 million more malaria cases and 47 000 more deaths in 2020 compared to 2019 (1). The elimination of malaria is difficult to accomplish to a great extent due to the extremely complex life cycle of *Plasmodium* species that occurs within both the human host and the *Anopheles* mosquito vector.

1.2. The life cycle of *P. falciparum* parasites

The human host is infected through the injection of sporozoites from the salivary glands of an infected *Anopheles* mosquito during a blood meal (Figure 1.1) (4). The sporozoites from the skin migrate through the peripheral blood circulation to the liver sinusoids for the invasion of hepatocytes (7,8). An asexual exoerythrocytic developmental cycle occurs (EDC, Figure 1.1),

where each sporozoite undergoes hepatic schizogony with multiple nuclear divisions to produce a hepatic schizont. Hepatocyte rupture releases thousands (about 10 000 to 40 000) of haploid merozoites per schizont into the bloodstream (9). The asexual intraerythrocytic developmental cycle (IDC, Figure 1.1), which is ~48 h, commences when the merozoites invade erythrocytes. Each haploid merozoite develops into a ring-stage parasite that has a thin discoidal shape. The ring-stage parasite subsequently develops into a metabolically active trophozoite with a compact cytoplasm (10). With maturation, the trophozoite parasite enters into schizogony where multiple nuclear divisions produce a multi-nucleated schizont (10). Erythrocyte rupture releases 8-24 merozoites per schizont that each infects a new erythrocyte for proliferation and continuation of the asexual IDC.

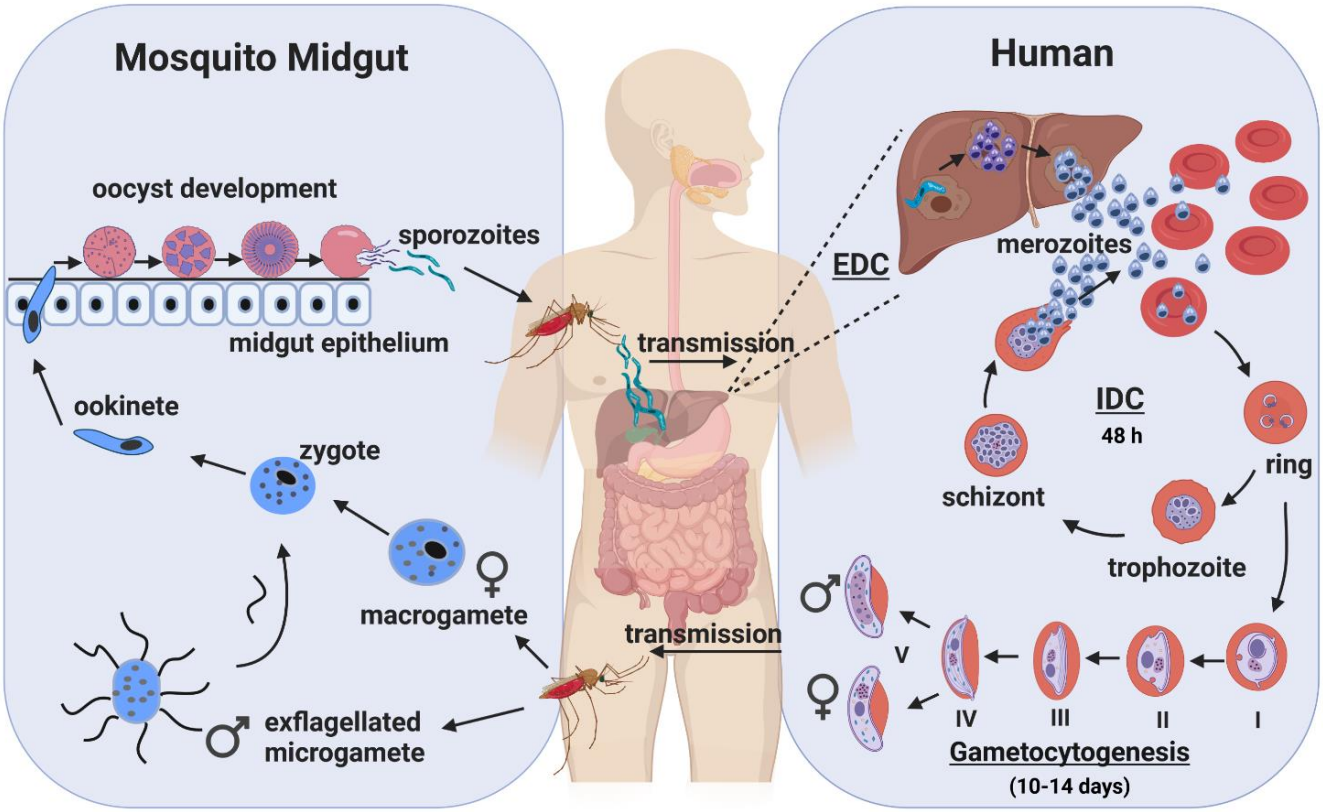

Figure 1.1: The life cycle of *P. falciparum* parasites. During a blood meal, the female *Anopheles* mosquito transmits sporozoites to the human host. The sporozoites migrate to the liver through peripheral circulation and form hepatic schizonts during an exoerythrocytic cycle (EDC). Hepatocyte rupture releases thousands of merozoites into the bloodstream for invasion of erythrocytes. This initiates an intraerythrocytic cycle (IDC) where the merozoites develop from rings to trophozoites and ultimately to schizont-stage parasites that rupture to release more merozoites for infection of more erythrocytes. A small proportion of intraerythrocytic parasites commit to differentiate into gametocytes through a process called gametocytogenesis. The mature stage V male and female gametocytes are transmitted to the female mosquito midgut through another blood meal, where differentiation occurs into gametes that fuse to form a zygote. The zygote matures into an oocyst that migrates across the epithelium midgut to form an oocyst. Once the oocyst bursts, sporozoites are released that migrate to the salivary glands of the mosquito for repetition of the life cycle. Figure created with Biorender.com under a standard academic licence.

Continuation of the asexual IDC in the human host results in malaria symptoms (10). Symptoms initially involve normal flu-like symptoms, such as fever, headache, sweats, and chills. Severe symptoms then form, however, if not treated within 24 h. These can involve severe anaemia, respiratory distress, multi-organ failure, or cerebral malaria, which could ultimately lead to death (11).

A small proportion (<10 %) of intraerythrocytic parasites commit to gametocytogenesis, a differentiation process resulting in sexual intraerythrocytic parasites. During gametocytogenesis, the parasites undergo five developmental stages over a 10-14 day period to form male and female gametocytes (Figure 1.1) (12). Each of these stages has a unique morphology, with a gradual change from round shaped in stage I, to various elongated forms in stages II-IV, to banana shaped in stage V (13). These stage-specific gametocytes sequester in extravascular spaces e.g., within the bone marrow. Only mature stage V male and female gametocytes return to the peripheral circulation for transmission to a feeding female *Anopheles* mosquito (14). This guarantees the survival of the parasites and ensures continuous malaria transmission. Within the midgut of the *Anopheles* mosquito, a change in the microenvironment (pH, temperature, and presence of xanthurenic acid) stimulates male and female gametocytes to differentiate into eight flagellated microgametes and one macrogamete, respectively (15). A single haploid microgamete fuses with the macrogamete to form a diploid zygote (15). The zygote matures into a motile ookinete that crosses the midgut epithelium to develop into an oocyst near the basal lamina (16). Asexual replication within the oocyst results in thousands of sporozoites that travel to the mosquito salivary glands and transmit to the human host when the mosquito takes another blood meal (17). This results in the continuation of the life cycle. Malaria control and eradication strategies depend on the disruption of parasite development and transmission through this multistage life cycle.

1.3. Strategies for malaria control

The intricate *P. falciparum* life cycle can be disrupted through either targeting the mosquito vector itself or by targeting the *P. falciparum* parasite.

1.3.1 Targeting the *Anopheles* vector

Vector control has made significant contributions in reducing malaria infections and death, and is mainly reliant on insecticide interventions such as indoor residual spraying (IRS) and long-lasting insecticide-treated nets (LLINs) (18). Other strategies include larviciding and environmental management (i.e., draining marshes and other breeding reservoirs). Pyrethroids are the only insecticide class currently used for LLINs, as the three other commonly used

insecticide classes cannot be safely applied at effective doses (19). These include the organochlorines, carbamates, and organophosphates, such as dichlorodiphenyltrichloroethane (DDT) that are used for IRS in conjunction with pyrethroids. However, vector control sustainability is hindered by the increasing emergence of insecticide-resistant *Anopheles* mosquitoes (19).

1.3.2 Targeting the *P. falciparum* parasite

The *P. falciparum* parasite can be targeted in different ways, for example, infections can be prevented with vaccines or prophylactic drug treatments, while established infections can be cleared by targeting the asexual intraerythrocytic parasites with antimalarial drugs (20). Lastly, targeting the transmissible sexual gametocytes prevents transmission within a population (21). Malaria vaccine development is challenging due to the complexity of the life cycle of the *P. falciparum* parasite and the extensive antigenic variation it employs (22). Antigenic variation occurs on the surface of an infected erythrocyte due to transcriptional switch among members (~60) of the *var* gene family of the parasite *P. falciparum* (23). RTS, S/ASO1 is the only malaria vaccine to have completed phase III clinical trials (24,25). This vaccine induces immune responses against the circumsporozoite protein of *P. falciparum* during the exoerythrocytic liver stage. It was recently approved (October 2021) for widespread use by the WHO for children living in areas with moderate to high malaria transmission (2,24,25). The vaccine has 36 % efficacy in reducing severe malaria cases in children aged 5 to 17 months after three doses of the vaccine plus a booster, and has a favourable safety profile (1,26). Although this vaccine provides only partial protection, it might reduce the burden of malaria in children and validates the development of a malaria vaccine (27). However, an ideal vaccine would require higher efficacy. R21/Matrix-M is a vaccine that has recently shown high-level efficacy. It is a modified version of the RTS, S/ASO1 vaccine, and uses a higher proportion of the circumsporozoite protein antigen with a different adjuvant to boost the immune response. The vaccine provided up to 80% protection for children aged 5 to 17 months in a phase IIb trial with three initial doses followed by a booster a year later, and is currently undergoing phase III clinical trials (28). Additional vaccine candidates have been developed that target asexual intraerythrocytic parasites or transmissible sexual gametocytes, but were not as successful in clinical trials (25,29).

Alternatively, malaria infections can be prevented by prophylactic drugs to reduce the risk that individuals visiting malaria-endemic areas contract the disease (30). Prophylactic antimalarials are based on either disruption of exoerythrocytic liver stage development or suppression of the emergent asexual intraerythrocytic parasite stages. The latter requires a continuation of

treatment when leaving a malaria-endemic area (up to four weeks) to eliminate the asexual intraerythrocytic parasites that could emerge from the development of the liver stage (31). These prophylactic drugs include mefloquine, doxycycline, and atovaquone-proguanil, where the latter also target the liver stage (32).

Apart from prophylaxis, antimalarial drugs also treat established malaria infections by targeting the asexual intraerythrocytic parasites to relieve symptoms. Artemisinin-based combination therapies (ACTs) are currently recommended as the first-line treatment in all malaria endemic countries (2). Since artemisinin derivatives are short-acting drugs, they are combined with a long-lasting partner drug, such as mefloquine, lumefantrine, and amodiaquine (33). This combination ensures that the majority of parasites are killed by the artemisinin component, while any remaining parasites are cleared by the partner drug with a slower elimination rate to reduce recrudescent infections (34). However, as with previously used antimalarials (i.e., quinolines, antifolates), resistance has emerged against artemisinin and the partner drugs (35,36). Therefore, research on new antimalarial drugs against the asexual intraerythrocytic stages is imperative to sustain malaria control strategies.

Along with the clear need to discover novel biological targets in these rapidly proliferating parasites to treat malaria, there is also a requirement for targets in the gametocyte stages to prevent transmission within a population. Primaquine is currently the only licensed drug recommended by the WHO as a transmission-blocking drug. Although it is an effective gametocidal drug, the use of primaquine is limited as it causes hemolytic anemia by affecting glucose-6-phosphate dehydrogenase (G6PD) activity (37,38). This is especially problematic for people who have G6PD deficiency, which is a widespread deficiency found in malaria endemic areas (39). Therefore, since malaria elimination cannot be accomplished without preventing transmission of *P. falciparum* parasites from the human host to the *Anopheles* mosquito vector (21), the identification of biological targets in gametocytes are urgently required. This requires a greater understanding of the important biological processes that occur during gametocytogenesis.

1.4. Ion homeostasis in *P. falciparum* parasites

During the asexual IDC, *P. falciparum* parasites adapt to dramatic variations in environmental ionic conditions. Within the blood plasma, *P. falciparum* parasites are exposed to a high-[Na^+]/low-[K^+] environment. Upon invasion, the erythrocyte cytosol has a low-[Na^+]/high-[K^+] environment (40). Erythrocytes maintain this intracellular environment with a Na^+/K^+-ATPase that counters the leak of Na^+ and K^+ down their respective concentration gradients by pumping K^+ into and Na^+ out of the cell (41). However, as *P. falciparum* parasites mature from

ring to trophozoite stages (~12 to 18 h after invasion), there is an increased leakage of Na^+ into and K^+ out of the infected erythrocyte down the respective concentration gradients (42). This is attributed to new permeability pathways (NPPs) that is induced by the *P. falciparum* parasite in the erythrocyte membrane to increase permeability to a wide range of organic and inorganic solutes (42) as well as to a range of organic cations (43) (Figure 1.2). Although the erythrocyte Na^+/K^+-ATPase increases its activity two-fold to counteract the dissipation of the Na^+ and K^+ concentration gradients across the erythrocyte membrane, it is ultimately overwhelmed (44), and the cytosol of the infected erythrocyte progressively approaches the high-[Na^+]/low-[K^+] environment of the extracellular blood plasma as the parasite matures (40).

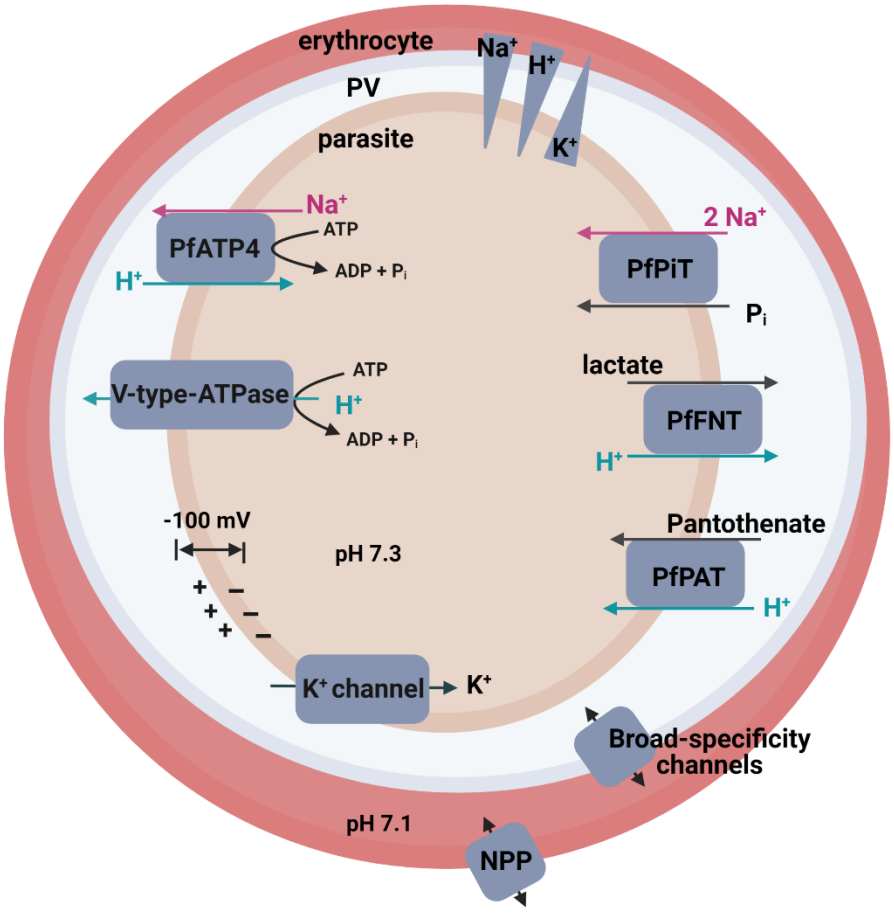

Figure 1.2: A schematic diagram of ion transport systems in mature *P. falciparum* parasites. As *P. falciparum* parasites develop into trophozoites, new permeability pathways (NPPs) are induced in the erythrocyte membrane that allow for an increased influx of Na^+ and K^+ down their respective gradients. This results in a high-[Na^+]/-low[K^+] in the erythrocyte cytosol similar to that of the extracellular blood plasma. Similar concentrations are expected in the parasitophorous vacuole (PV) due to broad-specificity channels in the parasitophorous vacuolar membrane (PVM). Alternatively, a high [K^+] is maintained in the parasite cytosol with K^+ being drawn into the cell with the high inwardly negative E_m against its concentration gradient through a plasma membrane K^+ channel. A low [Na^+] is maintained in the parasite cytosol with the efflux of Na^+ against its concentration gradient by a PfATP4 that simultaneously countertransport H^+. The large inwardly negative electrochemical gradient of Na^+ is used to import phosphate via PfPiT. Efflux of H^+ by a V-type H^+-ATPase generates the large inwardly negative E_m of approximately -100 mV and is critical to pH homeostasis. Additionally, efflux of H^+ occurs with the efflux of lactate by a PfFNT transporter. The inwardly negative H^+ gradient is used for the intracellular accumulation of the essential vitamin pantothenate via a PfPAT transporter. Figure created with Biorender.com under a standard academic licence.

Within the erythrocyte, the intraerythrocytic parasite resides within a parasitophorous vacuole (PV), which is enclosed by a parasitophorous vacuolar membrane (PVM) that forms through invagination of the erythrocyte during initial invasion (45). High-conductance broad-selectivity channels in the PVM are freely permeable to low molecular weight solutes, including anions and cations (46,47). Therefore, following the major transition to a high-[Na^+]/low-[K^+] in the erythrocyte cytosol, the ion concentrations in the PV are expected to be similar. The *P. falciparum* parasite maintains a low-[Na^+]/high[K^+] in its cytosol (40,48,49). Due to the resulting inward [Na^+] gradient across the parasite's plasma membrane and the parasite's high inwardly negative membrane potential (E_m) (approximately -100 mV) (50), a large inward electrochemical gradient for Na^+ exists. The parasite exploits this energy source, with Na^+ intake used to drive the import of inorganic phosphate, which is an essential nutrient required to sustain growth and does so using a Na^+/phosphate symporter (PfPiT) (Figure 1.2) (51). Although other potential Na^+-coupled transporters are encoded in the genome of *P. falciparum,* their functions have not been characterized and neither has their dependence on the Na^+ gradient (52).

With the high [Na^+] in the erythrocyte cytosol, the large inwardly directed [Na^+] gradient must be maintained by the active extrusion of Na^+ to counter the inward leak of Na^+ down its electrochemical gradient via unknown pathways. A P-type Na^+-ATPase (PfATP4) is responsible for the efflux of Na^+ and is simultaneously coupled to the influx of H^+ (Figure 1.2) (53,54). This places a significant acid load on the intracellular parasite that must be countered by the efflux of H^+ (54). The primary source of H^+ extrusion occurs by a vacuolar-type (V-type) H^+-ATPase on the parasite plasma membrane (55), which is also primarily responsible for the large inwardly negative E_m of approximately -100 mV (Figure 1.2) (50). Inhibition of V-type H^+ ATPase (concanamycin A/bafilomycin A_1 inhibitors) results in subsequent cytosolic acidification (55,56) and depolarization of the plasma membrane (50). In contrast to the pH of ~7.1 in the erythrocyte cytosol (57), the pH in the immediate vicinity of the external surface of the parasite's plasma membrane is ~6.9 due to the active extrusion of H^+ by the V-type H^+-ATPase (55,56). Thus, with a resting cytosolic pH of ~ 7.1 to 7.4 in the *P. falciparum* parasite (53,55,56), there is a significant inward [H^+] gradient with the inwardly negative E_m. The parasite exploits the resulting inward electrochemical gradient of H^+ is exploited to favour the intracellular accumulation of the essential vitamin pantothenic acid (precursor of coenzyme A) by an H^+/pantothenate symporter (PfPAT) (Figure 1.2) (58,59). Although the V-Type H^+-ATPase is the primary pathway for H^+ extrusion, the parasite uses a lactate/H^+ symporter (PfFNT) as a secondary pathway due to the substantial acid load of lactic acid generation within the cytosol (Figure 1.2). Therefore, PfFNT is associated with the regulation

of cytosolic pH, in which the efflux of lactate down its concentration gradient is used to efflux H^+ (60). Additionally, the uptake of Cl^- against its concentration gradient is coupled to the transport of H^+ equivalents to maintain a high cytosolic [Cl^-] and occurs via a H^+/Cl^- symporter or an OH^-/Cl^- antiporter (61). If the inward H^+ electrochemical gradient energizes the uptake of Cl^-, the transporter could mediate the recovery of cytosolic pH with alkalinization events (61). The involvement of other H^+ transporters that could be involved in the regulation of cytosolic pH is unknown.

With the efflux of H^+ by the V-Type H^+-ATPase, there is a partial countering of the associated current by the influx of K^+. This contributes to the maintenance of the resting inwardly negative E_m, which increases with membrane hyperpolarization when isolated *P. falciparum* parasites are exposed to either a reduced extracellular [K^+] or K^+ channel inhibitors (Ba^{2+} or Cs^+), and decreases with membrane depolarization when exposed to an increased extracellular [K^+] (50). These data are indicative of the presence of K^+ channels in the plasma membrane of *P. falciparum* parasites to mediate K^+ uptake, which is drawn into the parasite against its concentration gradient by the large inwardly negative E_m (50).

Multiple known biological processes of the asexual parasite are dependent on these ion transporters functioning together to regulate the asymmetric distribution of inorganic cations and anions across the plasma membrane. These biological processes have not been investigated during the gametocyte stages. The only information available on ion homeostasis during gametocytogenesis is based on drug inhibition of selected ion transport pathways (62,63).

1.5. Disruption of ion homeostasis in *P. falciparum* parasites

Multiple distinct chemical classes have been identified to inhibit Na^+ efflux by PfATP4 and consequently disrupt Na^+ homeostasis in *P. falciparum* parasites. These include spiroindolones (64-66), pyrazoleamides (67), aminopyrazoles (66), dihydroisoquinolones (68), and multiple compounds from the Medicines for Malaria Venture's (www.mmv.org) Malaria Box (69) that are potent inhibitors of the *in vitro* growth of asexual *P. falciparum* parasites. A spiroindolone (Cipargamin; KAE609) has progressed through phase I (70-72) and phase IIa (73,74) clinical trials, in which parasitaemia is rapidly cleared in adults with uncomplicated *P. vivax* or *P. falciparum* malaria. Exposure of *P. falciparum* parasites to each of these chemical compounds initiates an immediate progressive increase in cytosolic Na^+ with a simultaneous increase in cytosolic pH (Figure 1.3). With prolonged exposure at sublethal doses, the parasites develop resistance that is associated with mutations in the *pfatp4* gene (62). It is thus postulated that these compounds disrupt the low cytosolic [Na^+] by inhibiting the extrusion of

Na^+ by PfATP4. The continued leak of Na^+ into the cytosol down its electrochemical gradient is no longer countered, resulting in a progressive increase in the cytosolic [Na^+] (62).

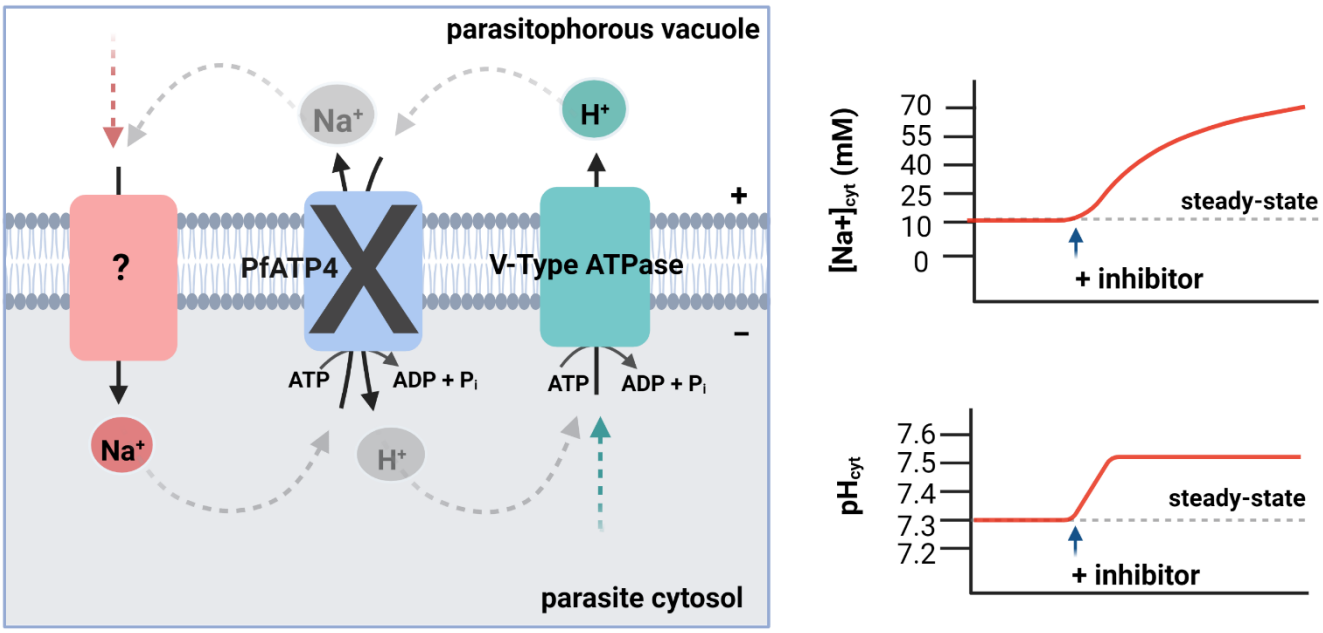

Figure 1.3: Disruption of the Na^+ gradient in *P. falciparum* parasites. The efflux of Na^+ by PfATP4 counters the influx of Na^+ down its electrochemical gradient (via unknown pathways) in order to maintain a low cytosolic [Na^+]. The efflux of PfATP4 is coupled to the influx of H^+ that places a significant acid load on the parasite. This is countered by the efflux of H^+ by a V-Type ATPase. Inhibition of Na^+ efflux by PfATP4 results in a progressive increase in cytosolic [Na^+] as Na^+ continues to leak into the cytosol. With elimination of the acid load, a progressive increase in cytosolic pH occurs with an overcompensation of H^+ efflux by the V-Type ATPase. Figure created with Biorender.com under a standard academic licence.

Additionally, inhibition of Na^+ efflux by PfATP4 prevents the counter transport of H^+ into the cytosol. This results in an overcompensation of H^+ extrusion by the V-Type H^+-ATPase that is no longer required to counteract the associated acid load of H^+ influx by PfATP4 (Figure 1.3). This leads to a progressive increase in cytosolic pH, which is postulated to account for the observed cytosolic alkalinization (62). This altered cytosolic pH is detrimental to enzyme function, while increased cytosolic [Na^+] triggers detrimental swelling and prevents essential uptake/export processes that are based on the Na^+ gradient (62). Although the mode of action has not been elucidated in gametocytes, Cipargamin has also shown potent dose-dependent inhibition against all stages of *P. falciparum* gametocyte development *in vitro* (75). It is clear that Na^+ homeostasis is essential for the viability of *P. falciparum* parasites.

Known eukaryote K^+ channel inhibitors (i.e., bicuculline methiodide and tubocurarine chloride) inhibit *P. falciparum* asexual parasites, but their effect on gametocyte development is unknown (76). However, a K^+-selective ionophore, salinomycin, inhibits asexual proliferation and gametocyte development of *P. falciparum* parasites (63). Although salinomycin does not directly target K^+ channels, it forms lipid-soluble complexes with the K^+ cation and carries it

through the plasma membrane lipid barrier through a passive diffusion process (77,78), which results in the dissipation of the K^+ gradient (Figure 1.4). The detrimental effects that this has on the viability of *P. falciparum* parasites indicate that maintaining K^+ homeostasis is essential for important biological processes in both asexual and gametocyte stages. Similar disruptive effects of the K^+ gradient are believed to occur with the inhibition of K^+ channels in the parasite *P. falciparum,* which necessitates a further study of what is known about these channels.

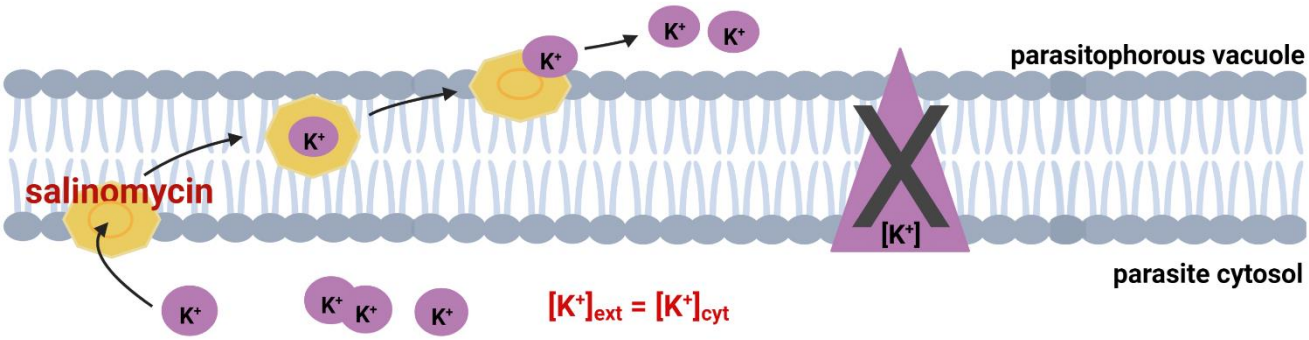

Figure 1.4: Salinomycin disrupts K^+ gradient of *P. falciparum* parasites. *P. falciparum* parasites maintain a high cytosolic [K^+]. With the addition of salinomycin, lipid soluble complexes form between the ionophore and the K^+ cations. This modifies the permeability of K^+, in which they are carried across the plasma membrane via a passive diffusion process. This disrupts the K^+ gradient with the extracellular [K^+] being equal to the intracellular [K^+]. Figure created with Biorender.com under a standard academic licence.

1.6. K^+ channels in *P. falciparum* parasites

Three putative K^+ channels are encoded in the *P. falciparum* genome, namely PfK1 (PF3D7_1227200), PfK2 (PF3D7_1465500), and PfK3 (PF3D7_1436100) (79). The diverse family of K^+ channels can be functionally grouped into five main classes: cyclic nucleotide-gated, inward rectifier, voltage-gated, Ca^{2+}-gated, and two-pore K^+ channels (80). Preliminary analyses indicate that the *P. falciparum* K^+ channels have a similarity with both voltage-gated as well as Ca^{2+}-gated K^+ channels (81).

Voltage-gated K^+ channels are the largest family of K^+ channels, present in both excitable and non-excitable cells. These proteins have a wide range of physiological functions, ranging from action potential repolarization in excitable cells to modulation of the membrane potential in non-excitable cells (82,83). In eukaryotes, the voltage-gated K^+ channel is typically a tetrameric structure in which four identical subunits arrange symmetrically to form a central pore with four surrounding voltage sensors (Figure 1.5 A) (84). Each subunit is composed of a hydrophobic region of six membrane-spanning α-helical segments that are denoted as S1-S6, with flanking hydrophilic amino and carboxyl-terminal domains in the cytoplasm (Figure 1.5 B) (84). The first four transmembrane segments (S1-S4) contain the voltage-sensor domain, where the fourth

transmembrane segment (S4) contains approximately four to eight positively charged amino acids (arginine or lysine) that provides sensitivity towards the membrane potential (85). These charges move across the electric field in response to changes in the membrane potential, in which the associated structural rearrangement of the voltage-sensor domains leads to conformational changes in the conduction pore to either open or close to the movement of K^+ ions through the channel (86).

The last two transmembrane segments (S5-S6) form the pore domain of each subunit, which are collectively arranged to form the central conducting pore (Figure 1.5 A) (87). The narrowest part of the pore is known as the selectivity filter and is responsible for K^+ selectivity. A highly conserved sequence of amino acids (TXGYG) resides in a re-entrant loop between S5 and S6 of each subunit, in which the re-entrant loops position together to form the selectivity filter (Figure 1.5 A) (88,89). The backbone carbonyl oxygen atoms located in the TXGYG sequences provide four K^+ ion binding sites (88). Each K^+ ion binds to eight carbonyl oxygen atoms in the exact same geometry as to their eight waters of hydration, which are shed upon entering the selectivity filter (90). Due to the smaller size of Na^+ ions, they are not properly solvated by the carbonyl oxygens and thus it is energetically favoured that they remain hydrated with water molecules (90). Therefore, the passage of K^+ ions through the selectivity filter is strongly favoured over the passage of Na^+ ions.

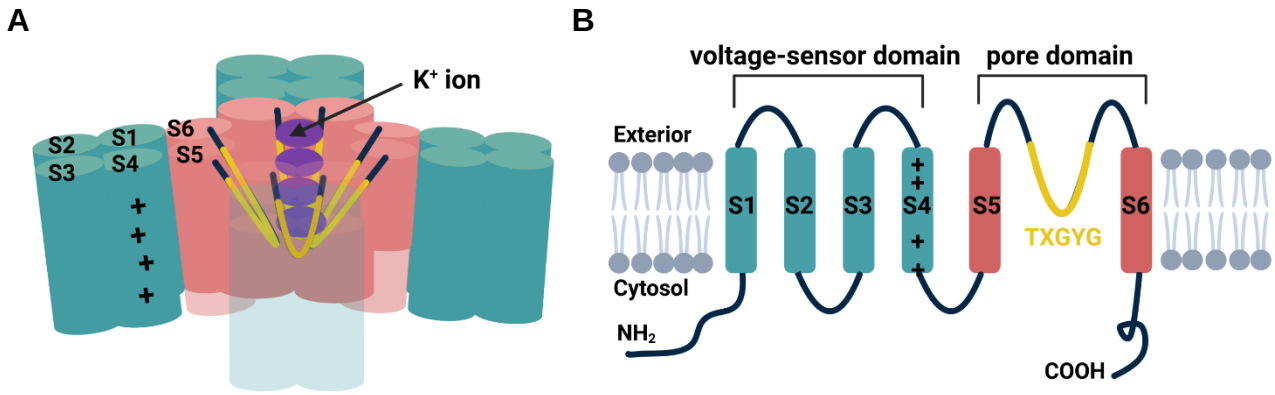

Figure 1.5: Schematic diagram of the general structure of voltage-gated K^+ channels. (A) Four subunits form a tetrameric structure with a central conduction pore (red) surrounded by four voltage sensor domains (blue). The selectivity filter is formed by the loops of the pore domains and provide binding sites for four K^+ ions. (B) Each subunit consists of six transmembrane segments (S1-S6) flanked by cytosolic amino and carboxylic termini. The voltage-sensor domain is formed by S1-S4 (blue), in which S4 is positively charged. The pore domain is formed by S5-S6 (red), and has an intervening re-entrant loop that contains a highly conserved amino acid sequence (yellow). Figure created with Biorender.com under a standard academic licence.

Ca^{2+}-gated K^+ channels consist of three main subfamilies, namely: small conductance (SK; ~4-14 pS), intermediate conductance (IK; ~32-39 pS), and big conductance (BK; ~200-300 pS) (91). As with voltage-gated K^+ channels, each subunit of the SK and IK channel

tetramers consist of six transmembrane segments (S1-S6), where the last two transmembrane segments form the pore domain (S5-S6) with the conserved sequence of amino acids (TXGYG) (Figure 1.6 A) (91). However, channel gating is activated by intracellular Ca^{2+} and is independent of membrane voltage (91-93). Ca^{2+} sensitivity is gained from the calmodulin (CaM) protein, which is tightly bound to a CaM binding domain (CaMBD) in the cytosolic C-terminus region of the channels (Figure 1.6 A) (93,94). Binding of Ca^{2+} to CaM induces conformational changes in the CaM-CaMBD monomers for subsequent channel pore opening (95,96).

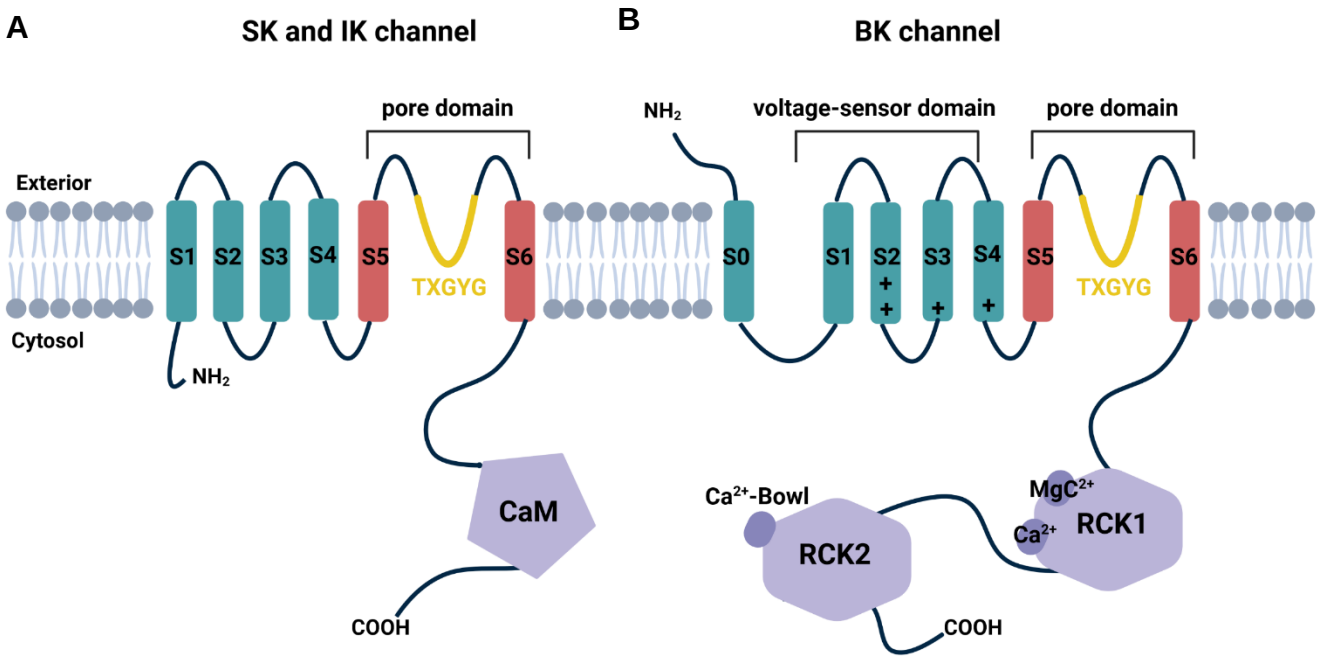

Figure 1.6: Schematic diagram of the general structure of Ca^{2+} -activated K^+ channels. (A) Membrane topology of an SK/IK channel subunit, which resembles the overall structure of voltage-gated K^+ channels (Figure 1.5). However, these channels are activated by intracellular [Ca^{2+}] based on a mechanism that involves a calmodulin (CaM) binding domain (CaMBD), and is independent of membrane voltage (B) Membrane topology of a BK channel subunit, which is activated through both membrane voltage and increase in intracellular [Ca^{2+}]. The channel subunit differs from SK/IK channels in an additional S0 segment. The cytosolic C-terminus functions as a Ca^{2+} sensor domain, which is constituted by the RCK1 (S7-S8) and RCK2 (S9-S10) domains. Figure created with Biorender.com under a standard academic licence.

In contrast to SK and IK channels, BK channels (also known as large conductance Ca^{2+}-activated K^+ channels) require allosteric activation by both membrane voltage changes and relatively high intracellular [Ca^{2+}] (97,98). The topology of the BK channel subunit is unique from the SK/IK group in the existence of an additional S0 transmembrane segment (N-terminal to S1), but also share homology in their membrane topology to voltage-gated K^+ channels with a voltage-sensor domain (S1-S4) and a pore domain (S5-S6) (Figure 1.6 B) (99). The membrane voltage is sensed within the S2, S3, and S4 transmembrane segments by

charged amino acids (100), while the Ca^{2+} sensing ability of BK channels is conferred by an extensive cytosolic C-terminal region that has four additional hydrophobic segments (S7-S10) (Figure 1.6 B) (101). The S7-S8 and S9-S10 segments are located within two non-identical tandem domains that serve as regulators of conductance of K^+ (RCK), RCK1 and RCK2, respectively (102). A high-affinity Ca^{2+}-binding site is present within each RCK1, while a high-affinity Ca^{2+} bowl-binding site is present within each RCK2, which results in eight high-affinity Ca^{2+} sites in the C-terminal domain of the tetramer that forms a Ca^{2+}-sensing apparatus known as the "gating ring" (103). The RCK domains additionally contains multiple regulatory domains for a variety of ligands (102,104) or divalent cations including Mg^{2+} (Figure 1.6 B) (105,106).

While it is unclear if PfK1 and PfK2 are gated by voltage changes, Ca^{2+} or both, both PfK1 and PfK2 are predicted to have the highly conserved TXGYG sequence (107) that is characteristic of almost every other member of the family (107). However, PfK3 has a highly unusual selectivity sequence where the highly conserved amino acid sequence in the selectivity filter has a GKG motif instead of the GYG. This questions the functionality of PfK3 as a voltage- or Ca^{2+}- gated K^+ channel. Both *pfk1* and *pfk2* are expressed throughout the asexual stages of *P. falciparum* parasites, with peak expression of *pfk1* during the trophozoite stages and peak expression of *pfk2* during the ring and schizont stages (Figure 1.7) (108,109). Immunolocalization indicated that PfK1 is exported to the EPM, whereas PfK2 is located on the PPM (107).

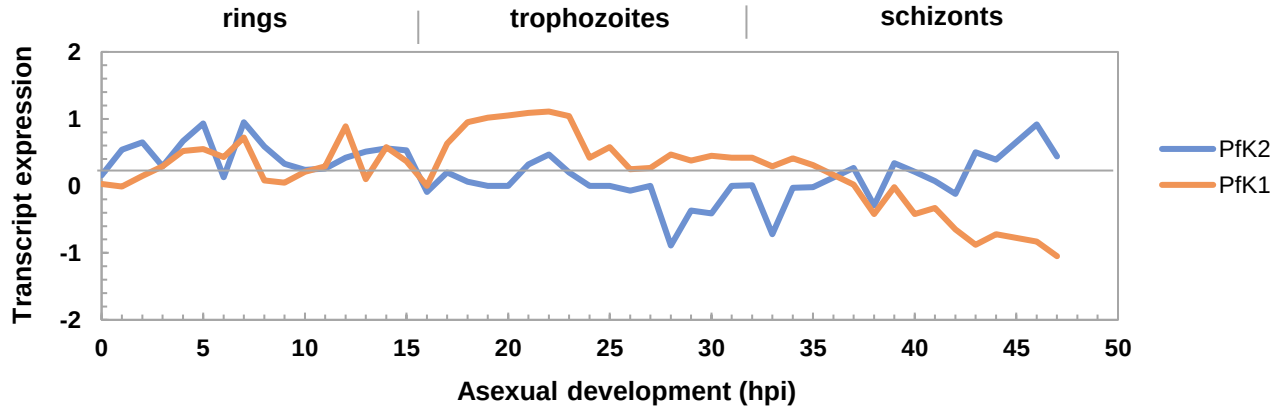

Figure 1.7: Transcriptome profile of PfK1 and PfK2 during asexual development of *P. falciparum* parasites. The transcript expression profiles of PfK1 (orange line) and PfK2 (blue line) are represented by $\log_2$(Cy5/Cy3) expression values (y-axis) for each time point throughout asexual development (x-axis). Ring stage development observed from 0-16 hpi, trophozoite development from 17-32 hpi, and schizont development from 33-47 hpi (hours post-invasion). Transcriptomic data obtained from Painter *et al.,* (2017) (109).

Both *pfk1* and *pfk2* were reported to be essential for asexual *P. falciparum* parasites following targeted gene disruption (TGD), where the genes of interest were altered at the genomic level with a truncated version to render non-functional proteins (107). However, contradictory data with transposon mutagenesis were obtained in asexual parasites of *P. falciparum* with insertion of *piggyBac* transposon into *pfk1* and *pfk2* (110), where only *pfk1* was confirmed as essential (Table 1.1). Due to the conflicting reports, further information would be required to confirm the essentiality of PfK1 and PfK2 for *P. falciparum* asexual parasites.

Table 1.1: Reported data on PfK1 and PfK2 essentiality in *P. falciparum* parasites

	Asexual stages		**Gametocytogenesis**
	genetic disruption **Ref** (107)	***piggyBac*** **Ref** (110)	**knockout/knockdown**
PfK1	essential	essential	unknown
PfK2	essential	dispensable	unknown

By contrast, the localization and essentiality of PfK1 and PfK2 during gametocytogenesis of *P. falciparum* parasites remain unknown (Table 1.1). With TGD (107), asexual parasites with the truncated *pfk1* and *pfk2* did not survive, which prevented the development and subsequent analysis of the proteins in sexual gametocyte stages. However, PfK2 is the only K^+ transporter that has expression during gametocytogenesis (Figure 1.8) (108,109), suggesting that it could be solely responsible for maintaining the K^+ gradient during gametocyte development of *P. falciparum* parasites.

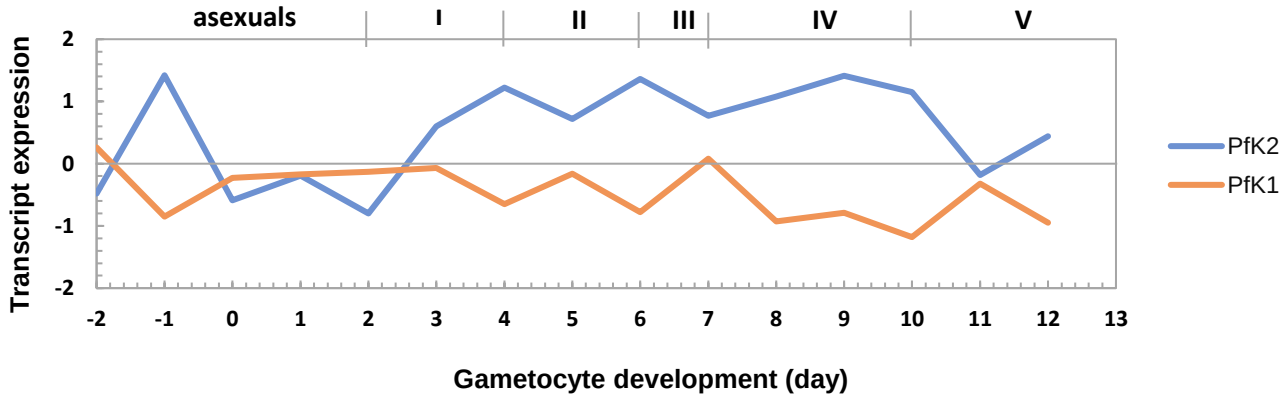

Figure 1.8: Transcriptome profile of PfK1 and PfK2 during gametocyte development of *P. falciparum* parasites. The transcript expression profiles of PfK1 (orange line) and PfK2 (blue line) are represented by log2(Cy5/Cy3) expression values (y-axis) for each time point throughout gametocyte development (x-axis). I-V represents the stages of gametocyte development. Stage I gametocytes observed from day 3-4, stage II from day 4-6, stage III from day 6-7, stage IV from day 7-10, and stage V from day 10-13. Transcriptomic data obtained from van Biljon *et al*., (2019) (111).

Since interference of the K^+ gradient inhibits gametocyte viability (Figure 1.4), it can be hypothesised that PfK2 is likely essential for important biological processes during gametocytogenesis of *P. falciparum* parasites. This project will thus generate transgenic *P. falciparum* parasites through genetic manipulation techniques. This will allow the future investigation of PfK2 functional relevance in *P. falciparum* parasites.

1.7. Genetic manipulation of *pfk2* in *P. falciparum* parasites

Ideally, the functional role of *P. falciparum* proteins during asexual parasite proliferation and sexual gametocyte differentiation must be determined using a reverse genetics approach. Specifically, a protein is dispensable if its disruption does not prevent proliferation or differentiation. On the contrary, disruption of essential proteins stops either proliferation or differentiation. Furthermore, while the parasite might survive the disruption of certain proteins, there may still be observable effects on the morphology and function of the parasite. Various genetic manipulation techniques are used in *P. falciparum* parasites, either to 'knockout' genes or to 'knockdown' the gene product (mRNA or protein). Knockout systems include the site-specific recombinase Cre/Lox system, zinc finger nucleases, and the CRISPR-Cas9 system, all of which act on the genome level. Additionally, in TGD, the gene can be replaced with a truncated sequence. Knockdown systems include the *glmS* system, the DiCre recombinase system and TetR aptamer system, amongst others (112).

This study will aim to generate transgenic parasite lines with truncated PfK2 (with a different truncation than previously tested) to obtain clarity on the essentially of PfK2 for asexual parasites (Figure 1.9). A shorter truncation (~300 bp) will be generated than what was previously tested (~1000 bp) to reduce the likelihood that the truncated fragment might still be functional (112). The TGD will be coupled with a selection-linked integration (SLI) system (112). Generally, during the genetic manipulation of *P. falciparum* parasites, asexual parasites are transfected with the appropriate plasmid that is maintained episomally due to the presence of a drug selection marker. Integration into the genome is then obtained through random homologous recombination, often over several months. By contrast, the SLI-system is based on a double selection system. The episomal presence of the plasmid is maintained by a selection marker (human dihydrofolate reductase, hDHFR), while parasites with genomic integration are selected through a second promoter-less resistance marker (neomycin resistance gene, NeoR) (112) (Figure 1.9). This NeoR marker is attached to the target gene through a T2A skip peptide, where a ribosomal "skip" will produce the NeoR protein separately from the PfK2 labelled with GFP (113). Therefore, the marker is only expressed if the construct is integrated and under the control of the native promoter of the gene under investigation. This

increases the speed and success rate in obtaining transgenic lines with genomic integration in *P. falciparum* parasites (112).

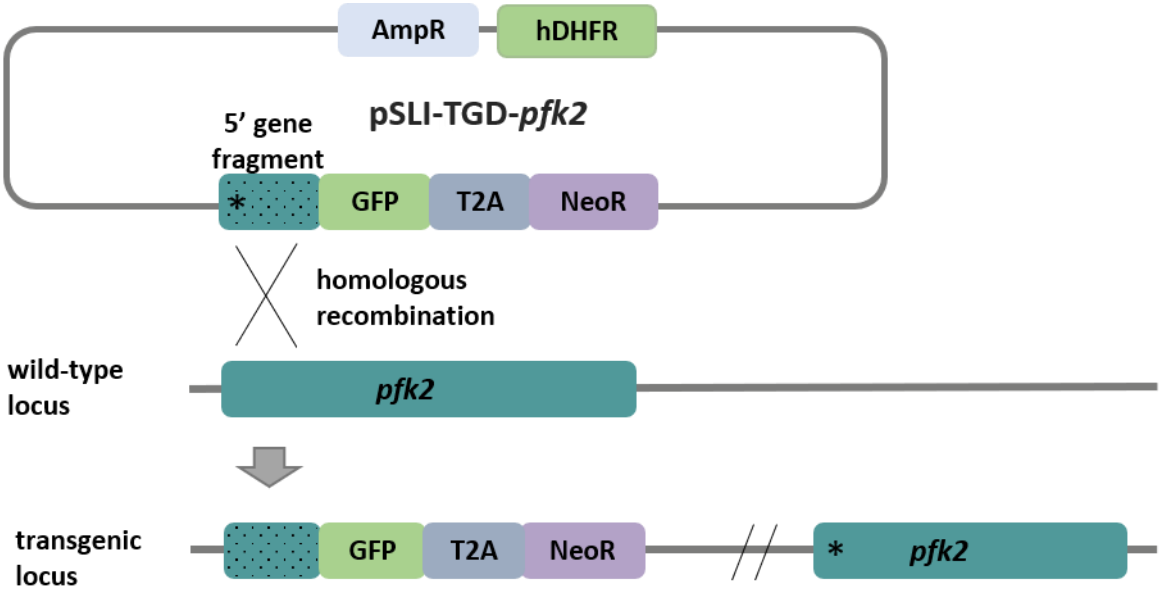

Figure 1.9: Schematic representation of the SLI-TGD system. The ampicillin resistance gene (AmpR) enable cloning of a 5' gene fragment of the *pfk2* gene into the pSLI-TGD plasmid. Following transfection of *P. falciparum* parasites, episomal uptake is selected for with the human dihydrofolate reductase gene (hDHFR). Parasites with successful homologous recombination has a truncated *pfk2* modified with a 3-terminal attachment of a green fluorescent protein (GFP) sequence, followed by a T2A skip peptide sequence, and a neomycin resistance (NeoR) gene to select for genomic integration. Asterisk (*) represents stop codon (TAA). Schematic not drawn to scale.

However, if *pfk2* is essential for asexual parasites then a conditional knockdown system will be required to investigate PfK2 function in gametocytes. This inducible system will allow for altering gene expression only after a portion of the parasites in the IDC have developed into gametocytes. This study will therefore also generate transgenic parasites lines with the *glmS* ribozyme conditional knockdown system coupled with the SLI system (114). The *glmS* ribozyme system is based on the incorporation of the *glmS* element downstream from the gene site, where the addition of glucosamine will activate the *glmS* ribozyme domain for self-cleavage of the mRNA to regulate the amount of gene product synthesized (Figure 1.10) (114). To ensure that the effects seen with knockdown are due to self-cleavage of the activated *glmS* ribozyme, a mutant form (M9 glmS) will be used as a control. This inactive version of the glmS ribozyme has a single point mutation at the ribozyme cleavage site that prevents mRNA self-cleavage with the addition of glucosamine (114).

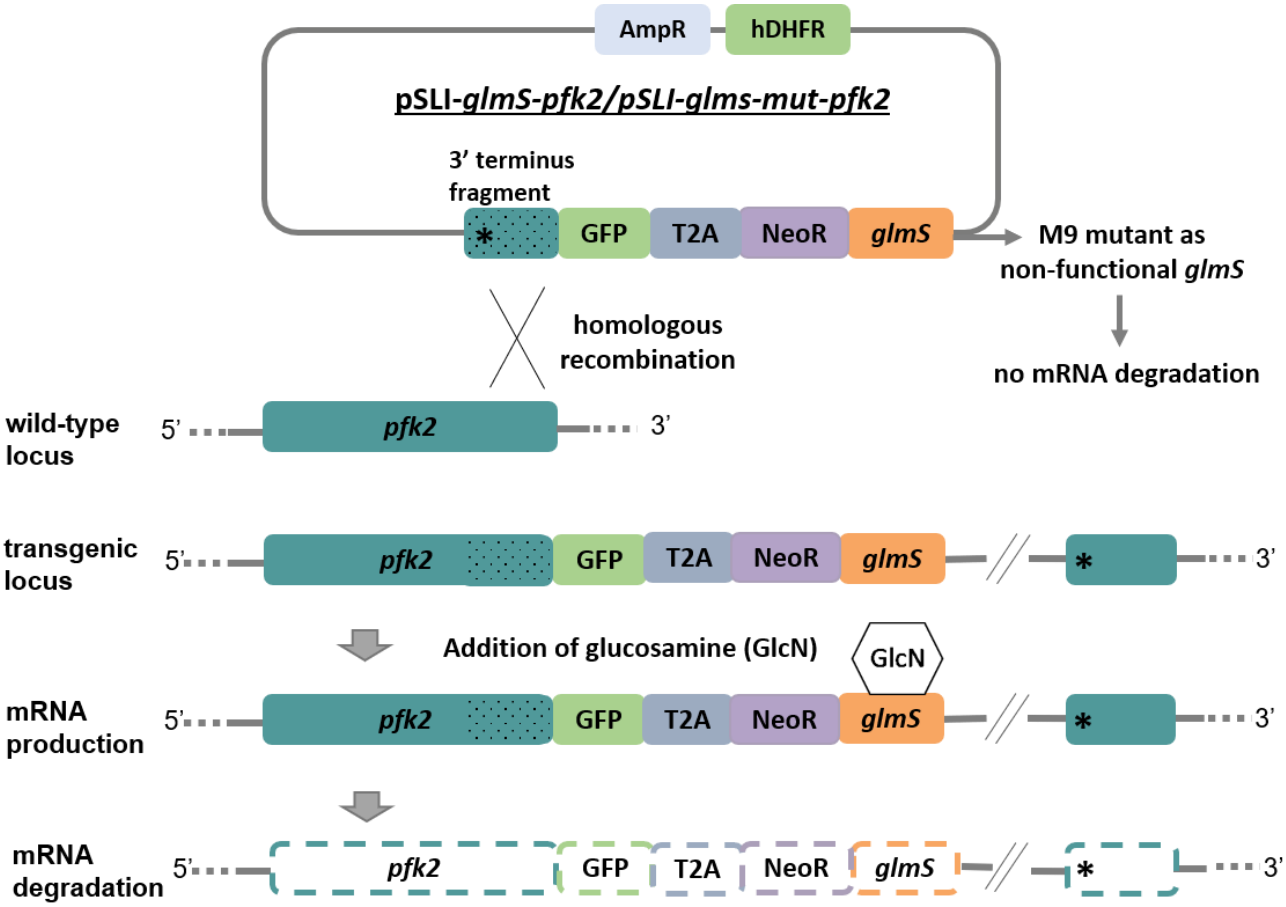

Figure 1.10: Schematic representation of the SLI-*glmS* system. The ampicillin resistance gene (AmpR) enable cloning of a 3' gene fragment of the *pfk2* gene into the pSLI-*glmS* plasmid. Following transfection of *P. falciparum* parasites, episomal uptake is selected for with the human dihydrofolate reductase gene (hDHFR). Parasites with successful homologous recombination have a *pfk2* modified with a 3-terminal attachment of a green fluorescent protein (GFP) sequence, and a *glmS* ribozyme sequence, followed by a T2A skip peptide sequence, and a neomycin resistance (NeoR) gene to select for genomic integration. The addition of glucosamine activates the *glmS* ribozyme for self-cleavage, which results in degradation of the mRNA and knockdown of protein expression. Asterisk (*) represents stop codon (TAA). Schematic not drawn to scale.

A study by a previous MSc student generated recombinant pSLI-*glmS* plasmids (p-GFP-*glmS*-*pfk2* and p-GFP-*glmS*-*mut*-*pfk2*) containing a 3-terminal fragment (~1000 bp) of the *pfk2* gene (115). These were transfected into *P. falciparum* parasites to select for episomal uptake [NF54-epi(SLI-*glmS*-*pfk2*) and NF54-epi(SLI-*glmS*-*mut*-*pfk2*)] and subsequently integration to generate NF54-*pfk2*-GFP-*glmS* and NF54-*pfk2*-GFP-*glmS*-*mut* transgenic lines. These transgenic lines only had partial integration, in which the original wild-type (WT) locus was still present for the respective populations. This study will aim to generate fully transgenic parasites for NF54-*pfk2*-GFP-*glmS* and NF54-*pfk2*-GFP-*glmS*-*mut* without observable WT parasites present. This will allow future functional analysis studies for *pfk2* through conditional knockdown with the *glmS* ribozyme domain in addition to TGD.

Aim

Develop transgenic *P. falciparum* parasites through genetic manipulation techniques for future functional studies of the importance of a putative K^+ channel (PF3D7_146550, PfK2) through genetic disruption and conditional knock-down approaches.

Hypothesis

The *pfk2* gene can be genetically modified with the pSLI-TGD and pSLI-*glmS* plasmid systems.

Objectives

I. *In silico* characterization of *pfk2*.
II. Construct a recombinant pSLI-TGD plasmid with the *pfk2* gene fragment and generate a transgenic *P. falciparum* parasite line with the SLI-TGD system for *pfk2.*
III. Generate fully transgenic NF54-*pfk2*-GFP-*glmS* and NF54-*pfk2*-GFP-*glmS*-*mut* parasite lines without the WT locus.

Research outputs:

Claassen E.B., Els F., Mugo E., Birkholtz L.M. and Niemand J. Investigating the role of a putative K^+ channel during gametocytogenesis in *Plasmodium falciparum* parasites. 6th South African Malaria Research Conference. Poster presentation. Virtual, 3 to 4 August 2021.

Claassen E.B., Els F., Mugo E., Birkholtz L.M. and Niemand J. Investigating the role of a putative K^+ channel during gametocytogenesis in *Plasmodium falciparum* parasites. 27th Congress of the South African Society of Biochemistry and Molecular Biology. Poster presentation. Virtual, 23 to 26 January 2022.

Chapter 2: Materials and Methods

2.1. Ethics statement

This study was approved by the Faculty of Natural and Agricultural Sciences Ethics Committee (ethics approval no: NAS096/2021) at the University of Pretoria, South Africa. All experiments were carried out at the Malaria Parasite Molecular Laboratory (M_2PL) biosafety level P2 facility according to relevant guidelines and regulations. The *in vitro* cultivation of malaria parasites, *P. falciparum*, in human erythrocytes was approved by umbrella ethics for the SARChI program under Prof. Birkholtz by the Faculty of Natural and Agricultural Sciences Ethics Committee (ethics approval number: 180000094). The use of human erythrocytes was additionally approved by the Faculty of Health Sciences Ethics Committee (ethics approval number: 506/2018).

2.2. *In silico* analysis of putative *P. falciparum* K^+ channel PfK2 (PF3D7_1465500)

Transmembrane domain predictions

The transmembrane domains of PfK2 were predicted from its amino acid sequence [accessed through PlasmoDB (https://plasmodb.org/plasmo/app)] by three transmembrane domain prediction servers, namely: DeepTMHMM (https://dtu.biolib.com/DeepTMHMM) (116), PSI-blast secondary structure PREDiction (PSIPRED) (http://bioinf.cs.ucl.ac.uk/psipred/) (117), and TOPCON (https://topcons.cbr.su.se/pred/) (118). The DeepTMHMM method was recently released (April 2022) as an improved version of TMHMM (119). It is based on a deep learning protein language model-based algorithm and is predicted to be the best-performing method for the prediction of the topology of both alpha-helical and beta-barrel transmembrane proteins (116). MEMPACK (TM Topology and Helix Packing) analysis was used within the PSIPRED server, which is based on machine learning-based tools and uses multiple sequence alignments from PSI-BLAST to sum the log-likelihood scores (117). The TOPCON method uses a consensus algorithm to combine the outputs of different predictors (namely, Philius (120), PolyPhobius (121), SCAMPI (122), OCTOPUS (123), and SPOCTOPUS (124) and predicts the final topology based on a hidden Markov model. This consensus prediction method has been reported to achieve the highest prediction accuracy based on benchmark datasets (125).

In addition, a hydropathy plot was used to investigate possible transmembrane domains based on hydrophobic regions. The plot was generated with the Kyte and Doolittle hydrophobicity scale (126) in Python with the Matplotlib library. This scale allocates hydropathy values to all

amino acids and is based on free energies from water-vapour transfer, as well as the interior-exterior distribution of residue side chains (126). Positive values correspond to hydrophobic regions, while negative values are associated with hydrophilic regions. These hydropathy values are then averaged over a window size, in which all the averages are plotted at the midpoint of the window. A window size of 7-11 amino acid residues is the most ideal for the detection of surface-exposed regions in globular proteins, while a window size of 19-21 amino acid residues is optimal for transmembrane regions (126). A window size of 21 amino acid residues was used to detect possible membrane-spanning regions for PfK2.

2.2.1. K^+ channel selectivity filter motif prediction

The CLUSTAL Omega (1.2.4) (https://www.ebi.ac.uk/Tools/msa/clustalo/) multiple sequence alignment program (127) was used (default settings) to confirm whether PfK2 contains the K^+ channel selectivity filter motif (TVGYG). Protein sequence alignment was performed with K^+ channels from other organisms, that is, *Rhizopus azygosporus* (accession number, RCH94169.1), *Mus musculus* (accession number, AAA39365.1), *Homo* sapiens (accession number, NP_000208.2), *Xenopus laevis* (accession number, XO_018120303.1), *Drosophila melanogaster* (accession number, NP_728783.1), *Escherichia coli* (accession number, MLC55274.1), *Caenorhabditis elegans* (accession number, NP_001256810.1), *Theileria parva* strain Muguga (accession number, KAF5153237.1), *Babesia bovis* T2Bo (accession number, EDO06445.2). The CLUSTAL Omega software performs multiple sequence alignment based on seeded guide trees and hidden Markov model profile-profile techniques (128). The amino acid sequences were accessed through the National Center for Biotechnology Information (NCBI; https://www.ncbi.nlm.nih.gov/), with GeneBank accession numbers indicated in parentheses.

2.2.2. Three-dimensional (3D) protein structure prediction

The 3D protein subunit structure of PfK2 was obtained from the AlphaFold Protein Structure Database (https://alphafold.ebi.ac.uk/), while a 3D protein homo-oligomer structure was obtained from the GalaxyHomomer server (http://galaxy.seoklab.org/homomer). AlphaFold is an artificial intelligence system that was developed in partnership between DeepMind and the EMBL-European Bioinformatics Institute. It incorporates both physical as well as biological knowledge about protein structure with multisequence alignments to generate a deep learning algorithm (129,130). AlphaFold provides accuracy at an atomic level even when no similar structure is known, and produces a per residue confidence score on a scale from 0 to 100 (higher scores correspond to higher confidence) based on the predicted local-distance

difference test (pLDDT) (131). Regions of very low confidence (pLDDT < 50) were trimmed off using UCSF Chimera version 1.15 (132). GalaxyHomomer uses both template-based modelling and *ab initio* docking to predict the homo-oligomer structure of a target protein from either a sequence or monomer structure (133). The *ab initio* method is a distinctive feature of the server that detects and refines unreliable regions for which template information is not available or inconsistent (133).

2.2.3. Protein domain and family predictions

The InterPro database (http://www.ebi.ac.uk/interpro/) was used to analyse the superfamily/family in which the PfK2 amino acid sequence [accessed through UniProt (https://www.uniprot.org/)] can be classified, as well as to predict the presence of highly conserved domains. InterPro combines predictive models (known as signatures) from several different databases to provide an integrated database and diagnostic tool (134).

2.3. *In vitro* cultivation of asexual *P. falciparum* parasites

Asexual *P. falciparum* parasites (NF54 strain) were maintained *in vitro* in human erythrocytes (A^+ or O^+) using standard procedures developed by Trager and Jensen (135). Parasites were cultured at 5 % haematocrit with daily replacement of RPMI-1640 cell culture medium (Sigma Aldrich, USA) supplemented with 23.81 nM $NaHCO_3$ (Sigma-Aldrich, USA), 0.024 mg/mL gentamycin (Hyclone, USA), 0.2 % (w/v) glucose (Merck, Germany), 25 nM 4-(2-hydroxyethyl)-1-piperazineethanesulfonic acid) (HEPES, Sigma-Aldrich, USA), 0.2 mM hypoxanthine (Sigma-Aldrich, USA), and completed with 5 g/L Albumax II (Invitrogen, USA, substitute for human serum). Parasite cultures were incubated at 37 °C with shaking at 60 rpm, and maintained in a hypoxic environment consisting of an atmosphere of 5 % CO_2, 5 % O_2, and 90 % N_2 (Afrox, South Africa). Parasitaemia, the percentage of parasite-infected erythrocytes, was determined daily through optical microscopy (1000x magnification, Nikon, Japan) using Rapi-Diff-stained thin blood smears (Merck, South Africa), and maintained at 2-6 % for ring- and 2-4 % for trophozoite-stage parasite cultures.

2.4. Cloning strategy to generate a recombinant pSLI-TGD construct

A recombinant pSLI-TGD construct was generated for essentiality studies of PfK2, in which the gene of interest is replaced by a truncated version to render it non-functional. The final construct (pSLI-TGD-*pfk2*) was generated by amplifying a 5' gene fragment of *pfk2* (332 bp) with flanking *Not*I and *Mlu*I restriction sites for directional cloning into the pSLI-TGD plasmid (112) (Figure 2.1).

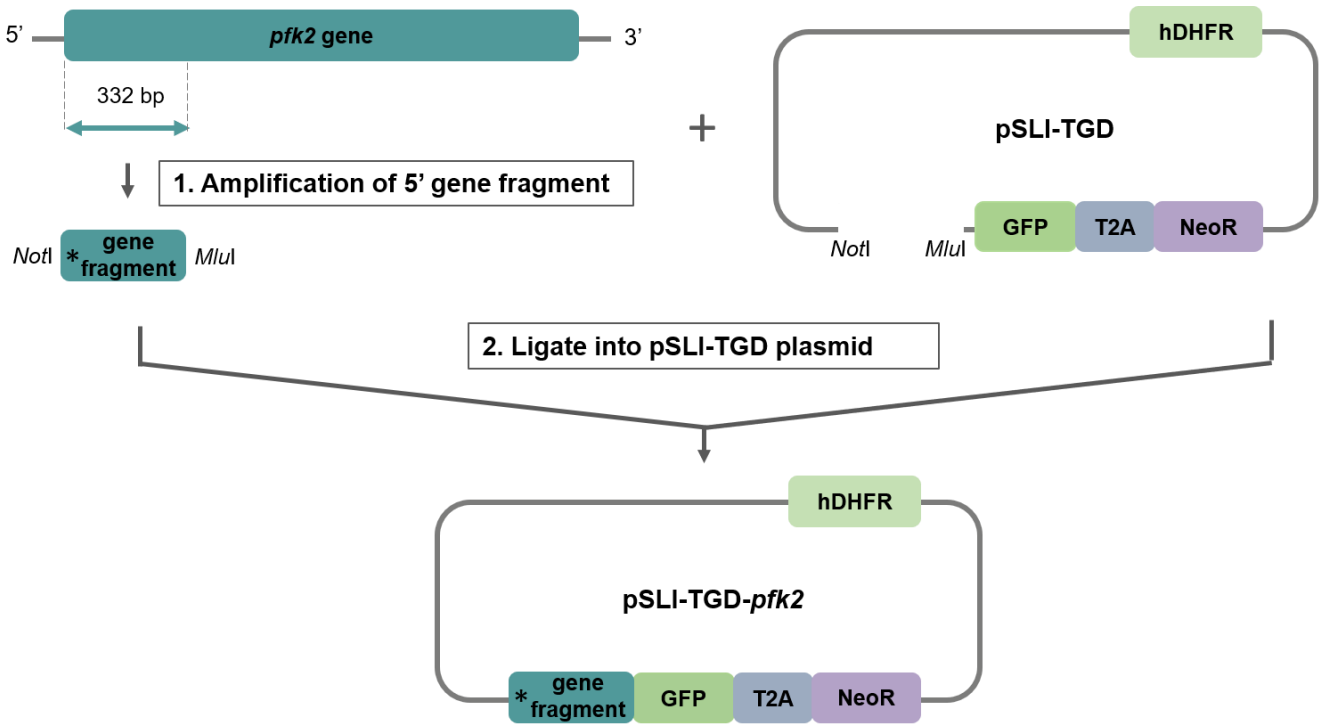

Figure 2.1: Cloning strategy to generate a pSLI-TGD-*pfk2* construct for transfection. A recombinant pSLI-TGD-*pfk2* construct was generated by amplifying a 5' gene fragment (332 bp) of *pfk2* and ligating it into the pSLI-TGD plasmid based on complementary *Not*I and *Mlu*I restriction enzyme sites. Asterisk (*) represents stop codon (TAA). Schematic not drawn to scale.

2.4.1. Total DNA isolation from *P. falciparum* parasites

Total DNA was isolated from asexual *P. falciparum* NF54 cultures (>3 % parasitaemia, >50 % trophozoite population) to act as template in PCR amplifications. The Quick DNA MiniPrep Kit (Zymo Research, USA) with proprietary buffers was used, in which the presence of a high concentration of chaotropic salts allows selective binding of DNA to a silica-based membrane. The DNA was isolated according to the manufacturer's instructions and quantified with a NanoDrop ND-1000 spectrophotometer (Thermo Fisher Scientific, USA) based on the maximal absorbance of purine and pyrimidine bases at a wavelength of 260 nm. The purity of the eluted DNA was determined on the basis of the maximal absorbance of proteins (aromatic amino acids) at 280 nm and the maximal absorbance of salts and phenolic compounds at 230 nm. The DNA was regarded as pure when A260/A280 and A260/A230 ratios were between 1.8 - 2.0. Purified DNA was stored at -20 °C until use.

2.4.2. Amplification of a *pfk2* 5' gene fragment to clone into the pSLI-TGD plasmid

Forward and reverse primers were designed in Benchling (www.benchling.com) to amplify a 5' gene fragment of ~332 bp of *pfk2* (PF3D7_1465500) for cloning into the pSLI-TGD plasmid (Table 2.1). The primer sequences were optimized with regard to melting temperature,

heterodimer and homodimer formation, as well as monomer secondary structure formation. The *Not*I (5' GC↓GGCCGC 3') and *Mlu*I (5' A↓CGCGT 3') restriction cleavage sites were added to the forward and reverse primer sequences, respectively, along with the overhang sequences to promote the binding efficiency of the restriction enzymes. Following the restriction site in the forward primer, a stop codon (TAA) was added to prevent expression prior to genomic integration. The primers were manufactured by Inqaba Biotechnical Industries (Pty) Ltd (South Africa) and dissolved in dddH_2O according to the manufacturer's instructions.

Table 2.1: Primer sequences used to amplify 5' gene fragment of *pfk2*. The restriction enzyme cut sites are underlined; the overhang nucleotide sequences are indicated in lower case; the stop codon is highlighted in bold.

primer code	primer sequence (5' – 3')		product length
P1	F	tgttGCGGCCGC**TAA**ATGAAAAGCGGATTATTTTCTATG	332 bp
P2	R	gtatACGCGTCCGATTCAATAACATTCCCG	

PCR amplification was performed in a 2720 Thermal Cycler (Applied Biosystems, Foster City, USA) with 5 pmol each of the forward and reverse gene-specific primers (Table 2.1), 30 - 50 ng of isolated gDNA (section 2.4.1.) and 1x KAPA Taq Ready Mix [KAPA Taq DNA polymerase (0.5 U/25 µL), proprietary KAPA Taq buffer, dNTPs (0.2 mM each), $MgCl_2$ (1.5 mM), proprietary stabilizers, KAPA Biosystems, Wilmington, USA]. The optimized thermal cycling profile included an initial denaturation step at 95 °C for 3 min, followed by 35 cycles of denaturation at 95 °C for 30 s, annealing at 60 °C for 30 s, and extension at 68 °C for 1 min, with a final extension at 68 °C for 3 min.

The amplified product was loaded with 1x purple loading dye (2.5 % w/v Ficoll 400, 10 mM EDTA, 3.3 mM Tris-HCI, 0.08 % w/v SDS, 0.02 % proprietary Dye 1, and 0.001 % proprietary Dye 2) (New England Biolabs, USA) on a 1.5 % (w/v) agarose gel (Lonza, Basel, Switzerland) / Tris-Acetate-EDTA (TAE) (20 mM Tris, 20 mM acetic acid and 1 mM EDTA, pH 8.0) gel containing ethidium bromide (EtBr) (1 µg/mL). A 100 bp DNA ladder (Promega, USA) was used as a molecular marker. A Gel Doc XR Imaging system (Bio-Rad, USA) was used for visualization, and Image Lab version 6.1 (Bio-Rad, USA) was used to analyse and invert the gel images. The amplified fragment of the *pfk2* gene was excised from the agarose gel and purified according to the manufacturer's instructions with the NucleoSpin Gel and PCR Clean-up Kit (Machery Nagel GmbH & Co.KG, Germany), which is based on DNA binding to a silica membrane. The eluted sample was quantified as described in section 2.4.1. and stored at -20 °C until use.

2.4.3. Cloning of the amplified *pfk2* 5' gene fragment into the pSLI-TGD plasmid

Competent *E. coli* DH5*α* cells were prepared for the uptake of plasmid DNA by inoculating the cell strain in 5 mL of Luria Bertani (LB) broth [1 % (w/v) tryptone, 1 % (w/v) NaCl, 0.5 % (w/v) yeast extract, pH 7.5], incubated overnight at 37 °C with shaking (150-180 rpm). The overnight culture was diluted in LB broth (1:50) and incubated with shaking at 37 °C until the logarithmic growth phase [OD_{600} of ~0.4, measured on a NanoDrop ND-1000 spectrophotometer (Thermo Fisher Scientific, USA)]. The cells were incubated on ice for 20 min, centrifuged at 1870 x*g* for 30 min at 4 °C in a Thermo Scientific SL 8R centrifuge (Thermo Fischer Scientific, USA), and the pellet resuspended in ice-cold 0.1 M $CaCl_2$ (25 mL). Centrifugation was repeated as above, and the pellet resuspended in ice-cold 0.1 M $CaCl_2$ (2.5 mL) and 13 % (v/v) glycerol (375 µL). The cells were incubated on ice for 1 h, then stored in 100 µL aliquots at -80 °C until used.

For transformation, competent *E. coli* DH5*α* cells (100 µL) were thawed from -80 °C on ice, and 10 ng of the pSLI-TGD plasmid added. The plasmid-cell mixture was incubated on ice for 30 min, heat shocked at 42 °C for 90 s and immediately incubated on ice for 2 min, followed by the immediate addition of pre-warmed LB-glucose (900 µL) (LB broth, 20 mM glucose) and incubation for 1 h at 37 °C with shaking. The cell suspension (100 µL) was plated onto LB-agar-amp plates [LB broth, 1.5 % (w/v) agar, 100 µg/mL ampicillin], and incubated overnight at 37 °C. Colonies of *E. coli* DH5*α* cells, transformed with the pSLI-TGD plasmid, were inoculated into 8 mL LB-amp (LB broth with 100 µg/mL ampicillin) and incubated overnight at 37 °C with shaking. The plasmid DNA was isolated from the saturated culture based on alkaline denaturation with the proprietary buffers of the NucleoSpin Plasmid (NoLid) Isolation Kit (Macherey-Nagel GmbH & Co.KG, Germany) according to the manufacturer's instructions. The purified plasmid DNA was quantified as described in section 2.4.1. and stored at -20 °C.

To generate corresponding 5' and 3' sticky ends for ligation, the isolated pSLI-TGD plasmid (2 µg) and the amplified gene fragment (1.2 µg) were digested with 10 U of *Not*I-HF (New England Biolabs, USA) and *Mlu*I-HF in 1 x CutSmart buffer (50 mM Potassium Acetate, 20 mM Tris-acetate, 10 mM Magnesium Acetate, 100 µg/mL BSA, New England Biolabs, UK) for 3 h at 37 °C. The digested plasmid backbone was excised from a 1 % (w/v) agarose/TAE gel and purified as for the digested gene fragment with the NucleoSpin Gel and PCR Clean-up Kit (Machery Nagel GmbH & Co.KG, Germany) according to the manufacturer's instructions,

The digested 5' gene fragment was ligated to the complementary sticky ends of the digested pSLI-TGD plasmid with 400 U of T4 DNA ligase (New England Biolabs, USA) and 1 x T4 DNA ligase buffer (50 mM Tris-HCI, 10 mM $MgCl_2$, 1 mM ATP, 10 mM DTT). A

3:1 insert to vector molar ratio was used in the equation below to calculate the amount of insert DNA required, and the reaction was incubated overnight at 4 °C.

$$\frac{\text{ng of vector x kb size of insert}}{\text{kb size of vector}} \times \text{insert: vector molar ratio} = \text{ng of insert}$$

The ligation reaction (10 µL) was added to competent *E. coli* DH5*α* cells (100 µL), transformed as described previously, and plated onto LB-agar-amp plates. The plates were incubated overnight at 37 °C.

2.4.4. Screening of recombinant pSLI-TGD plasmid

Recombinant clones were identified from the LB-agar-amp plates by colony screening PCR. Single colonies were randomly selected, each inoculated in 100 µL LB-amp, and incubated for 2 h at 37 °C with shaking (150-180 rpm). PCR amplification was performed with 5 pmol each of the gene-specific forward primer (P1; Table 2.1) and the reverse plasmid-backbone reverse primer (P4: Table 2.2), 1 µL of bacterial culture as template, and 1x KAPA Taq Ready Mix. The thermal cycling profile included an initial denaturation step at 95°C for 3 min, followed by 35 cycles of denaturization at 95 °C for 30 s, annealing at 60 °C for 30 s, and extension at 68 °C for 1 min, with a final extension at 68 °C for 3 min. The PCR products were analysed on a 1.5 % (w/v) agarose gel with a 100 bp DNA ladder (Promega, USA) to identify recombinant clones based on the presence of a correctly sized DNA band. The bacterial culture (50 µL) of selected recombinant clones was inoculated into 8 mL of LB-amp and incubated overnight at 37 °C with shaking. The plasmid DNA was isolated with the NucleoSpin Gel and PCR Clean-up Kit (Machery Nagel GmbH & Co.KG, Germany) according to the manufacturer's instructions, quantified spectrophotometrically, and stored at -20 °C until use.

Table 2.2: Primer sequences used to screen for recombinant pSLI-TGD constructs

	primer code		primer sequence (5' – 3')	product length
colony PCR	P1	F	tgttGCGGCCGC**TAA**ATGAAAAGCGGATTATTTTCTATG	416 bp
	P4	R	ACAAGAATTGGGACAACTCCAGTGA	
sequencing	P3	F	AGCGGATAACAATTTCACACAGGA	496 bp
	P4	R	ACAAGAATTGGGACAACTCCAGTGA	

Restriction enzyme digestion was used to further validate that the *pfk2* gene fragment ligated successfully into the pSLI-TGD plasmid. The isolated plasmid DNA (0.5 µg) was digested with

10 U of *Not*I-HF and *Mlu*I-HF in 1 x CutSmart buffer for 1.5 h at 37 °C. The digested product was analysed on a 1.5 % (w/v) agarose gel with a 1 kb DNA ladder (Promega, USA) to identify DNA bands that correlate with the size of the pSLI-TGD plasmid backbone and the *pfk2* gene fragment.

The sequence of the *pfk2* insert was validated by Sanger sequencing, which is based on the incorporation of fluorescently labelled dideoxynucleotides that cause chain termination of each amplified extension at a different base. Each sequencing reaction (20 µL) was performed with 1 x BigDye proprietary mix (2 µL) and 2 x BigDye proprietary buffer (4 µL) from the BigDye Terminator v3.1 Cycle Sequencing kit (Applied Biosystems, Foster City, USA), 100 ng of plasmid DNA, and 5 pmol of forward or reverse backbone-specific primers (P3 and P4; Table 2.2). The thermal cycling profile included an initial denaturization step at 96 °C for 1 min, followed by 25 cycles of denaturation at 96 °C for 10 s, annealing at 50 °C for 5 s, and extension at 60 °C for 4 min. The sequencing reactions were cleaned with ethanol precipitation by mixing each with a solution of 3 M sodium acetate (pH 5.2, 2 µL) and ice-cold 100 % absolute ethanol (50 µL). The mixtures were incubated on ice for 15 min and centrifuged at 13 000 x*g* for 30 min at 4 °C in a 5415 R Eppendorf centrifuge (Hamburg, Germany). The pellet was washed by adding ice-cold 70 % (v/v) ethanol (250 µL), followed by centrifugation for 10 min as above. The supernatant was discarded and the pellet dried *in vacuo* (Bachofer BA-VC-300H vacuum concentrator, Germany) to evaporate residual ethanol. The sequencing was carried out at the DNA Sanger Sequencing facility at the University of Pretoria (Faculty of Natural and Agricultural Sciences) with an ABI3500xL Genetic Analyser (Applied Biosystems, Thermo Fischer Scientific, USA). Analysis of the DNA sequences was carried out with the sequence alignment tool in Benchling.

2.5. Generate transgenic *P. falciparum* parasites with the SLI-TGD system

2.5.1. Large-scale isolation of recombinant pSLI-TGD plasmid

To isolate sufficient plasmid DNA for transfection, the recombinant pSLI-TGD plasmid was transformed into competent *E. coli* DH5*α* cells as described in section 2.4.3. The transformed cell suspension (200 µL) was transferred to 10 mL LB-amp and incubated overnight at 37 °C with shaking (150-180 rpm). This bacterial culture (2 mL) was subsequently inoculated in 200 mL of LB-amp and incubated overnight at 37 °C with shaking. Plasmid DNA was isolated from the saturated bacterial culture (OD_{600} >2) with the NucleoBond Xtra Midi / Maxi purification kit (Macherey-Nagel GmbH & Co.KG, Germany) according to the manufacturer's instructions. The eluent was further purified with isopropanol precipitation. Ice-cold isopropanol (3.5 mL)

was added to the eluent (5 mL), briefly vortexed (10-15 s), and centrifuged at 15000 x*g* for 30 min at 4 °C. The pellet was washed with ice-cold 70 % (v/v) ethanol (2 mL) by centrifugation as above for 5 min. The DNA pellet was dried *in vacuo* and resuspended in 250 µL $dddH_20$. A day before transfection, the plasmid DNA (100-250 µg) was precipitated with ethanol as previously described in section 2.4.4. but with an additional wash step at the end with 1 mL of ice-cold 100 % ethanol by centrifugation at 13000 x*g* for 15 min at 4 °C. The pellet was air dried at room temperature in a laminar flow hood, and resuspended in 250 µL of Cytomix [120 mM KCl (Minema, South Africa), 0.15 mM $CaCl_2$ (Merck, Germany), 2 mM Egtazic acid (Sigma-Aldrich, USA), 5 mM $MgCI_2$ (Merck, Germany), 10 mM K_2HPO_4 (Scharlau, Germany), 25 mM HEPES (Sigma-Aldrich, USA), pH 7.6].

2.5.2. Transfection of asexual *P. falciparum* parasites with the recombinant pSLI-TGD plasmid

A *P. falciparum* NF54 parasite culture (4 mL) was used for transfection at a 5 % haematocrit and with a ring-stage population >5 %. The culture was centrifuged at 3500 x*g* for 4 min in a Heraeus Megafuge 40 centrifuge (Thermo Fisher Scientific, USA), the media aspirated, and the 200 µL pellet resuspended in equal volume of Cytomix. Following centrifugation at 3500 x*g* for 3 min, the cell pellet was resuspended in Cytomix containing a total of 200 µg of recombinant pSLI-TGD plasmid DNA (section 2.5) to a produce a final volume of 450 µL. The mixture was transferred to a pre-chilled 2 mm electroporation cuvette and electroporated with a Gene Pulser Xcell Electroporation System (BioRad, USA). Electroporation took place at a capacitance of 950 µF, a voltage of 0.31 kV, and at maximum resistance to obtain an optimal time constant of 10-25 ms. The electroporated sample was immediately added to 5 mL of complete media in a 25 cm^2 culture flask, and allowed to recover in a stationary incubator for 2 h at 37 °C in a 5 % CO_2, 5 % O_2, and 90 % N_2 atmosphere. The recovered parasites were centrifuged (3500 x*g* for 3 min) to aspirate the lysed erythrocytes with the media. The pellet was resuspended in 5 mL of pre-warmed culture medium and 100 µl of erythrocytes added to maintain a 5 % haematocrit. The culture was transferred back a stationary incubator at 37 ° C with a 5 % CO_2, 5 % O_2, and 90 % N_2 atmosphere.

2.5.3. Drug selection for episomal uptake of recombinant pSLI-TGD plasmid

Twenty-four hours after transfection, parasites with episomal uptake of the recombinant pSLI-TGD plasmid were selected for with the addition of 4 nM WR99210 (Jacobs Pharmaceutical Company, USA). This antifolate drug stops nucleic acid synthesis in *P. falciparum* parasites by inhibiting the dihydrofolate reductase (DHFR) of the parasites (136).

The expression of the human hDHFR resistance marker from the pSLI-TGD plasmid allows the parasites to survive, albeit only those that have taken up the recombinant pSLI-TGD plasmid episomally. The transfected parasites were placed under drug pressure for 10 days in a stationary incubator, after which the parasites were transferred back to a shaking incubator and allowed to recover in drug-free culture medium. During recovery, the culture medium was replaced every 3 to 4 days, and fresh erythrocytes were added once a week to replace lysed erythrocytes and maintain a 5 % haematocrit. The parasitaemia was monitored throughout drug selection and recovery to monitor parasite proliferation.

2.6. Generate transgenic *P. falciparum* parasites with the SLI-*glmS* system

2.6.1 Validate NF54-epi(SLI-*glmS-pfk2*) and NF54-epi(SLI-*glmS-mut-pfk2*) lines

Recombinant pSLI-*glmS* plasmids (p-GFP-*glmS-pfk2* and p-GFP-*glmS*-mut-*pfk2*) with a 3' gene fragment of *pfk2* were generated by a previous MSc student and transfected into asexual *P. falciparum* NF54 parasites, resulting in lines containing the plasmids episomally **[**NF54-epi(SLI-*glmS-pfk2*) and NF54-epi(SLI-*glmS*-mut-*pfk2*)] (115).

2.6.1.1 Sanger Sequencing of the recombinant p-GFP-*glmS-pfk2* and p-GFP-*glmS-mut-pfk2* constructs

The p-GFP-*glmS-pfk2* and p-GFP-*glmS*-mut-*pfk2* constructs were validated by Sanger sequencing as described in section 2.4.4. to confirm that there were no unwanted insertions, deletions, or frameshift mutations that could interfere with downstream conditional knockdown experiments with the *glmS* ribozyme domain. The sequencing amplification reaction was performed with both gene-specific primers (P5 and P6; Table 2.3) as well as plasmid-backbone primers (P3 and P4; Table 2.3) to generate a consensus sequence.

Table 2.3: Primer sequences used for sequencing of p-GFP-*glmS-pfk2* and p-GFP-*glmS*-mut-*pfk2* constructs.

	primer code	primer sequence (5' – 3')		product length
plasmid-specific	P3	F	AGCGGATAACAATTTCACACAGGA	332 bp
	P4	R	ACAAGAATTGGGACAACTCCAGTGA	
gene-specific	P5	F	gcatCTTAAGACATAAACACATGCTACAGCG	332 bp
	P6	R	ataGGTACCCAATATATAAACTATATCATCGAATCG	

2.6.1.2 PCR analysis of episomal presence for NF54-epi(SLI-*glmS*-*pfk2*) and NF54-epi(SLI-*glmS*-mut-*pfk2*) lines

The NF54-epi(SLI-*glmS*-*pfk2*) and NF54-epi(SLI-*glmS*-mut-*pfk2*) lines were validated by PCR analysis to confirm the episomal presence of the recombinant p-GFP-*glmS*-*pfk2* and p-GFP-*glmS*-mut-*pfk2* constructs. The Quick DNA Miniprep Kit was used according to the manufacturer's instructions to isolate DNA from the respective parasite cultures. Table 2.4 lists the primer pairs used for detection with the expected amplification size for the episomal presence of the recombinant constructs, while Figure 2.2 provides a schematic representation of the primer binding sites.

Table 2.4: Primer sequences used to confirm episomal presence for the SLI-*glmS* system.

purpose	primer code		primer sequence (5' – 3')	product length (bp)
episomal uptake	P7 ■	F	gcatGCGGCCGCtaaGCCATTTACTTTTGAATTATAAAAAGC	1161
	P4 ◇	R	ACAAGAATTGGGACAACTCCAGTGA	

The episomal presence of the recombinant pSLI-*glmS* constructs was detected by amplification with a gene-specific primer (P7; Table 2.4) and a plasmid-backbone primer (P4; Table 2.4). PCR amplification was performed with 5 pmol each of the forward and reverse primers (Table 2.4), 32 ng of DNA, and 1x KAPA Taq Ready Mix. The thermal cycling profile included an initial denaturation step at 95 °C for 3 min, followed by 35 cycles of denaturation at 95 °C for 1 min, annealing at 50 °C for 1 min, and extension at 68 °C for 2 min, with a final extension at 68 °C for 5 min. The PCR products were analysed on a 1 % (w/v) agarose gel with a 1 kb DNA ladder (Promega, USA) to identify the DNA fragment sizes.

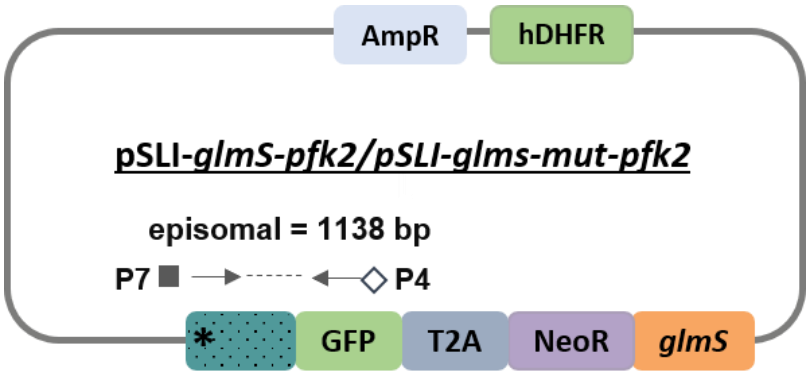

Figure 2.2: Schematic representation of the primer pairs used to detect episomal presence of p-GFP-*glmS*-*pfk2* and p-GFP-*glmS*-mut-*pfk2*. Primer pair number P7 and P4 (Table 2.4) was used to detect episomal presence of the recombinant constructs. Schematic diagram not drawn to scale.

2.6.2. Drug pressure to generate fully transgenic NF54-*pfk2*-GFP-*glmS* and NF54-*pfk2*-GFP-*glmS-mut* lines

The NF54-epi(SLI-*glmS-mut-pfk2*) line with episomal presence of the p-GFP-*glmS-mut-pfk2* construct was previously placed under drug pressure with G418 (Thermo Fischer Scientific, USA) over a 14-day period to obtain genomic integration (115). In this study, the same concentration of G418 was used to select the NF54-epi(SLI-*glmS-pfk2*) episomal line for integration over a 16-day drug pressure period. G418 (geneticin; an analog of neomycin sulphate) blocks polypeptide synthesis by inhibiting elongation, and selects integrated parasites based on the neomycin resistance marker expressed under the *pfk2* endogenous promoter. Complete culture medium containing 400 µg/mL G418 was changed every day for the first 10 days and then every second day for six days (NF54-epi(SLI-*glmS-pfk2*). In a second set of experiments, partially integrated NF54-*pfk2*-GFP-*glmS* and NF54-*pfk2*-GFP-*glmS-mut* parasites were placed under drug pressure with G418 and WR99210 to remove the WT locus. Complete culture medium containing G418 (800 µg/mL) was changed every day for 10 days and then every second day for six days. WR99210 (4 nM) was added to the complete culture medium in combination with G418 (800 µg/mL) for the first four days of drug pressure. In a third set of experiments, partially integrated NF54-*pfk2*-GFP-*glmS* and NF54-*pfk2*-GFP-*glmS-mut* lines were placed under drug pressure with WR99210 for removal of the WT locus. Complete culture medium containing WR9910 (8 nM) was changed every day for 10 days (NF54-*pfk2*-GFP-*glmS*) or every day for 16 days (NF54-*pfk2*-GFP-*glmS-mut*).

During drug pressure, the cultures were maintained in a stationary incubator. With the removal of the drug pressure, the cultures were transferred to a shaking incubator for recovery, with the medium changed every 3 to 4 days. To replace lysed erythrocytes, fresh erythrocytes (100 µL; 50 % haematocrit) were added once a week or as necessary to maintain a 5% haematocrit. Parasitaemia was monitored throughout drug pressure and recovery to monitor parasite proliferation. The DNA of parasites recovered from drug pressure was isolated at a sufficient parasitaemia (>3 %) using the Quick-DNA Miniprep Kit according to the manufacturer's instructions. To detect integration and the absence of the WT locus, PCR analysis was performed with the same conditions as in section 2.6.1.2., and the primer pairs used for screening with their respective binding sites are indicated in Table 2.5 and Figure 2.3, respectively. Integration was analysed by amplification of 5' (primer P8 and P4; Table 2.5) and 3' (primer P3 and P9; Table 2.5) flanking loci regions of the *pfk2* gene. The detection of WT parasites was determined by amplification across the locus (primer P8 and P9; Table 2.5). Following PCR analysis, parasites pellets (100 % packed erythrocytes) were

resuspended in freezing medium (28 % (v/v) glycerol, 3 % (w/v) D-sorbitol, 0.65 % (w/v) NaCl) in a 1:1 ratio and frozen in liquid nitrogen for future studies.

Table 2.5: Primer sequences used to confirm integration for the SLI-*glmS* system.

purpose	primer code		primer sequence (5' – 3')	product length (bp)
5' integration	P8 ●	F	GGTGAATTTAATGAAACAAAATTATATCATC	1368
	P4 ◇	R	ACAAGAATTGGGACAACTCCAGTGA	
3' integration	P3 ◆	F	AGCGGATAACAATTTCACACAGGA	1259
	P9 ○	R	CAAAATATTTAATGTAACCATTTGGATG	
transgenic locus	P8 ●	F	GGTGAATTTAATGAAACAAAATTATATCATC	8836
	P9 ○	R	CAAAATATTTAATGTAACCATTTGGATG	
wild-type locus	P8 ●	F	GGTGAATTTAATGAAACAAAATTATATCATC	1416
	P9 ○	R	CAAAATATTTAATGTAACCATTTGGATG	

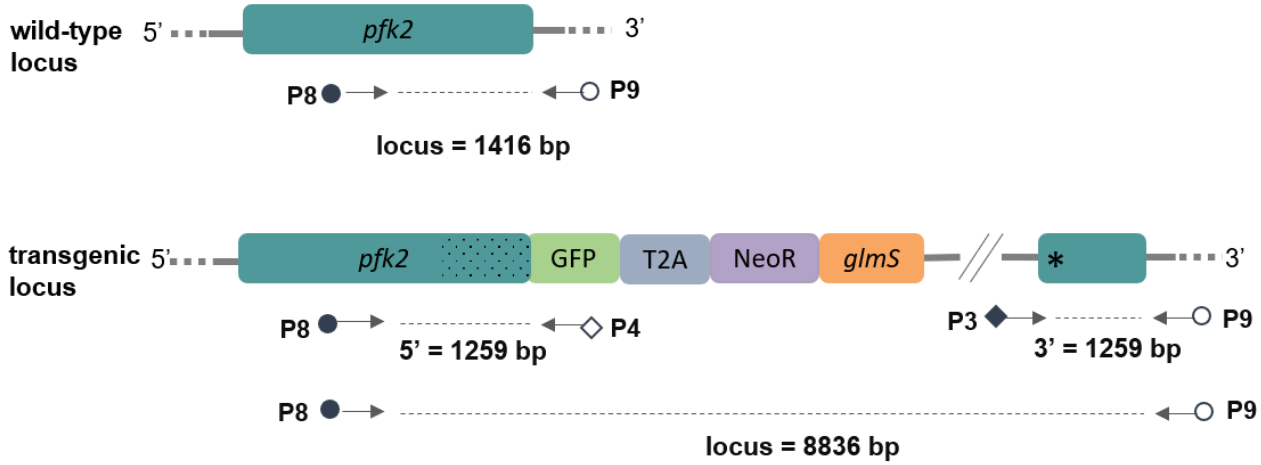

Figure 2.3: Schematic representation of the primer pairs used to detect integration for NF54-*pfk2*-GFP-*glmS* and NF54-*pfk2*-GFP-*glmS*-mut lines. Primers used for screening are represented by their respective primer codes as listed in Table 2.5. Primer pair number P8 and P4 was used to detect integration at the 5' end of *pfk2*, while P3 and P9 was used to detect integration at the 3' end of *pfk2*. The WT locus was detected with primer pair number P8 and P9, which are located upstream and downstream of the 3' homology region, respectively. Schematic diagram not drawn to scale.

2.6.3. Limiting dilution to obtain fully transgenic NF54-*pfk2*-GFP-*glmS* and NF54-*pfk2*-GFP-*glmS*-mut lines

Asexual parasite cultures of partially integrated NF54-*pfk2*-GFP-*glmS* and NF54-*pfk2*-GFP-*glmS* mut parasite populations were cloned by limiting dilution. Parasitaemia was determined

by microscopic examination of Rapi-Diff-stained thin blood smears. Since 1mL of packed erythrocytes contain 10^{10} cells, the number of infected erythrocytes per mL packed cells were calculated using the parasitaemia determined. Parasite suspensions at 2% haematocrit (200 µL in each well) were prepared to obtain final concentrations of 0.5 parasites/well (± 48 wells with a single parasite), 1 parasite/well (± 96 wells with a single parasite) and 3 parasites/well for each 96-well microtiter plate. The 96-well microtiter plates were incubated in a sealed gas chamber in a stationary incubator at 37 °C, with an atmosphere of 5% CO_2, 5 % O_2, and 90 % N_2 maintained daily. Complete media changes were made weekly with 0.4 % fresh erythrocytes. Parasite proliferation was detected visually through a change in media colour. Rapid proliferation of asexual parasites relies on anaerobic glycolysis to maintain its energy supply (137), resulting in an accumulation of lactate. The efflux of lactate results in acidification of the medium with a change in colour from pink to yellow due to the presence of the indicator Phenol Red. The proliferation in wells with a yellow media colour was subsequently validated by microscopic evaluation of Rapi-Diff-stained thin blood smears. However, detecting integration and the absence of WT parasites through PCR analysis would require isolation of gDNA from a sufficient culture volume (5 to 10 mL). This is a costly procedure that also requires an extensive time period. As an alternative, PCR conditions in which *in vitro* cultures could be screened directly from 96-well microtiter plates without increasing the culture volume or isolating gDNA were investigated (138).

Different template sources were compared using standard PCR conditions to amplify 18S *P. falciparum* ribosomal RNA gene. This reaction was chosen since this is a robust PCR amplification that is routinely used in the M_2PL laboratory. A partially integrated NF54-*pfk2*-GFP-*glmS*-mut culture was serially diluted 10-fold at a 2 % haematocrit from a 1.5 % to 0.00015 % parasitaemia. For each dilution, three different conditions were tested in 20 µL PCR amplification reactions with 5 pmol each of the gene-specific primers in Table 2.6 and 1x KAPA Taq Ready Mix. For the first condition, 20 µL of each diluted parasite suspension was centrifuged at 3500 x*g* for 3 min in a 5415 R Eppendorf centrifuge. The pellets were each resuspended in 32 µL ice-cold dddH_2O and flash frozen 3 times in liquid nitrogen. The supernatant (8 µL) at each dilution was added as a template to the PCR reactions. The second condition involved the use of 4 µL of the culture of each diluted parasite suspension directly in the PCR reactions, while the third condition involved the addition of 2 µL of settled cells of each diluted parasite suspension to the PCR reactions. The thermal cycling profile included an initial denaturation step at 95 °C for 3 min, followed by 40 cycles of denaturation at 95 °C for 30 s, annealing/extension at 60 °C for 2 min, with a final extension at 60 °C for 7 min. The PCR

products were analysed on a 1 % (w/v) agarose gel with a 1 kb DNA ladder (Promega, USA) to evaluate the amplification from three template conditions at different parasitaemias.

Table 2.6: Primer sequences used to optimize *P. falciparum* whole-cell PCR for amplification of the 18S ribosomal RNA gene.

primer code	primer sequence (5' – 3')		product length
P10	F	CCTGTTGTTGCCTTAAACTTC	1200 bp
P11	R	TTAAAATTGTTGCAGTTAAAACG	

The template source (4 μL parasite culture at 2% haematocrit) that allowed PCR amplification of the 18s rRNA gene at the lowest parasitaemia was subsequently tested to detect whether it can be used in the PCR to investigate integration at the 5' loci as well as to detect the absence of WT parasites. Asexual *P. falciparum* parasite cultures (4 µL; partially integrated NF54-*pfk2*-GFP-*glmS*-mut) were used at a 2 % haematocrit as a template for each 20 µL PCR reaction with 5 pmol each of the primers (P4 and P8, integration; P8 and P9; WT locus) in Table 2.5 and 1x KAPA Taq Ready Mix. The same PCR conditions were used as described above for the detection of integration at the 5' loci. The thermal cycling profile for the detection of the WT locus included an initial denaturation step at 95 °C for 3 min, followed by 40 cycles of denaturation at 95 °C for 1 min, annealing at 50 °C for 1 min, and extension at 68 °C for 2 min, with a final extension at 68 °C for 5 min. The PCR products were analysed on a 1 % (w/v) agarose gel with a 1 kb DNA ladder (Promega, USA) to identify the DNA fragment sizes.

These PCR conditions were used to screen the clones after limiting dilution for integration (5' loci) and the absence of the WT locus. Selected clones identified as integrants were increased in volume (200 µL to 10 mL) and haematocrit (2% to 5 %). gDNA was isolated as above for PCR analysis to screen for integration (5' and 3' loci) and the absence of WT parasites as previously described (section 2.6.2).

2.7. Visualization of GFP-tagged parasites for partially integrated NF54-*pfk2*-GFP-*glmS* and NF54-*pfk2*-GFP-*glmS*-mut line

For detection of GFP fluorescence of the partially integrated NF54-*pfk2*-GFP-*glmS* and NF54-*pfk2*-GFP-*glmS*-mut line, imaging was performed on an EVOS Cell Imaging System (Thermo Fischer Scientific, USA). The respective parasite cultures (10 µL each; 5 % haematocrit) were sealed with a 1 mm coverslip (Menzel-Gläser, Thermo Fisher Scientific, USA) onto a microscope slide (25 mm x 75 mm). A 100x oil immersion objective was used for

imaging. GFP has an excitation wavelength of 488 nm and an emission wavelength of 500 nm, which has detection through the green channel. Background signal was subtracted with ImageJ version 1.53a (based on Java 1.8.0_112) (139).

Chapter 3: Results

3.1. *In silico* analysis of PF3D7_1465500 in *P. falciparum* parasites

In silico analysis was performed with various bioinformatic tools to confirm and expand on the annotation of PF3D7_1465500 (PfK2) as a putative K^+ channel. As K^+ channels are integral membrane proteins, the transmembrane topology of PfK2 was investigated using three different transmembrane predictive tools, namely: DeepTMHMM (116), PSIPRED (117), and TOPCON (118). Multiple programs were used as the prediction algorithm of each is based on different principles (hydrophobicity, charge, machine learning techniques, evolutionary information, etc.), in which the final topology predictions by the different programs often differ from each other (140). A consensus based on similarity between all three tools suggested that PfK2 has eight transmembrane domains (Table 3.1).

Table 3.1: Predicted transmembrane domains (TMMs) of PfK2 with DeepTMHMM, PSIPRED, and TOPCON. Numbers in the table represent amino acid locations of predicted transmembrane domains.

Predicted transmembrane domain locations										
DeepTMHMM	11-20	47-64	144-165	183-203	217-232	242-251	278-299	347-364	-	-
PSIPRED	12-35	45-72	143-162	185-204	212-236	241-259	277-299	344-364	534-551	-
TOPCON	13-33	48-68	142-162	185-205	217-237	241-261	278-298	344-364	-	1199-1219
Consensus location (TMM domain)	**11-35 (TMM 1)**	**45-72 (TMM 2)**	**141-164 (TMM 3)**	**181-205 (TMM 4)**	**214-236 (TMM 5)**	**241-261 (TMM 6)**	**277-300 (TMM 7)**	**344-364 (TMM 8)**	**-**	**-**

To provide further validation, these results were compared to a hydropathy plot. The Kyte-Doolittle scale was used with a window size of 21, as this yields a plot in which transmembrane domains stand out sharply (126). The eight predicted transmembrane domains from the three predictive tools (Table 3.1: consensus sequence) correspond to hydrophobic peaks on the plot as seen in Figure 3.1 (highlighted in blue; labelled 1-8). These peaks, with the exception of 3 and 6, have a hydropathy index score ≥1.6, which indicated that there is a high probability that these are membrane-spanning regions (126). The remaining two-thirds of the plot has additional hydrophobic peaks towards the C-terminus, although at an overall lower hydrophobicity than that of the predicted transmembrane regions (Figure 3.1).

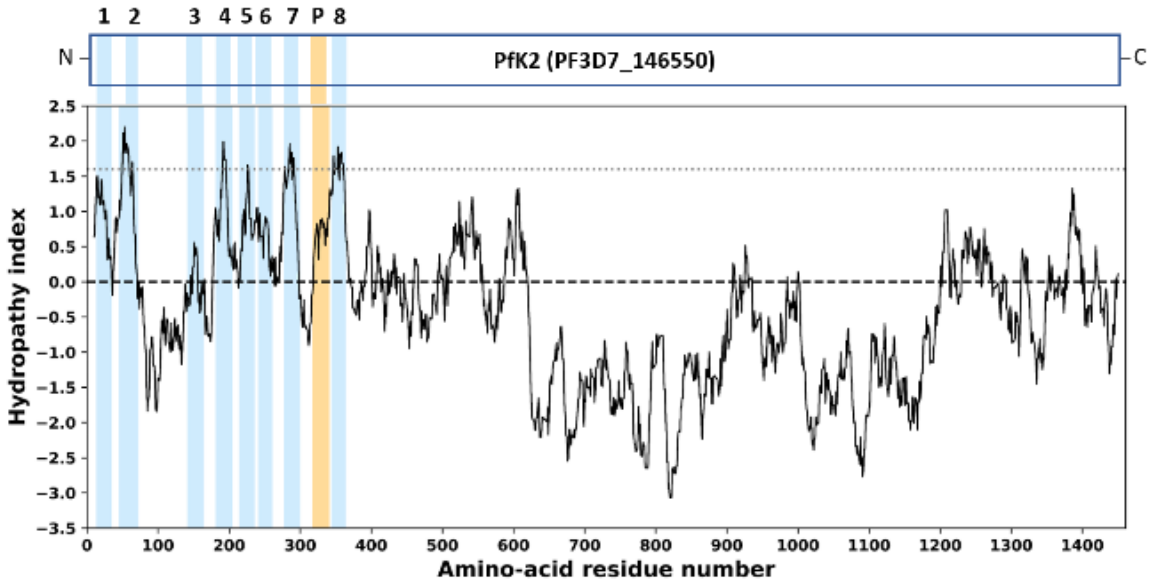

Figure 3.1: Hydropathy plot of the amino acid sequence of PfK2. The plot was made with Python (Matplotlib library) using the Kyte-Doolittle method (window size = 21). The line at 1.6 depicts the threshold value for predicting transmembrane regions. Values above and below 0.0 represent hydrophobic and hydrophilic residues, respectively. Peaks highlighted in blue represent predicted transmembrane domains by predictive tools (Table 3.1), while the peak highlighted in yellow represent the predicted pore loop (re-entrant helix) with the conserved signature sequence (TXGYG) (Figure 3.1).

Furthermore, characteristic to all K^+ channels is a highly conserved signature sequence (TXGYG) that forms the selectivity filter in a re-entrant loop between the S5 and S6 transmembrane segments, which collectively forms the pore domain (Figure 1.5) (141). To determine whether PfK2 contains the conserved signature sequence, amino acid sequence alignments to other K^+ channels was made with Clustal Omega.

The sequence alignment confirmed the presence of the conserved signature sequence for PfK2 at residues 332-336 (Figure 3.2). This signature sequence (TVGYG) occurs within a re-entrant loop (residues 307-341) that was predicted by PSIPRED. These results supported the annotation of PfK2 as a K^+ channel.

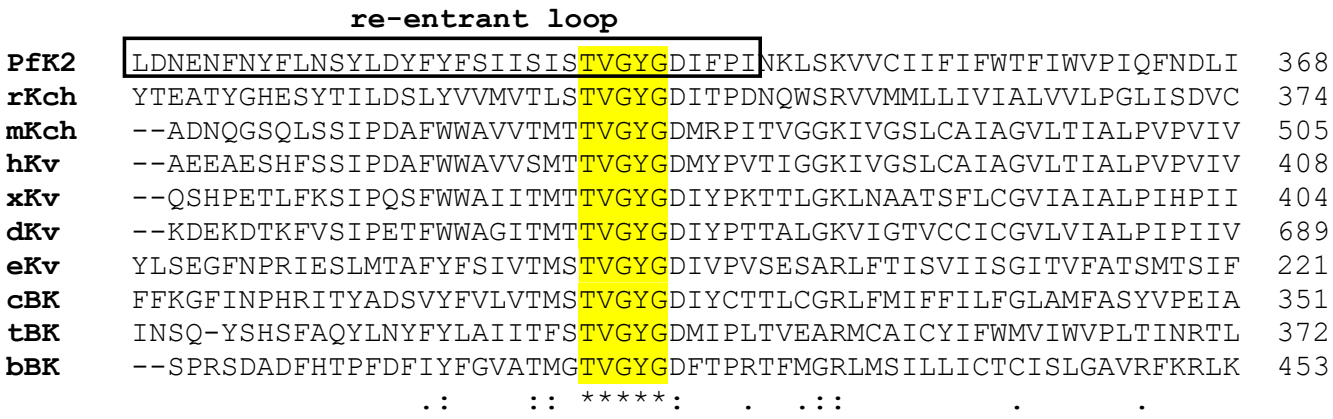

Figure 3.2: The conserved signature (TXGYG) sequence of PF3D7_1465500 aligned with various K^+ channels. GeneBank accession numbers are shown in parentheses. PfK2, *P. falciparum* K^+ channel K2 (XP_001348796.2); (rKch, *R. azygosporus* K^+ channel, sub T, member 2 (RCH94169.1); mKch, *M. musculus* K^+ channel protein (AAA39365.1); hKv, *H.* sapiens K^+ voltage-gated channel subfamily A member 1 (NP_000208.2); xKv, *X. laevis* K^+ voltage-gated channel subfamily F member 1 (XO_018120303.1); dKv, *D. melanogaster* voltage-gated shaker-related K^+ channel cognate b, isoform A (NP_728783.1); eKv, *E. coli* voltage-gated K^+ channel protein (MLC55274.1); cBK, *C. elegans* BK channel (NP_001256810.1); tBK, *T. parva* strain Muguga Ca^{2+}-activated BK K^+ channel alpha subunit family (KAF5153237.1); bBK, *B. bovis* T2Bo Ca^{2+}-activated BK K^+ channel alpha subunit family (EDO06445.2). The amino acids of the K^+ channel signature sequence (TXGYG) is highlighted in yellow. The alignment was generated with the CLUSTAL Omega (1.2.4) multiple sequence alignment program.

These results were compared to the predicted 3D protein structure of PfK2 (Figure 3.3 A). This predicted subunit structure was obtained by DeepMind's AlphaFold Protein Structure Database (https://alphafold.ebi.ac.uk/) (129,130), which uses a machine-learning approach based on both physical and biological principals to provide atomic-scale accuracy. The AlphaFold database predicted the entire protein sequence of a single subunit of PfK2 (amino acid residues 1-1461) with the majority of the structure calculated with confidence (90 > pLDDT > 70) (Figure S1; light blue regions), indicating high model accuracy. Regions of very low confidence (amino acid residues 624-896 and 945-1176) (Figure S1; red regions) was trimmed off using UCSF Chimera version 1.15 (132). UCSF Chimera was additionally used to edit the colour schemes based on the number and location of the predicted transmembrane domains in Table 3.1, which has an exact correlation to the predicted 3D structure subunit of PfK2 (Figure 3.3 B; S1-S8). The predicted re-entrant helix that contains the conserved signature sequence (TXGYG) (Figure 3.2) additionally correlates with the structure.

.

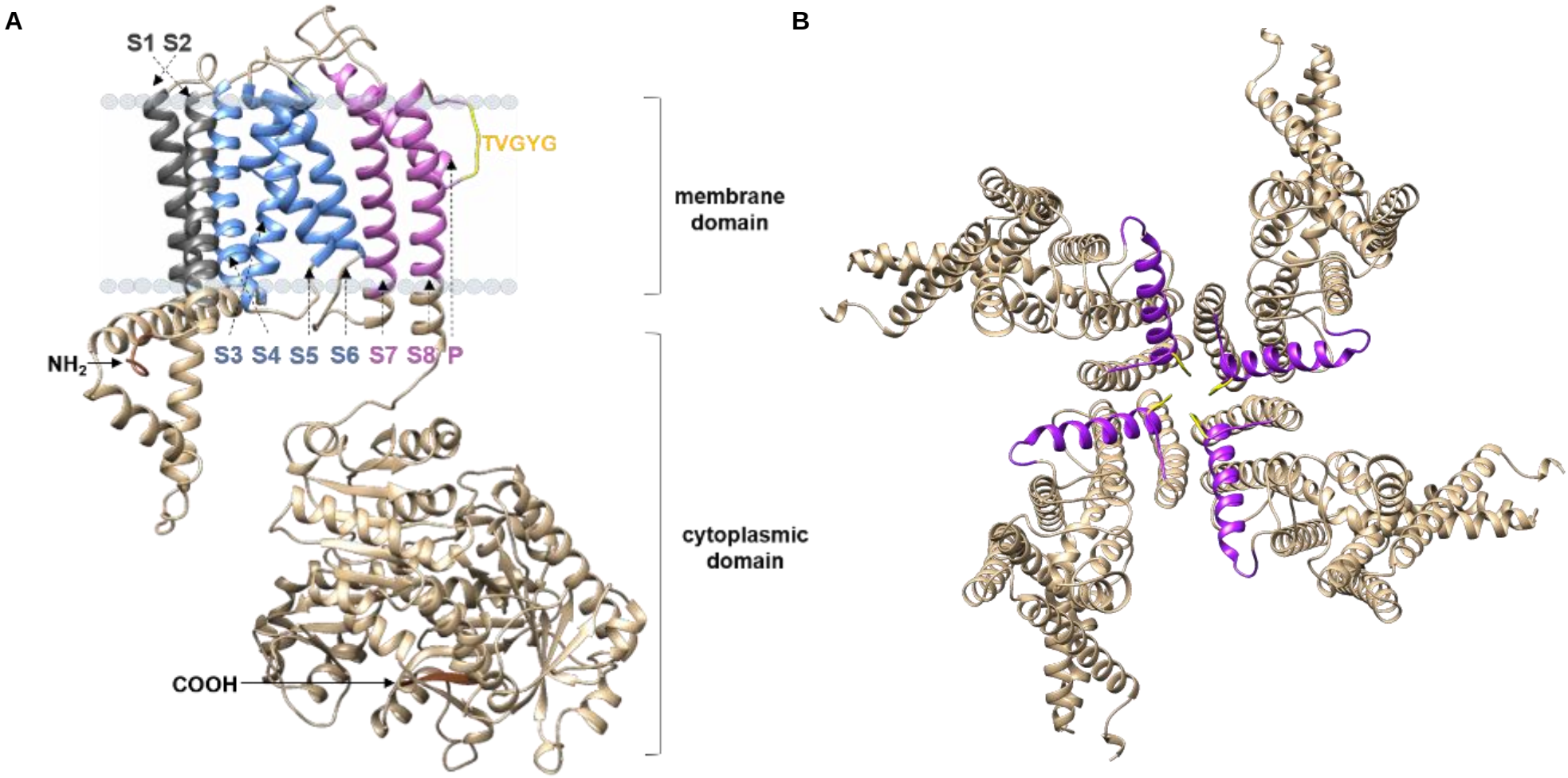

Figure 3.3: AlphaFold predicted three-dimensional structure of a single subunit of PfK2 in *P. falciparum* parasites. A: AlphaFold predicted structure of PfK2 (side view) with colour schemes corresponding to the number and location of predicted transmembrane domains in Table 3.1. Blue segments represent a possible voltage-sensor domain (S3-S6), while purple represents a possible pore domain (S7-S8) with the conserved signature sequence (TXGYG) in yellow. **B:** GalaxyWEB predicted tetrameric structure of PfK2 (residues 1-373) (top view) in *P. falciparum* parasites. Purple segments represent re-entrant loops that form a central pore, with the conserved signature sequences (yellow) pointing toward the centre of the pore to form a possible selectivity filter.

Since K^+ channels have a tetrameric structure, in which four identical subunits arrange to form a central ion conducting pore (Figure 1.5 A), the tetrameric structure of PfK2 was predicted through GalaxyWEB (https://galaxy.seoklab.org/cgi-bin/submit.cgi?type=HOMOMER). The predicted structure indicated that the re-entrant loop of each PfK2 subunit arrange symmetrically to form a central pore (Figure 3.3 B). Additionally, the predicted TXGYG signature sequence within each re-entrant loop points toward the central axis of the pore (Figure 3.3 B). This is characteristic of K^+ channels to provide K^+ selectivity from the backbone carbonyl oxygen atoms within the TXGYG sequence (section 1.6), which provided strong evidence that PfK2 is a K^+ channel.

Furthermore, it was investigated whether PfK2 has voltage-gated or Ca^{2+}-gated features. Conserved protein domain and family predictions were identified by InterPro, which provides model predictions from different databases. PfK2 contained a transmembrane cation channel superfamily (InterPro: IPR013099; Pfam: PF07885) at residues 285-371, a voltage-gated K^+ channel family signature (InterPro: IPR028325; Panther: PTHR11537) at residues 49-1004, as well as a BK channel alpha subunit domain at residues 524-618 (InterPro: IPR003929; Pfam: PF03493) (Figure 3.4). PfK2 is thus likely a BK channel, which has structural homology to the family of voltage-gated K^+ channels.

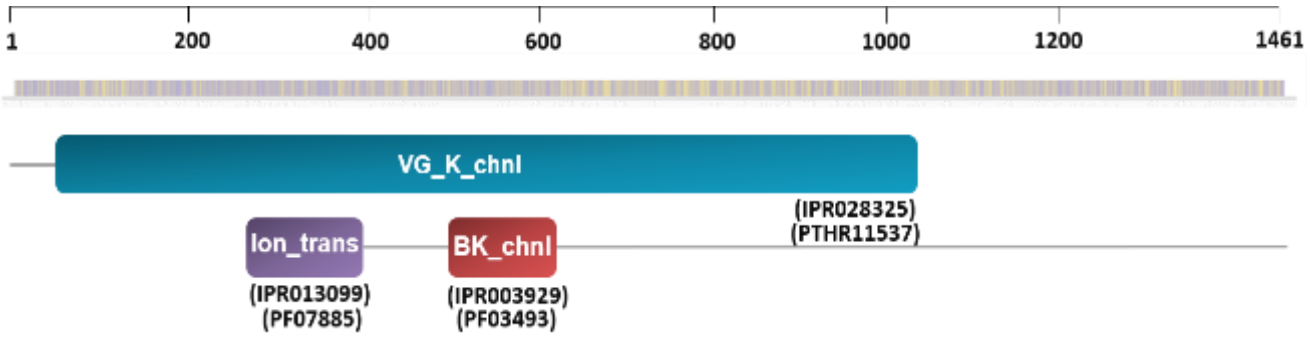

Figure 3.4: Schematic representation of predicted protein domains and families for PF3D7_1465500. VG_K_chnl: voltage-gated potassium channel family (residues 49-1048, IPR028325 and PTHR11537, blue). Ion_trans: transmembrane cation channel superfamily domain (residues 285-371, IPR013099 and PF07885, purple). BK_chnl: BK channel alpha subunit (residues 524-618, IPR003929 and PF03492, red). Predicted protein domains and families were obtained from InterPro. Figure created with PowerPoint 2019.

Previously (142), RCK1 and RCK2 domains, which act as a Ca^{2+} sensor in BK channels, were predicted through Phyre2 software (http://www.sbg.bio.ic.ac.uk/phyre2) (143). The Phyre2 analysis produced 3D structures of PfK2, in which the C-terminus was modelled based on homology alignments to RCK gating structures of K^+ channels from eukaryotic, prokaryotic, and archaeon origin (142). The highest scoring template was the human BK channel gating

ring (144,145), in which 579 residues that compromise the RCK1 and RCK2 domains aligned to a stretch of PfK2 that spans residues 421 to 1461 in the C-terminus (142). These results suggested that PfK2 has a possible RCK1 and RCK2 domain that spans residues 421 to 715 and 1166 to 1461 (142), respectively. Located within the predicted regions of the RCK domains are four hydrophobic peaks (two per domain) from the hydropathy plot in Figure 3.2. This supports the possibility that PfK2 has hydrophobic S9-S10 and S11-S12 cytosolic segments that are present within the RCK1 and RCK2 domains, respectively, as is characteristic of BK channels. Furthermore, PfK2 has positively charged amino acids present for the S5 (two lysine) and S6 (arginine and lysine) transmembrane segments, which could possibly be involved with voltage sensing.

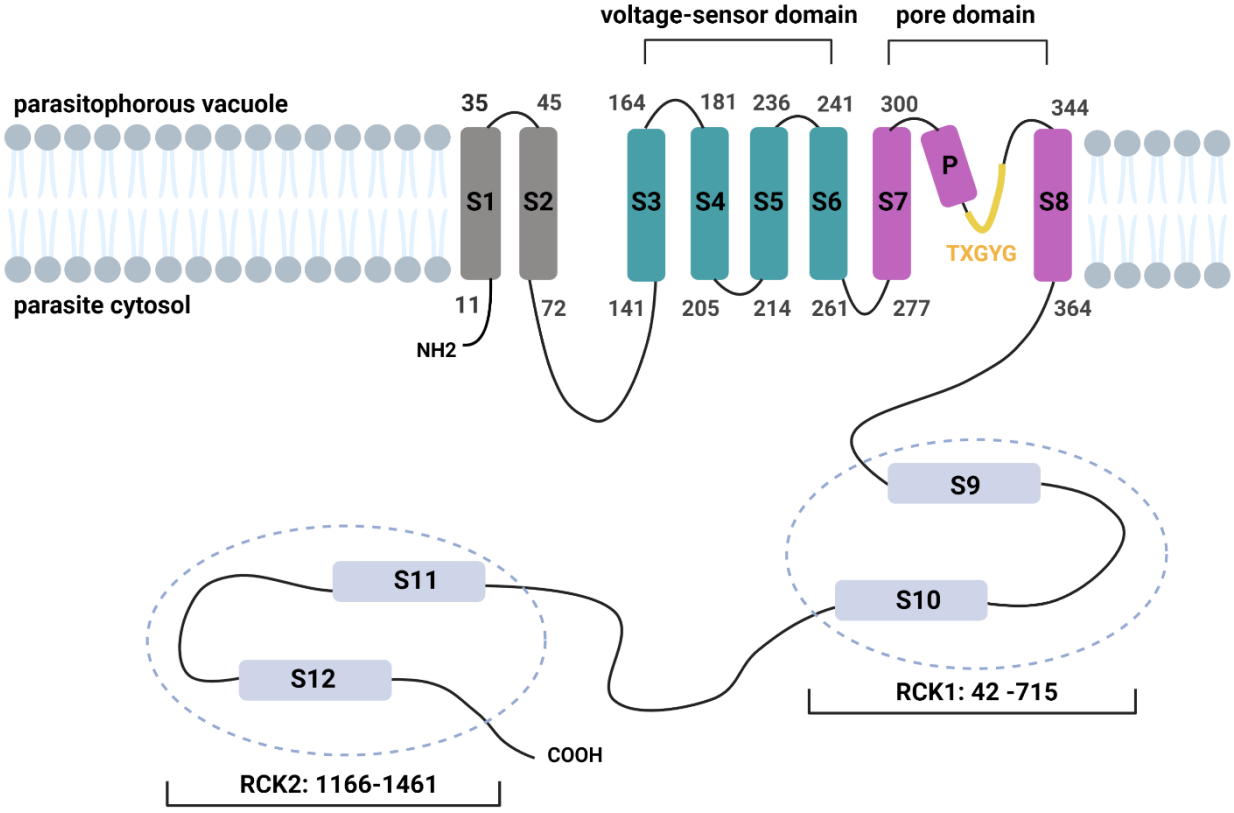

Figure 3.5: Membrane topology schematic of a single subunit of PfK2 in *P. falciparum* parasites. PfK2 is predicted to have eight transmembrane segments (S1-S8), with a possible voltage-sensor domain (S3-S6; blue) and pore domain (S7-S8; purple) that contains the conserver K^+ channel signature sequence (TXGYG; yellow). The cytosol is predicted to have four additional hydrophobic segments, S9-S10 and S11-S12, which occur within predicted RCK1 (residues 421-715) and RCK2 (residues 1166-1461) domains, respectively. Figure created with Biorender.com under a standard academic licence.

In conclusion, PfK2 is thought to have a membrane topology similar to BK channels. PfK2 has a possible pore forming unit comprising segments S7-S8 (Figure 3.5) that contain the conserved signature sequence (TXGYG) that is characteristic of K^+ channels. Furthermore, PfK2 has a possible voltage-sensor domain comprising segments S3-S6, with possible voltage

sensing charges in the S5 and S6 transmembrane segments, while the C-terminus of PfK2 is predicted to act as a Ca^{2+} sensor domain with possible RCK1 and RCK2 domains that is characteristic of BK channels. Although PfK2 has a similar structure to BK channels, its functional relevance remains unknown in *P. falciparum* parasites.

3.2. *In vitro* cultivation of asexual *P. falciparum* parasites

Asexual *P. falciparum* NF54 parasites were cultured *in vitro* to isolate DNA and to generate transgenic lines**.** The developmental stages of asexual *P. falciparum* parasites were observed *in vitro* over a 48 h time period (Figure 3.6). After invasion of the erythrocyte by the merozoite at 0 hpi, the development of the ring stage began with the parasite appearing as a thin discoidal shape at ~10-17 hpi. The early trophozoites, visible from ~18 hpi, were characterized by the formation of the hemozoin crystal, which increased in size along with the cytoplasm density as the late-stage trophozoites developed at ~30-37 hpi. The schizont stage parasites, consisting of multiple nuclei, burst at ~48 hpi to release merozoites that invade new erythrocytes for continuation of the IDC (146).

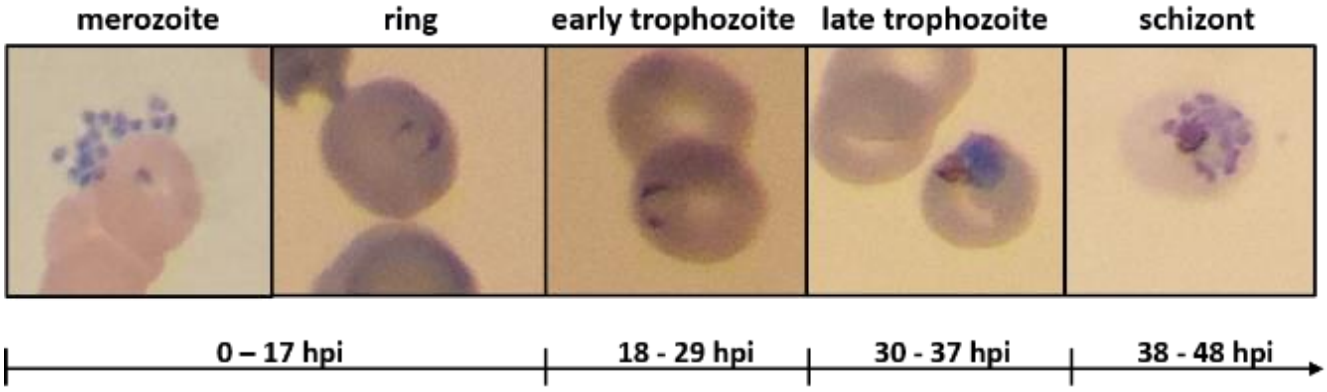

Figure 3.6: Developmental stages of asexual *P. falciparum* parasites *in vitro*. Morphological representation of the asexual stages of *P. falciparum* parasites with the respective hours post invasion (hpi) of the merozoite, ring, early trophozoite, late trophozoite, and schizont. Parasites were visualized from Rapi-Diff-stained thin blood smears with optical microscopy at 1000x magnification.

3.3. DNA isolation from asexual *P. falciparum* parasites

Total DNA was isolated from *in vitro* cultures of asexual *P. falciparum* NF54 parasites (>3 % parasitaemia, > 50 % trophozoite population) to use as a template in downstream PCR amplification experiments. Spectrophotometric analysis was used to quantify the yield and purity of the isolated DNA, with concentrations ranging from 11.8 ng/µL to 24.4 ng/µL and purity ratios of A260 / A280 and A260 / A230 ranging from 0.73 to 1.91.

3.4. Generate a transgenic *P. falciparum* parasite line with non-functional PfK2

3.4.1. Cloning of a 5' gene fragment of pfk2 into the pSLI-TGD plasmid

With the SLI-TGD system, *pfk2* would be altered at the genomic level to render a non-functional protein by replacing the gene with a truncated version (~332 bp) (Figure 3.7). This truncated version would have a loss of the predicted voltage-sensor domain (S3-S6), the pore domain (S7-S8), as well as the Ca^{2+} sensor domain (S9-S12) in the C-terminus (Figure 3.5).

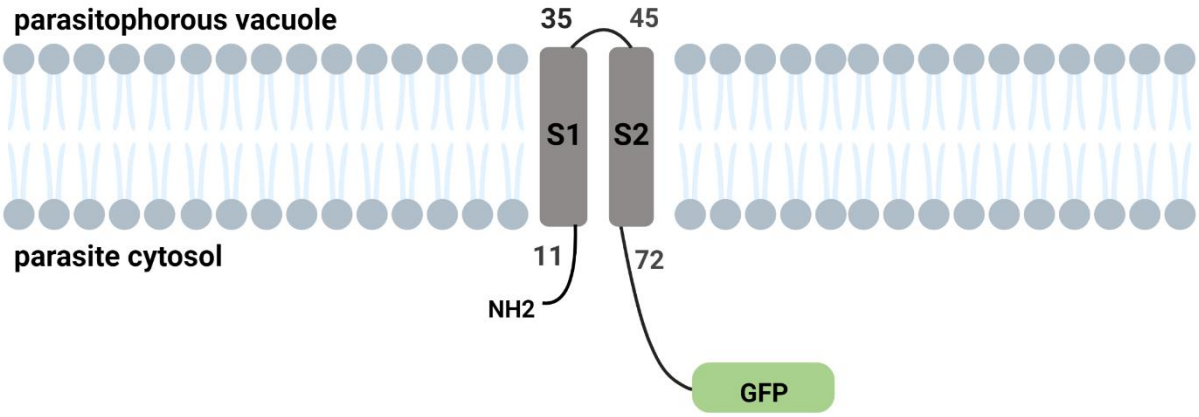

Figure 3.7: Membrane topology schematic of PfK2 truncated with the SLI-TGD system. Genetic modification with the SLI-TGD system results in a truncated version of PfK2 (110 amino acids), with loss of the predicted voltage-sensor domain, pore domain, and Ca^{2+} sensor domain of the native protein (1461 amino acids) (Figure 3.6). Figure created with Biorender.com under a standard academic licence.

A 5'-gene fragment of *pfk2* with flanking *Not*I and *Mlu*I restriction cleavage sites was amplified from isolated gDNA for directional cloning into the pSLI-TGD plasmid. The PCR conditions for amplification with the gene specific primers (Table 2.1) were investigated to determine the annealing temperature that resulted in the greatest amplification of the product, and this was estimated using the visual intensity after EtBr staining. PCR amplicons corresponding to the expected fragment size (~332 bp) were obtained at all three annealing temperatures tested (50 °C, 55 °C and 60 °C, Figure 3.8), with an annealing temperature of 60 °C resulting in the most intense band. Faint nonspecific bands were additionally observed at ~300 bp and ~200 bp at all three annealing temperatures tested. These bands remained present even when using an annealing temperature of 60 °C, which are closest to the predicted melting temperatures of the designed primers (forward primer: 64 °C; reverse primer: 62 °C). The PCR amplicon corresponding to the gene fragment of interest (~332 bp) was excised and purified from the gel for further downstream experiments. The purified product was analysed spectrophotometrically to have a DNA concentration of 69.3 ng/µL, with A260/A280 and A260/A230 purity ratios of 1.80 and 1.21, respectively.

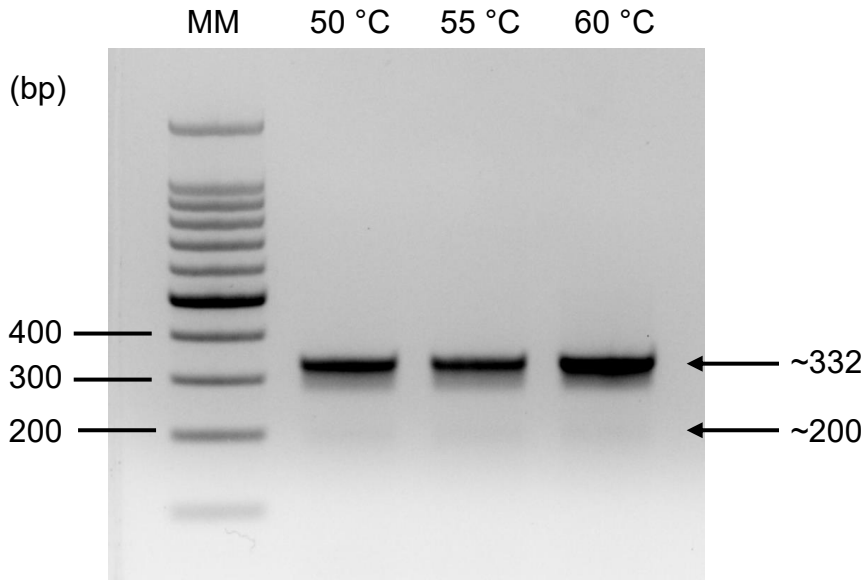

Figure 3.8: Amplification of 5'-gene fragment of *pfk2* from gDNA.PCR optimization to amplify a 5'-gene fragment of *pfk2* with designed primers (Table 2.1) included annealing temperatures of 50 °C, 55 °C and 60 °C. The most intense expected band (~332 bp) was obtained at an annealing temperature of 60 °C. The amplified DNA and 100 bp DNA ladder (Lane MM; Promega, USA) were separated with a 1 % w/v agarose/TAE gel that contained EtBr (1 µg/mL) for visualization under UV light.

The pSLI-TGD plasmid with a control gene fragment was isolated from *E. coli* DH5*α* cells and purified to produce a concentration of 596.8 ng/µL with purity ratios of A260/A280 and A260/A230 of 1.83 and 2.07, respectively. The isolated pSLI-TGD plasmid, as well as the amplified 5'-gene fragment, was digested with *Not*I-HF and *Mlu*I-HF restriction enzymes to generate compatible sticky ends. Digestion of the plasmid yielded a larger band (~6760 bp) corresponding to the plasmid backbone and a smaller band (~1700 bp) corresponding to the control gene fragment (PF3D7_1463000) (Figure 3.9). This not only confirmed the identity of the pSLI-TGD plasmid, but also allowed for subsequent gel extraction and purification of the plasmid backbone for downstream experiments. A concentration of 35 ng/µL was obtained for the isolated, cut plasmid backbone with A_{260}/A_{230} and A_{260}/A_{280} ratios of 1.78 and 1.57, respectively. Purification of the digested 5'-gene fragment yielded a concentration of 38 ng/µL with A260/A280 and A260/A230 ratios of 1.82 and 1.37, respectively.

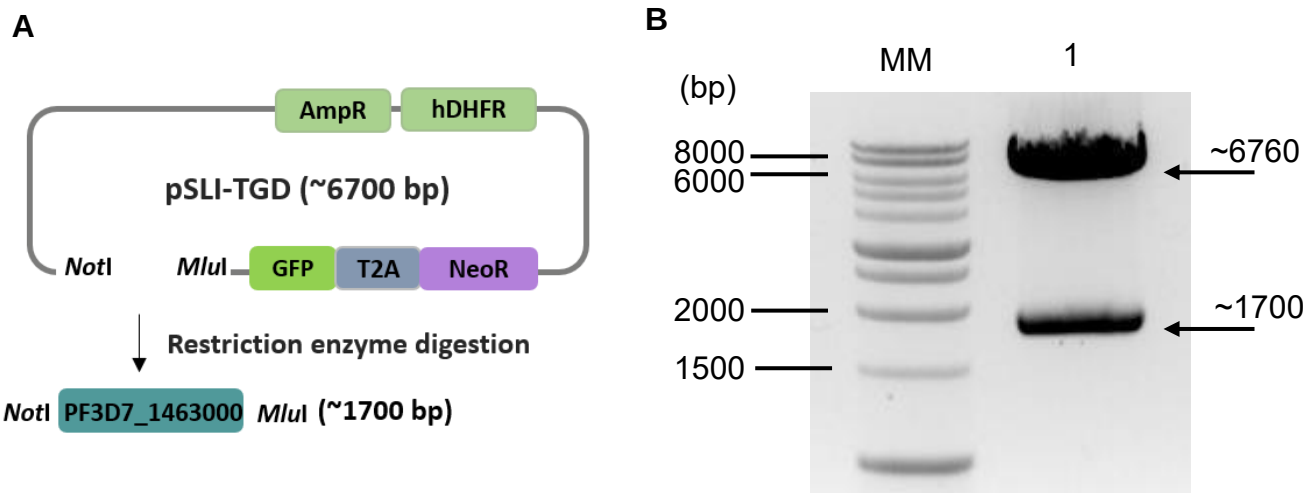

Figure 3.9: Restriction enzyme digestion of the pSLI-TGD plasmid to generate sticky ends for ligation. (A) Schematic representation of restriction enzyme digestion of the pSLI-TGD plasmid, with the expected size of the plasmid backbone and the control insert indicated. (B) Digestion of the pSLI-TGD plasmid with *Not*I-HF and *Mlu*I-HF produced the expected band sizes corresponding to the plasmid backbone (6760 bp) and the control insert (1700 bp). Digested product was separated with a 1 % (w/v) agarose/TAE gel that contained EtBr (1 µg/mL) for visualization under UV light. MM: 1 kb DNA ladder (Promega, USA) as a molecular marker.

The digested 5' gene fragment of *pfk2* was ligated to the digested pSLI-TGD plasmid. Following transformation into *E. coli* DH5*α* cells, colony screening PCR was performed to identify positive bacterial clones. All the clones screened had a recombinant pSLI-TGD plasmid with the correct sized 5' gene fragment inserted (~400 bp, Figure 3.10 B), based on amplification with a gene-specific forward primer (P1) and plasmid backbone reverse primer (P4) (Table 2.2).

A positive bacterial clone was grown overnight in LB broth and the plasmid DNA was isolated at a concentration of 287 ng/µL with purity ratios of A260/A280 and A260/A230 of 1.92 and 1.93, respectively. Restriction enzyme digestion mapping with *NotI*-HF and *MluI*-HF resulted in a larger band corresponding to the pSLI-TGD backbone (~6700 bp) and a smaller band corresponding to the expected size of the 5' gene fragment (~332 bp) (Figure 3.10 C). This provided further confirmation that the 5' gene fragment was successfully cloned into the respective pSLI-TGD plasmid.

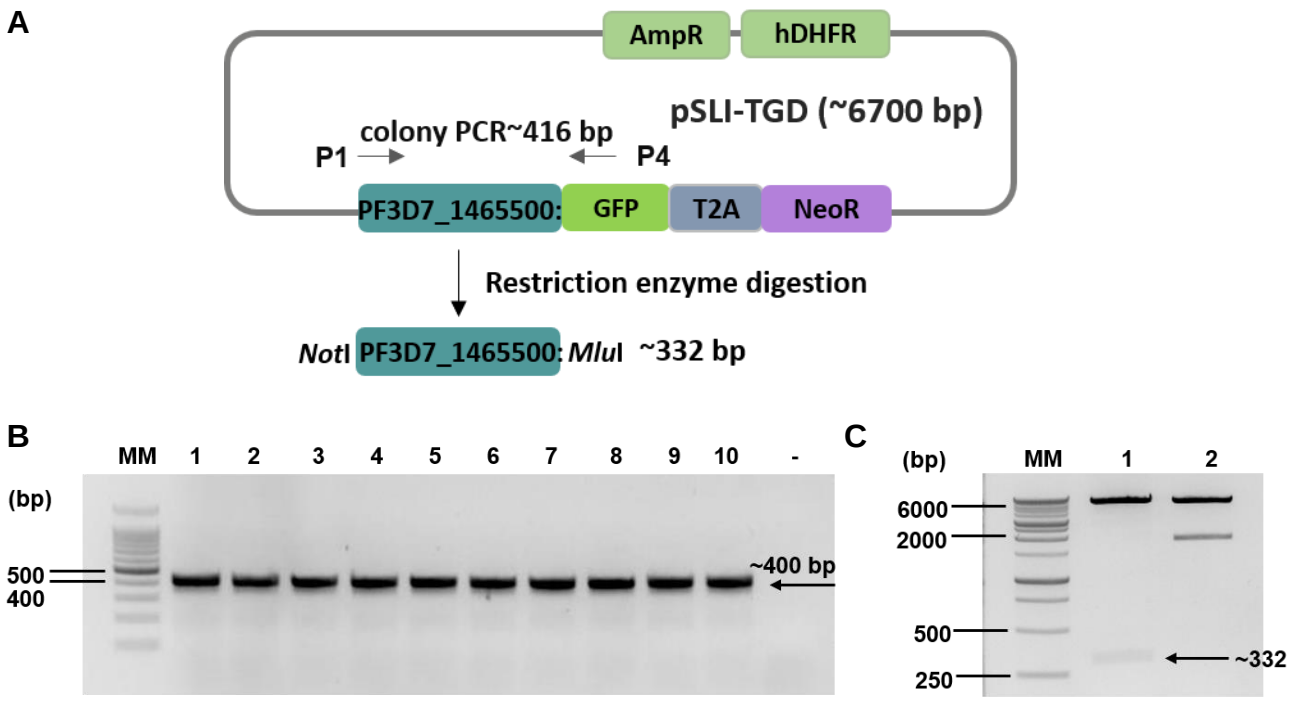

Figure 3.10: Validation of recombinant pSLI-TGD-*pfk2* plasmids. (A) Schematic representation showing the primer pair (P1 and P4; Table 2.2) used for colony screening PCR, as well as the expected size for restriction enzyme digestion with *Not*I-HF and *Mlu*I-HF. (B) Colony screening PCR of the 5' gene fragment of *pfk2* cloned into the pSLI-TGD plasmid. The expected band size (~400 bp) was obtained for all clones screened (lane 1-10) based on amplification with a forward gene-specific primer (P1) and a reverse plasmid backbone primer (P4). (C) Restriction enzyme digestion, for which the expected insert size (~332 bp) was excised from the pSLI-TGD-*pfk2* plasmid using the *Not*I-HF and *Mlu*I-HF restriction enzymes. Amplified and digested products were separated with a 1.5 % (w/v) agarose/TAE gel that contained EtBr (1 µg/mL) for visualization under UV light. MM: 1 kb DNA ladder (Promega, USA) as a molecular marker.

As a final verification step, Sanger dideoxy sequencing was performed to confirm the identity of the cloned insert and the absence of any insertions, deletions, or frameshift mutations. The sequencing alignment results (Figure 3.11) confirmed that the 5' gene fragment of *pfk2* was successfully cloned into the pSLI-TGD plasmid to generate a pSLI-TGD-*pfk2* construct for downstream transfection experiments.

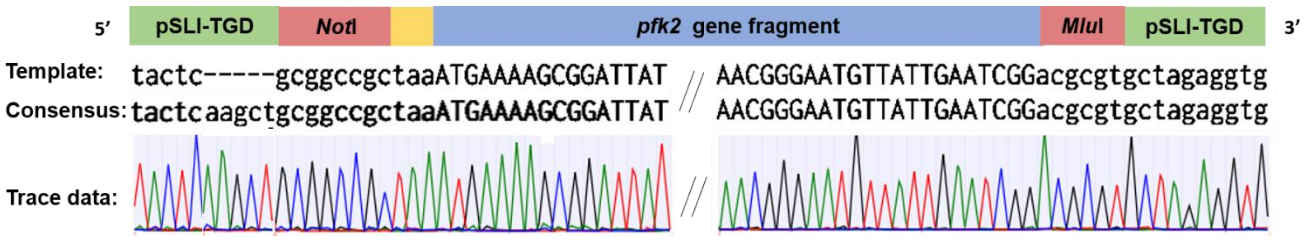

Figure 3.11: Sanger sequencing of 5' gene fragment of pSLI-TGD-*pfk2* construct. Alignment of consensus sequence of pSLI-TGD-pfk2 to the expected reference sequence. Consensus sequence of each construct was formed from analysis of two sequences obtained from plasmid backbone primers (Table 2.2). A forward or reverse chromatogram (trace data) is represented below the alignments. Schematic of DNA fragments not drawn to scale.

3.4.2. Generate transgenic *P. falciparum* parasites lines with the SLI-TGD system

Transfection of asexual *P. falciparum* NF54 parasites with the pSLI-TGD-*pfk2* construct was repeated twice, with ~200 µg of plasmid DNA used in each instance. Electroporation resulted in an expected rapid drop in parasitaemia (from ~7 % to ~1 %) for each transfection, possibly due to erythrocyte lysis caused by the transfection itself (Figure 3.12).

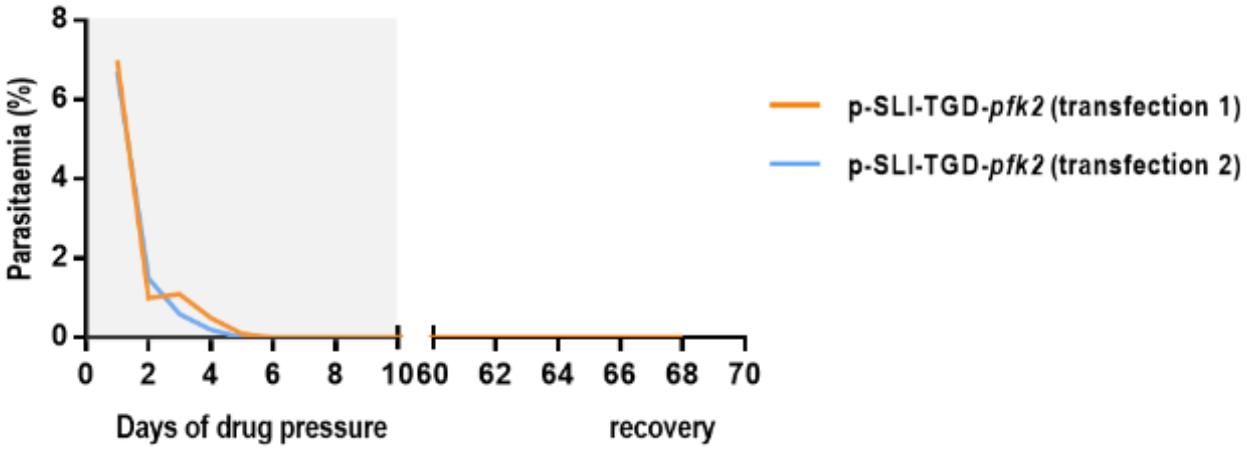

Figure 3.12: Intraerythrocytic *P. falciparum* parasitaemia during selection for episomal uptake of pSLI-TGD-*pfk2* following transfection. Asexual *P. falciparum* NF54 parasites was transfected with pSLI-TGD-*pfk2* and selected for episomal uptake through drug pressure with WR99210 (4 nM) for 10 days. Transfection was repeated twice, in which parasites did not recover in either instance. The parasitaemia was determined from Rapi-Diff-stained thin blood smears with optical microscopy at 1000x magnification. Figure was created with GraphPad Prism version 7.

Following transfection with the pSLI-TGD-*pfk2* construct, the asexual *P. falciparum* parasites were placed under drug pressure with WR99210 (4 nM) for 10 days to select for parasites that contains the plasmid episomally. During this 10-day period, the parasitaemia decreased further to undetectable levels (Figure 3.12). Subsequently, the WR99210 drug pressure was removed and the parasites were in recovery for 58 and 48 days in drug-free medium for the respective transfections. In both instances, the parasites never recovered, thus no parasites with episomal uptake of the pSLI-TGD-*pfk2* construct were obtained. Due to the low transfection efficiency of plasmids into *P. falciparum* parasites (147), an increased number of independent transfections might increase the chances for successful transfection (138).

3.5. Development of transgenic NF54-*pfk2*-GFP-*glmS* and NF54-*pfk2*-GFP-*glmS*-mut lines for inducible knockdown of PfK2

To obtain NF54-*pfk2*-GFP-*glmS* and NF54-*pfk2*-GFP-*glmS*-mut transgenic lines, the *pfk2* locus was modified at the 3' terminal with the attachment of a GFP sequence for localization studies, a *glmS* ribozyme sequence for conditional knockdown, as well as a T2A ribosomal

skip peptide by which genomic integration is selected for through the separate translation of an attached NeoR gene (Figure 3.13).

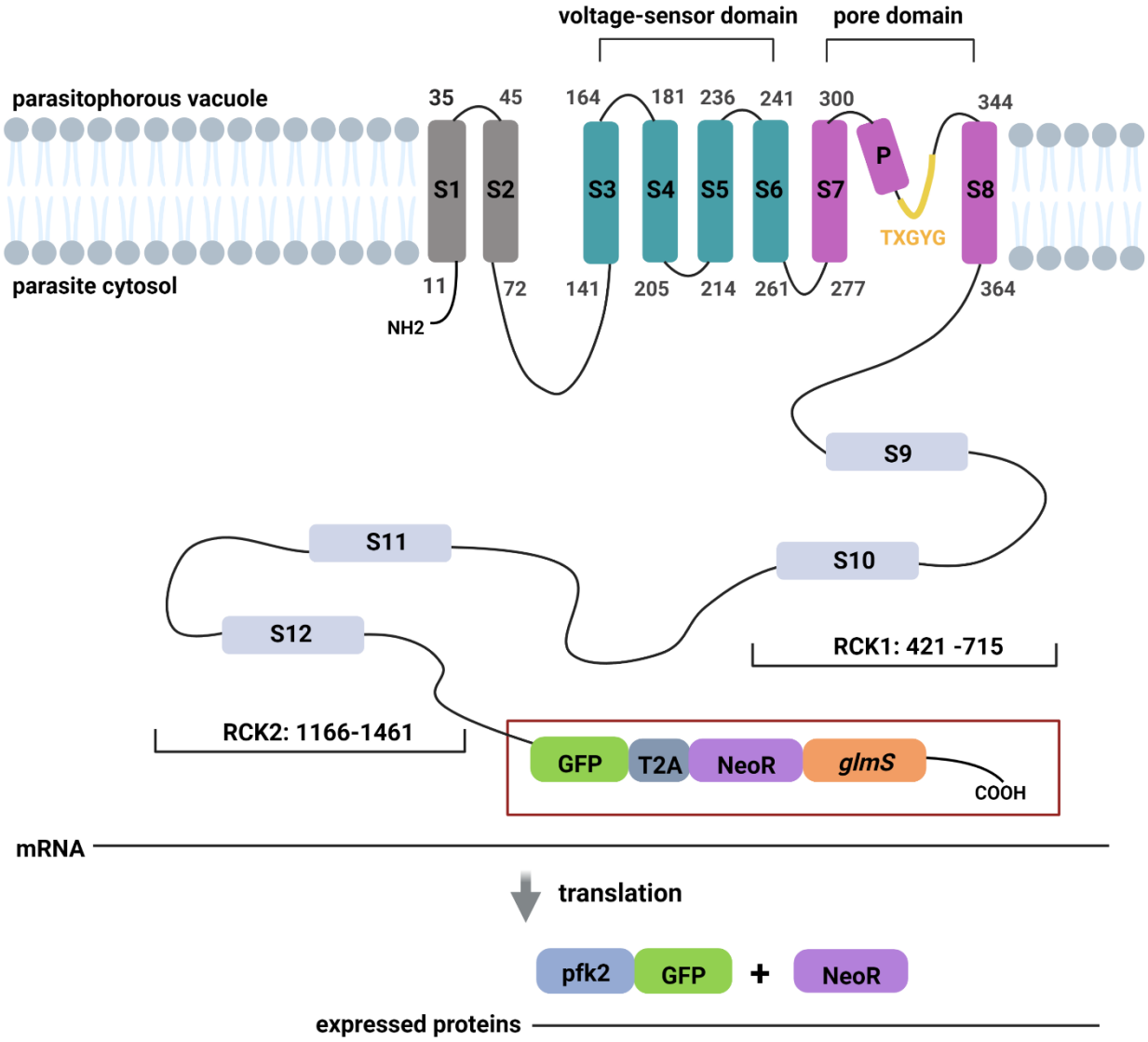

Figure 3.13: Schematic representation of PfK2 modified with the SLI-*glmS* system. *pfk2* was genetically modified with the SLI-*glmS* system through homologous recombination and was modified with the 3' terminal attachment of a GFP fluorescent reporter gene, a *glmS* ribozyme sequence, a T2A ribosomal skip peptide, and a neomycin resistance gene. Following transcription, a single mRNA is produced, from which a GFP-tagged PfK2 protein and the NeoR protein is translated. Figure created with Biorender.com under a standard academic licence.

Recombinant pSLI-*glmS* plasmids (p-GFP-*glmS*-*pfk2* and p-GFP-*glmS*-mut-*pfk2*) were previously generated by an MSc student and successfully transfected into asexual intraerythrocytic *P. falciparum* parasites to generate NF54-epi(SLI-*glmS*-*pfk2*) and NF54-epi(SLI-*glmS*-*mut*-*pfk2*) episomal lines (115).

3.5.1. Validate recombinant p-GFP-glmS-pfk2 and p-GFP-glmS-mut-pfk2 plasmids

The recombinant plasmids were validated in this study by assessing the *pfk2* 3'-gene fragment (1075 bp) of the constructs through Sanger sequencing (Figure 3.16).

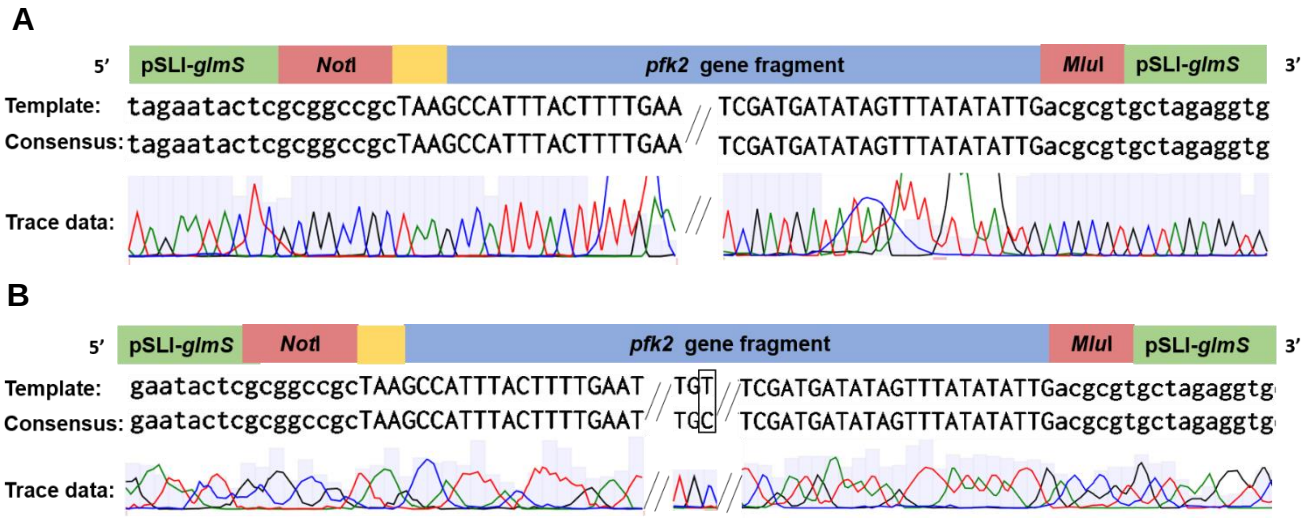

Figure 3.14: Sanger sequencing of p-GFP-*glmS*-*pfk2* and p-GFP-*glmS*-mut-*pfk2* plasmids. Alignment of the consensus sequence of (A) p-GFP-*glmS*-*pfk2* and (B) p-GFP-*glmS*-mut-*pfk2* to the expected reference sequence. Consensus sequence of each construct was formed from analysis of six sequences obtained from either gene-specific or plasmid backbone primers as seen in Table 2.3. A forward or reverse chromatogram (trace data) is represented below the alignments. Schematic of DNA fragments not drawn to scale.

A consensus sequence for either p-GFP-*glmS*-*pfk2* or p-GFP-*glmS*-mut-*pfk2* confirmed that the *pfk2* 3'-gene fragment was successfully cloned into the respective p-GFP-*glmS* and p-GFP-*glmS*-*mut* plasmids (Figure 3.14). A mutation from a thymine (T) to a cytosine (C) was present at nucleotide position 5258 of the 3' gene fragment for p-GFP-*glmS*-mut-*pfk2* (Figure 3.14 B). This was a synonymous mutation that did not change the encoded amino acid (cysteine) of the associated codon, and consequently did not affect structural changes to the translated protein. The sequencing analysis thus confirmed that neither the p-GFP-*glmS*-*pfk2* or p-GFP-*glmS*-mut-*pfk2* construct had any insertions, deletions, or frameshift mutations that could interfere with the downstream conditional knockdown of *pfk2* with the *glmS* ribozyme system.

3.5.2. Validate NF54-epi(SLI-*glmS-pfk2*) and NF54-epi(SLI-*glmS*-mut-*pfk2*) lines for the episomal presence of p-GFP-*glmS-pfk2* and p-GFP-*glmS*-mut-*pfk2*

The episomal presence of p-GFP-*glmS-pfk2* and p-GFP-*glmS*-mut-*pfk2* was subsequently validated for the NF54-epi(SLI-*glmS-pfk2*) and NF54-epi(SLI-*glmS-mut-pfk2*) transfected parasite populations. DNA from the respective parasite populations was isolated from the asexual parasite cultures. PCR amplification included a pair of primers that span the 3'terminal of the *pfk2* gene (P7; Table 2.4) and the pSLI-*glmS* backbone (P4; Table 2.4) (Figure 3.15 A). A single band of the expected size (1150 bp) indicated the presence of the correct sized recombinant plasmids within the parasite populations (Figure 3.15 B and C).

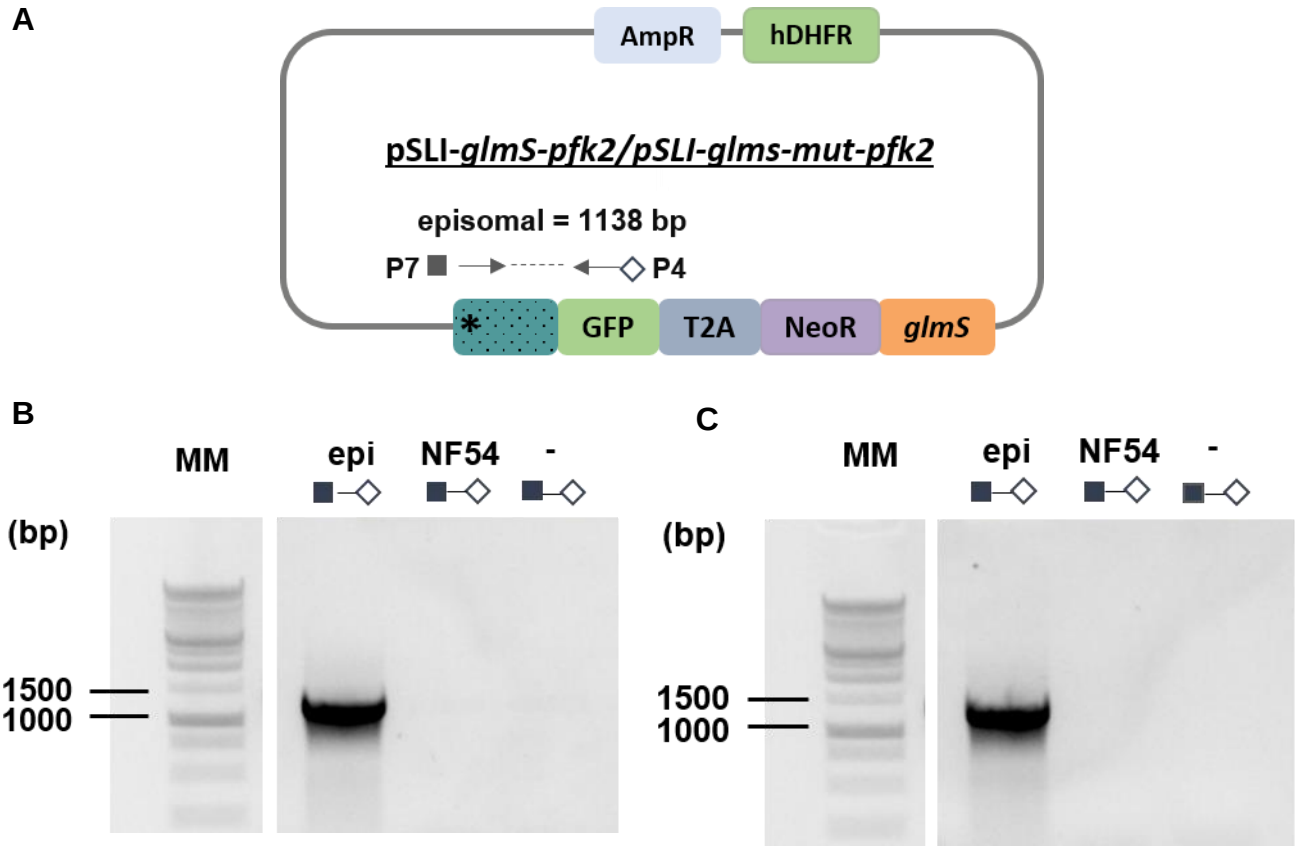

Figure 3.15: PCR analysis of episomal presence of the recombinant p-GFP-*glmS-pfk2* and p-GFP-*glmS-mut-pfk2* plasmids.(A) Schematic representation of the primer pairs used for screening with the expected amplification size for episomal presence of the recombinant plasmids. PCR screening for (B) NF54-epi(SLI-*glmS-pfk2*) parasites and (C) NF54-epi(SLI-*glmS-mut-pfk2*) parasites. Amplification for episomal confirmation produced the expected band size (1150 bp) for both parasite lines. The amplified DNA was separated with a 1 % w/v agarose/TAE gel that contained EtBr (1 µg/mL) for visualization under UV light. MM: 1 kb DNA ladder as molecular marker, epi: episomal parasite line, NF54: WT parasite control. Negative control (-) with no template DNA was included.

3.5.3. Selection and validation of genomic integration for the p-GFP-*glmS-pfk2* and p-GFP-*glmS*-mut-*pfk2* plasmids

The NF54-epi(SLI-*glmS-mut-pfk2*) parasite population was previously placed under a 14 day drug pressure period with G418 (400 µg/mL), after which partial integration was obtained (115). In this study, the NF54-epi(SLI-*glmS-pfk2*) parasite population was exposed to the same concentration of G418 over a 16 day drug pressure period to select for integration. The parasitaemia decreased from day 3 of drug pressure for NF54-epi(SLI-*glmS-pfk2*) parasites, and were completely undetectable after 7 days (Figure 3.16). Parasites that underwent integration were able to survive the drug pressure due to the NeoR marker, and increased in parasitaemia after 22 days in drug-free medium (Figure 3.16).

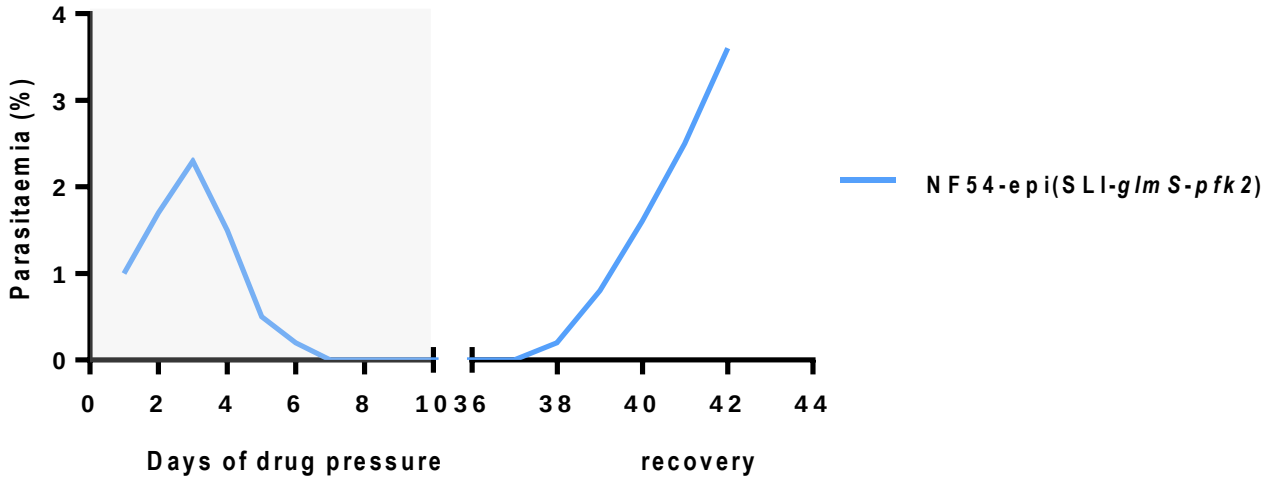

Figure 3.16: Intraerythrocytic *P. falciparum* parasitaemia during selection for genomic integration of NF54-epi(SLI-*glmS-pfk2*). NF54-epi(SLI-*glmS-pfk2*) was subjected to drug pressure for 16 days with G418 (400 µg/mL) to select for parasites that integrated the p-GFP-*glmS-pfk2* construct into the genome through homologous recombination. The parasitaemia was determined from Rapi-Diff-stained thin blood smears with optical microscopy at 1000x magnification. Figure was created with GraphPad Prism version 7.

To confirm successful integration of the p-GFP-*glmS-pfk2* and p-GFP-*glmS-mut-pfk2* plasmids, DNA was isolated from the respective parasite populations. To confirm integration at the 5' loci region, PCR amplification was performed with a primer binding to the *pfk2* gene (P8, upstream of the homology region; Table 2.5) and a reverse primer specific for the GFP tag (P4; Table 2.5) (Figure 3.17 A). To confirm integration at the 3' loci region, PCR amplification was performed with a primer binding to the plasmid backbone (P3; Table 2.5) and a reverse primer that binds downstream to the *pfk2* gene (P9; Table 2.5) (Figure 3.17 A).

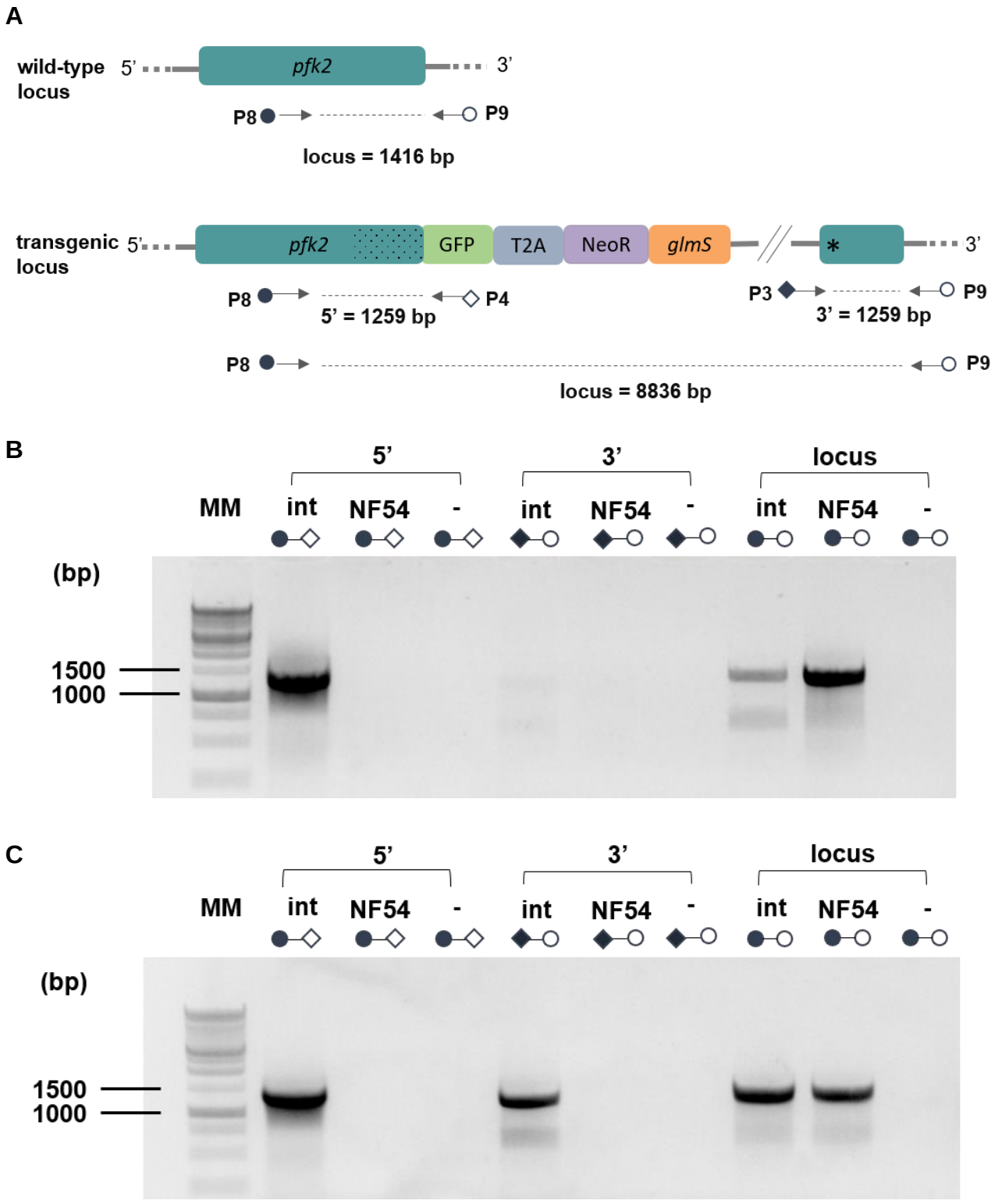

Figure 3.17: PCR analysis of p-GFP-*glmS*-*pfk2* and p-GFP-*glmS*-*mut*-*pfk2* integration into the *pfk2* locus of *P. falciparum* parasites. (A) Schematic representation of the primer pairs used for screening with the expected amplification sizes for integration (5', 3' and loci) checks. PCR screening for (B) NF54-*pfk2*-GFP-*glmS* parasites and (C) NF54-*pfk2*-GFP-*glmS*-mut parasites. The presence of 5' (1368 bp) and 3' (1259 bp) bands confirmed successful integration, but the presence of the original WT locus (1416 bp) indicates that WT parasites were still present for both parasite populations. The amplified DNA was separated with a 1 % w/v agarose/TAE gel that contained EtBr (1 µg/mL) for visualization under UV light. MM: 1 kb DNA ladder as molecular marker, int: integrated parasite line, NF54: WT parasite control. Negative control (-) with no template DNA was included.

As expected, no amplification was obtained for the WT *P. falciparum* NF54 control parasites, while 5' (~1368 bp) and 3' loci (~1259 bp) bands confirmed integration for both the p-GFP-glmS-pfk2 and p-GFP-*glmS*-mut-*pfk2* plasmids (Figure 3.17 B and C). However, both parasite populations were heterogeneous, with WT parasites still present, as seen by an amplicon of ~1416 bp at the locus (P8 and P9; Table 2.5). This band should be absent from fully integrated parasite lines due to the extensive size (>8000) of the incorporated plasmid cassette. Additionally, a constant amplicon of less than 1000 bp was present in the locus PCR. The PCR conditions were not optimized to obtain a single amplicon, given that the reaction is used for screening and not for downstream experiments. The identify of this amplicon is unknown, and it was not considered when evaluating integration. From these results, it was determined that only partially integrated NF54-*pfk2*-GFP-*glmS* and NF54-*pfk2*-GFP-*glmS*-mut parasite populations were obtained.

3.5.4. Drug pressure with G418 to generate fully transgenic NF54-*pfk2*-GFP-*glmS* and NF54-*pfk2*-GFP-*glmS*-mut lines

One approach to eliminate the WT locus was to subject the partially integrated NF54-*pfk2*-GFP-*glmS* and NF54-*pfk2*-GFP-*glmS-mut* parasite populations to another round of drug pressure with G418 to select for parasites that express NeoR under the control of the *pfk2* promoter. The drug pressure was applied for 16 days and the concentration of G418 was increased to 800 µg/mL to ensure that all parasites without the NeoR marker would be eliminated. WR99210 (4 nM) drug pressure was additionally applied in combination with G418 for the first 4 days. The parasitaemia of the parasites started to decline early into drug pressure (day 4), and was completely undetectable from day 7 (Figure 3.18)

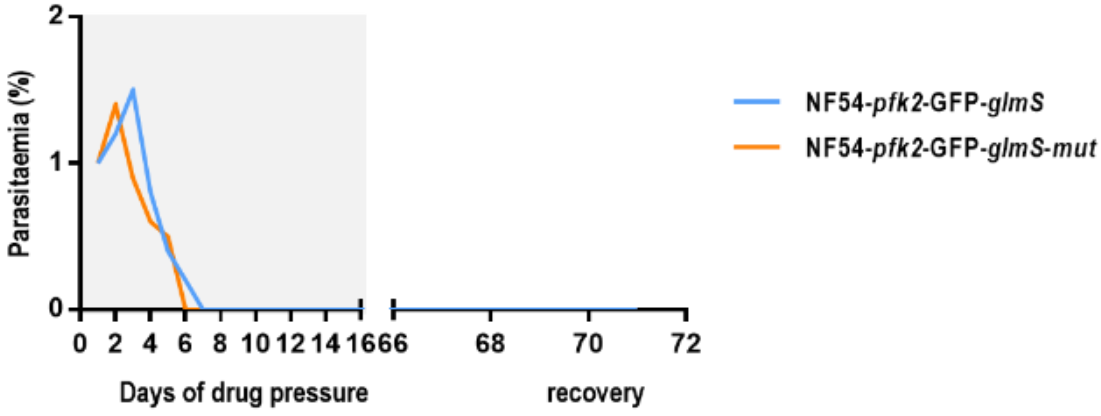

Figure 3.18: Intraerythrocytic *P. falciparum* parasitaemia during selection with G418 on the partially integrated NF54-*pfk2*-GFP-*glmS* and NF54-*pfk2*-GFP-*glmS-mut* parasite populations. The partially integrated NF54-*pfk2*-GFP-*glmS* and NF54-*pfk2*-GFP-*glmS-mut* parasites were subjected to drug pressure with WR99210 (day 1 to 4; 4 nM) and G418 (day 1 to 16; 800 µg/mL) to eliminate the WT locus. The parasitaemia was determined from Rapi-Diff-stained thin blood smears with optical microscopy at 1000x magnification. Figure was created with GraphPad Prism version 7.

Parasites were recovered in drug-free medium for 55 days, but neither of the partially integrated NF54-*pfk2*-GFP-*glmS* or NF54-*pfk2*-GFP-*glmS-mut* parasite populations recovered (Figure 3.18).

3.5.5. Limiting dilution to obtain clonal lines of NF54-*pfk2*-GFP-*glmS* and NF54-*pfk2*-GFP-*glmS*-mut lines

Limiting dilution was used as another approach to obtain homogeneous populations of integrated parasites for the partially integrated NF54-*pfk2*-GFP-*glmS* and NF54-*pfk2*-GFP-*glmS-mut* lines. This technique is based on the generation of clonal lines by performing serial dilutions at a theoretical concentration of less than one cell per unit of volume plated per well. Asexual parasite cultures from partially integrated NF54-*pfk2*-GFP-*glmS* and NF54-*pfk2*-GFP-*glmS-mut* parasite populations were diluted at a 2 % haematocrit to final concentrations of 0.5 parasites/well, 1 parasite/well, and 3 parasites/well in a 96-well microtiter plate. The latter two dilutions were used as a positive control for the detection of parasite proliferation, which was detected visually through a change in the colour of the medium. Proliferating parasites produce lactate, which results in acidification of the medium to a yellow colour in comparison to the pink colour of the medium in wells without parasites. Proliferating cultures with a yellow media colour was additionally confirmed by microscopic evaluation. The dilutions were maintained for three weeks with weekly media changes (with 0.4 % haematocrit erythrocytes) before parasite proliferation was detected using the 0.5 parasites per well dilution. About 33 % of the samples from the partially integrated NF54-*pfk2*-GFP-*glmS* population were positive for proliferation, while approximately 41 % of the samples from the partially integrated NF54-*pfk2*-GFP-*glmS-mut* population contained parasites.

Previously, parasite populations were tested for integration by isolating DNA from ~ 5 to 10 mL of asexual *P. falciparum* parasite culture (>3 % parasitaemia, 5 % haematocrit) to use as template in the 5', 3', and locus PCR (Figure 3.19). It was not feasible to amplify all the samples that had to be screened for integration to this parasitaemia and culture volume. Therefore, different template preparations were investigated for PCR amplification directly from the *in vitro* cultures. These investigations for amplification from *in vitro* culture were carried out using a robust PCR that amplifies the *P. falciparum* 18S ribosomal RNA gene. It was reasoned that if amplification was unsuccessful for this reaction for a specific template preparation, it was unlikely to be effective in the screening PCR reactions. An intraerythrocytic *P. falciparum* parasite culture (2 % haematocrit) was serially diluted 10-fold from 1.5 % to 0.0005 % parasitaemia. For each dilution, three different conditions were tested for amplification. For the

first condition, the parasite cultures were flash-frozen (3 x) in liquid nitrogen, and the supernatant (8 µL) added as a template to the PCR reactions. The second condition used the parasite culture (4 µL) directly in the PCR reactions, while the third condition involved using settled cells (2 µL) for amplification. The parasite culture (4 µL) was the most successful template for amplifying the 18S ribosomal RNA gene (~1200 bp band, Figure 3.19 A) (P10 and P11; Table 2.6), since amplification could be detected at a parasitaemia ranging from 0.015 % to 1.5 %. By contrast, the settled cells allowed amplification from 0.15 % parasitaemia, while the freeze-thaw preparation was the least successful, with amplification only obtained at 1.5% parasitaemia.

Subsequently, the parasite culture (4 µL; partially integrated NF54-*pfk2*-GFP-*glmS*-mut) as a template for PCR amplification, was determined to be sufficient to detect integration (Figure 3.19 B; ~1368 bp band) at the 5' loci as well as WT parasites (Figure 3.19 C; ~1416 bp band) at a parasitaemia ranging from 0.15 % to 1.5 %.

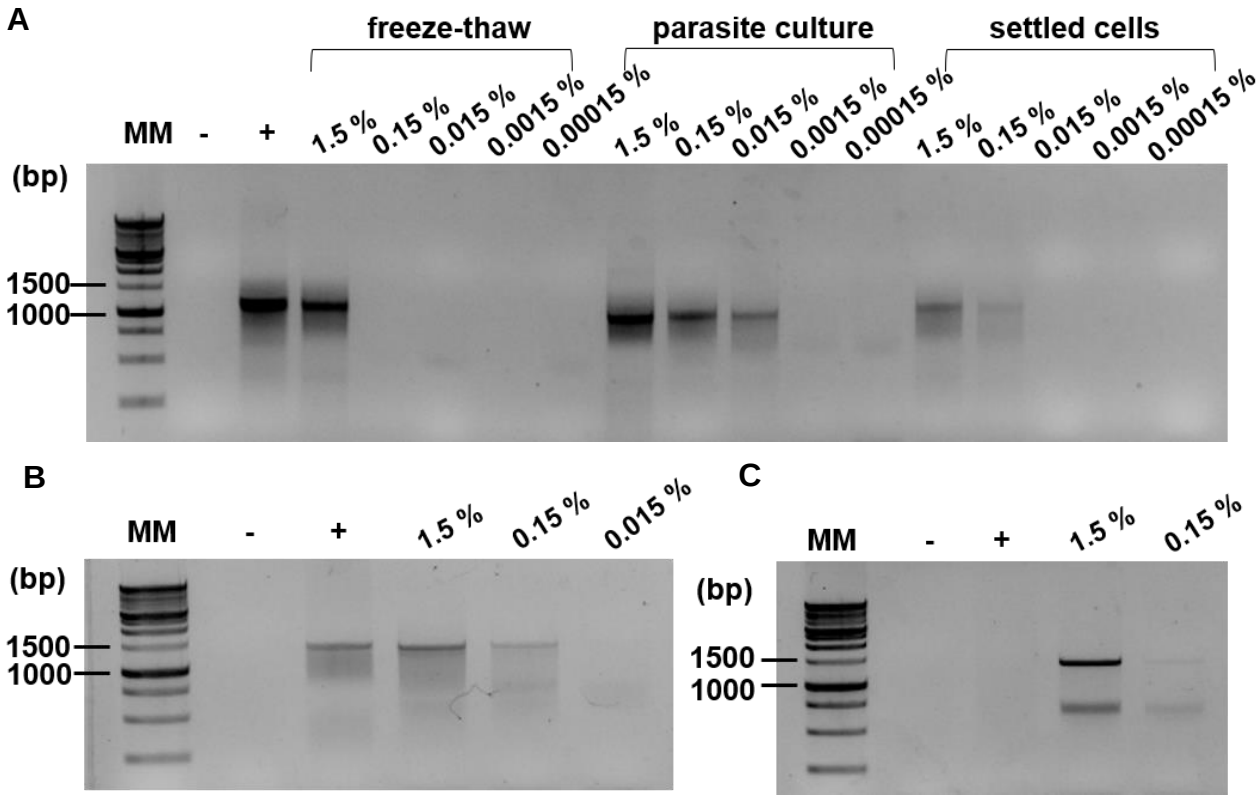

Figure 3.19: Evaluation of template preparations for PCR amplification directly from *in vitro P. falciparum* cultures. (A) PCR amplification of the 18S ribosomal RNA gene (B) Integration (5' loci; ~1368 bp) and (C) WT parasites were detected at a parasitaemia ranging from 0.15 % to 1.5 % using 4 µL parasite culture. The amplified products were separated with a 1 % w/v agarose/TAE gel that contained EtBr (1 µg/mL) for visualization under UV light. Positive control (+) isolated gDNA (32 ng) was included, along with a negative control (-) with no template DNA. MM: 1 kb DNA ladder as molecular marker.

Following limiting dilution of both NF54-*pfk2*-GFP-*glmS* and NF54-*pfk2*-GFP-*glmS-mut* populations, the samples that had parasite proliferation were screened for integration (5' loci) and the absence of WT parasites in the same manner as above, using parasite cultures (4 µL each) as template in the PCR reactions.

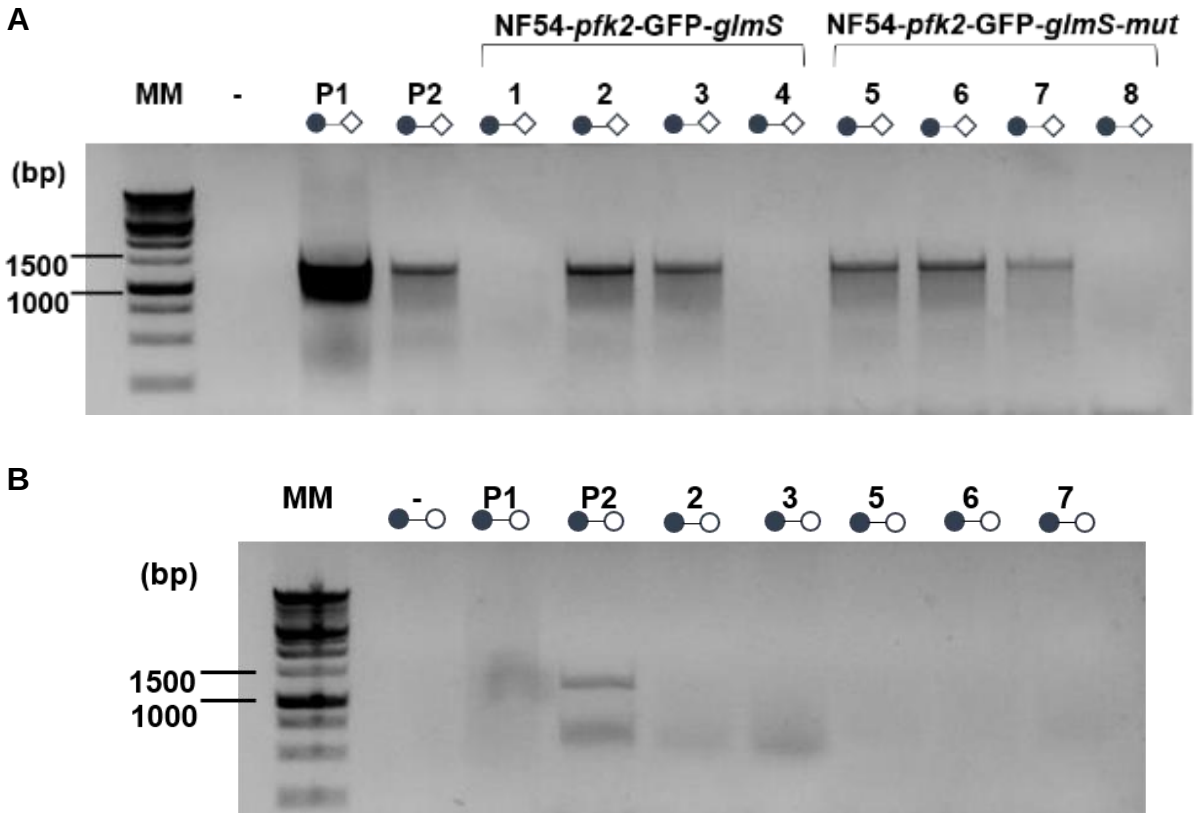

Figure 3.20: Screening for clonal lines of NF54-*pfk2*-GFP-*glmS* and NF54-*pfk2*-GFP-*glmS-mut.* Screening samples with parasite proliferation (0.5 parasites/well dilution) for (A) integration (5' loci; ~1368 bp band) and (B) WT parasites (~1416 bp band). The parasite cultures (4 µL each) were used as template in the PCR reactions. Positive control (P1) of isolated gDNA was included as well as a positive control (P2) with 4 µL of an NF54-*pfk2*-GFP-*glmS-mut* culture and a negative control (-) with no template. The amplified products were separated with a 1 % w/v agarose/TAE gel that contained EtBr (1 µg/mL) for visualization under UV light. MM: 1 kb DNA ladder as molecular marker.

Integration at the 5' loci (~1368 bp) was confirmed for 50 % (2 out of 4) and 75 % (3 out of 4) of the samples screened for the NF54-*pfk2*-GFP-*glmS* and NF54-*pfk2*-GFP-*glmS-mut* respectively (Figure 3.20 A). Additionally, these samples had no detectable WT parasites as seen by the absence of a band of ~1416 bp (Figure 3.20 B). These putative clonal isolates were increased in both volume (200 µl to 10 mL) and haematocrit (2 % to 5 %). At a sufficient parasitaemia (>3 %), DNA was isolated for PCR analysis to confirm that clonal isolates were obtained. Integration was confirmed through amplification of 5' (~1368 bp) and 3' (~1259 bp) bands (Figure 3.21 A to E). However, amplification across the locus yielded a band of ~1416 bp for all of the parasite populations, indicating that these were still heterogenous with the WT locus present (Figure 3.21 A to E).

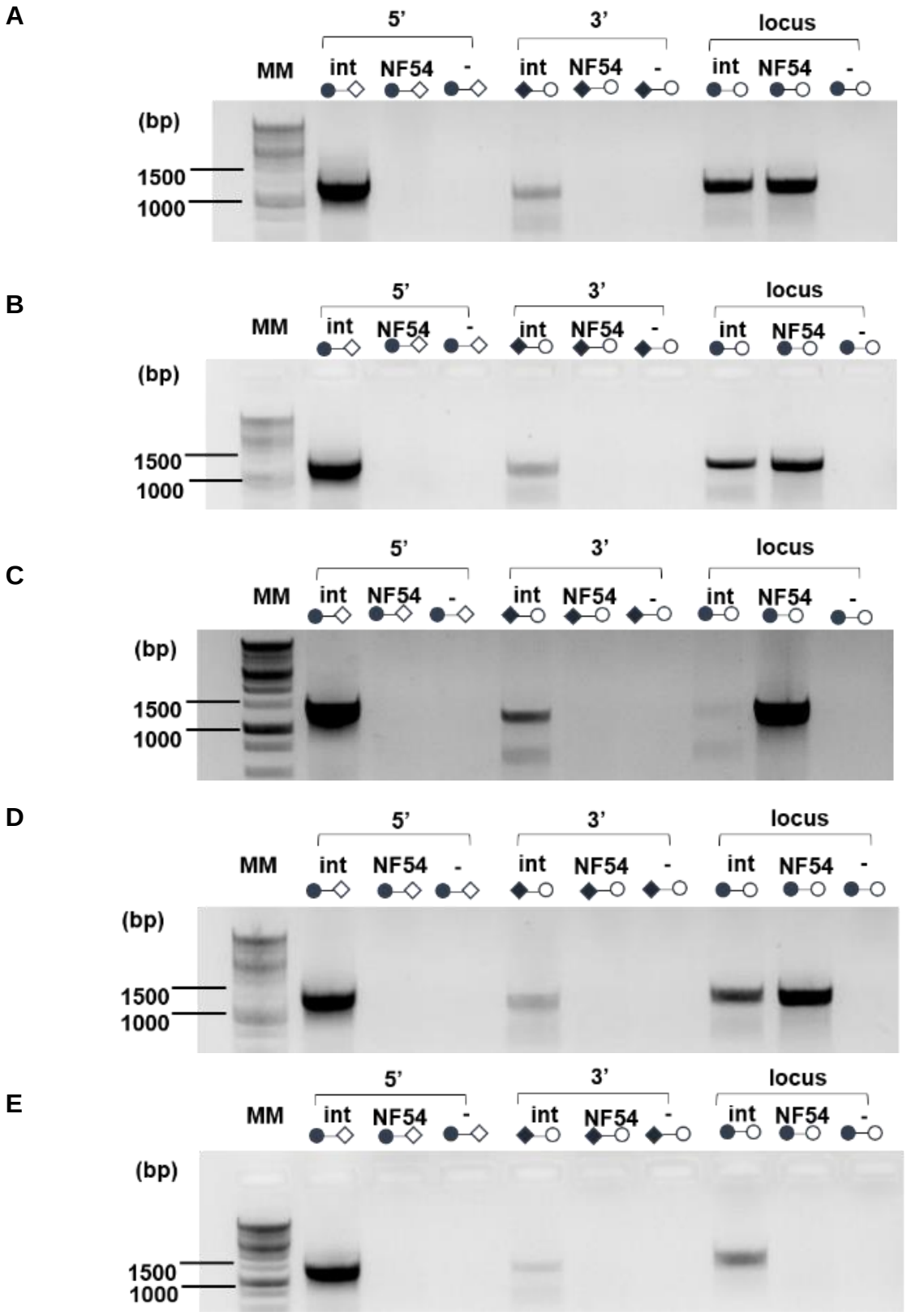

Figure 3.21: PCR analysis of the putative clonal isolates for NF54-*pfk2*-GFP-*glmS* and NF54-*pfk2*-GFP-*glmS-mut.* Screening for clonal isolates of (A and B) NF54-*pfk2*-GFP-*glmS* and (C, D, and E) NF54-*pfk2*-GFP-*glmS-mut*. The presence of 5' (1368 bp) and 3' (1259 bp) bands confirmed successful integration, but the presence of the WT locus (1416 bp) indicated that WT parasites were still present for all of the above parasite populations. The amplified DNA was separated with a 1 % w/v agarose/TAE gel that contained EtBr (1 µg/mL) for visualization under UV light. MM: 1 kb DNA ladder as molecular marker, int: integrated parasite line, NF54: WT parasite control. Negative control (-) with no template DNA was included.

The proportion of WT parasites in each of the samples was likely below the detection limit (<0.15 %) when the parasite cultures were used as a template for screening (Figure 3.20 B). The undetectable WT population likely proliferated to a detectable range with the extensive time period that was required to increase the volume of the cultures (200 µL to 10 mL). Alternatively, drug resistance is the only selective advantage that the integrated plasmid cassette provides to the transgenic parasites. Without drug pressure, the parasites could possibly lose the plasmid cassette through a random homologous recombination event with prolonged periods in culture (Figure 3.22).

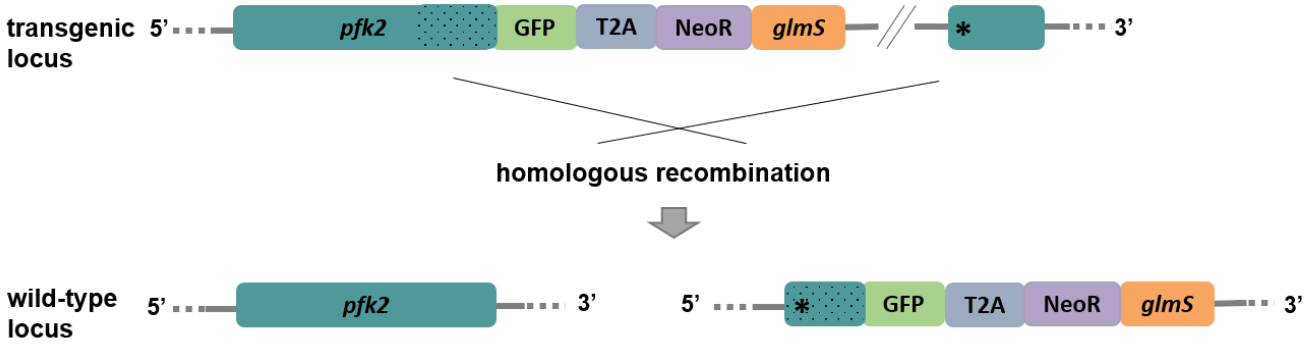

Figure 3.22: Schematic representation for the loss of the integrated plasmid cassette through random homologous recombination. The integrated plasmid cassette provides drug resistance as the only selective advantage to *P. falciparum* parasites. It is a possibility that these parasites lose the plasmid cassette through a random homologous recombination event with prolonged periods in culture with no drug pressure.

3.5.6. Evaluation of the feasibility of fluorescence-based separation of integrant and WT parasite populations

Both NF54-*pfk2*-GFP-*glmS* and NF54-*pfk2*-GFP-*glmS-mut* parasite populations express the PfK2 protein with a GFP fluorescent tag. Theoretically, it is possible that *P. falciparum* parasites containing this GFP protein can be separated from the WT parasites using a technique such as Fluorescence Activated Cell Sorting (FACS). To determine whether this would be feasible, fluorescence microscopy was first used to ascertain whether GFP fluorescence could be detected in the integrant parasites of the partially integrated NF54-*pfk2*-GFP-*glmS* and NF54-*pfk2*-GFP-*glmS-mut* lines. For both of the respective partially integrated lines, GFP expression was barely detectable with a weak fluorescent signal (Figure 3.23 A and B). A stronger fluorescent signal was detected for the transmissible sexual gametocytes (images on the left) than for the asexual parasites (images on the right) (Figure 3.23 A and B).

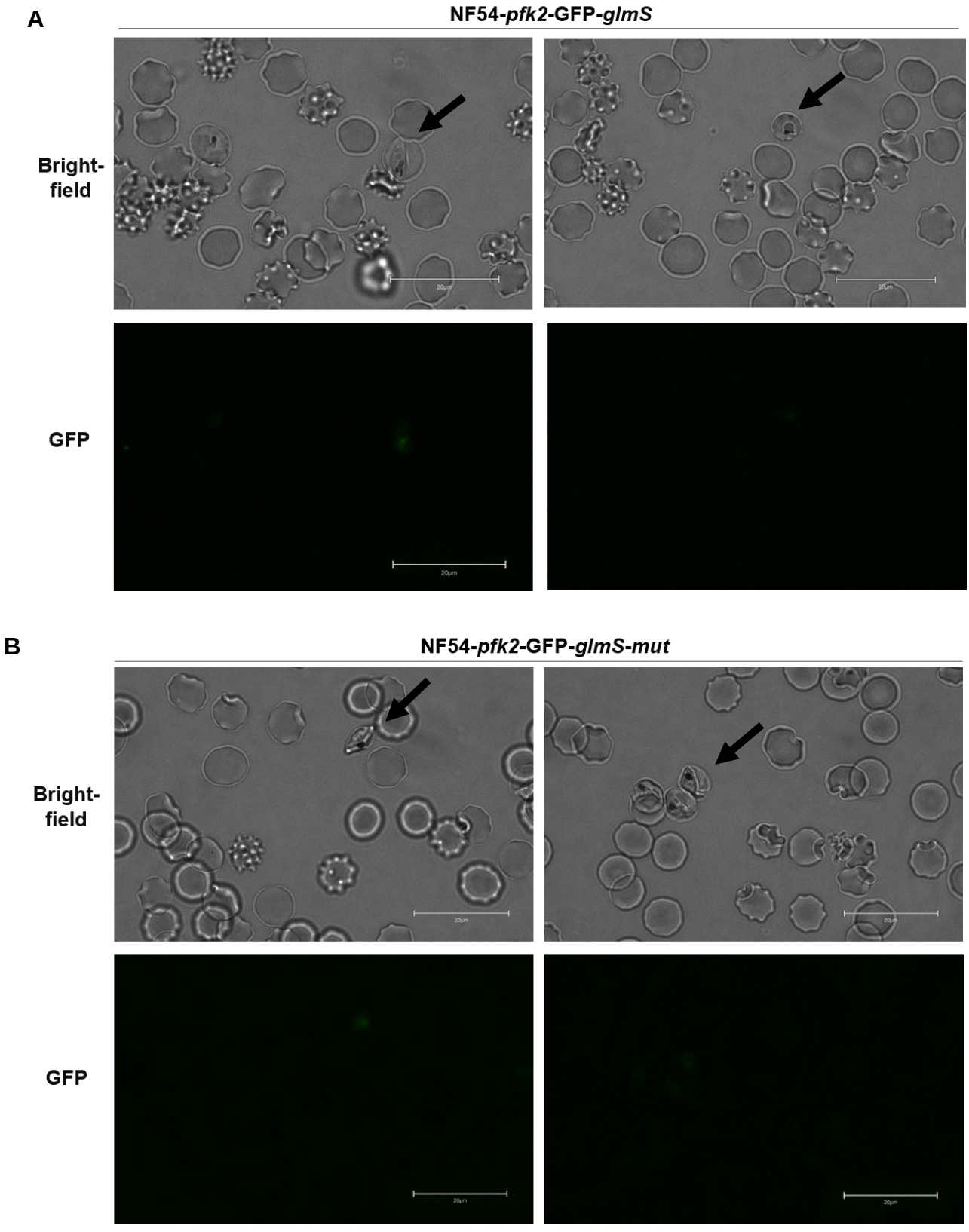

Figure 3.23: GFP fluorescence analysis of the partially integrated NF54-*pfk2*-GFP-*glmS* and NF54-*pfk2*-GFP-*glmS*-mut lines. GFP signal was detected for both the partially integrated (A) NF54-*pfk2*-GFP-*glmS* and (B) NF54-*pfk2*-GFP-*glmS*-mut lines. The GFP signal was slightly higher during the sexual gametocyte stages (images on the left, indicated with an arrow) than during the asexual stages (images on the right, indicated with an arrow).

Since the expression of GFP is driven by the *pfk2* promoter, the intensity of the fluorescent signal is dependent on the expression profile of PfK2. As indicated in Figure 1.8, PfK2 has low expression throughout the asexual stages but higher expression throughout gametocyte development. This correlates with the stronger GFP fluorescent signal picked up for these developmental stages compared to the asexual stages. The low expression profile of PfK2 is likely correlated to the annotation of PfK2 as a putative BK channel. These channels compromise the largest single-channel conductance (up to 300 pS) of all K^+ channels, which means that the opening of relatively few of these channels are required to have a significant impact on membrane potential (148).

Due to the weak GFP fluorescent intensity signal, FACS was not considered in this study to separate the integrated parasites from the WT parasites. Additionally, this method is associated with the exposure of the parasite cultures to a non-sterile environment prior to introduction to the sorter, which could possibly lead to contamination, while the viability of the parasites could also be affected through the sorting process itself (time outside of incubator, pressure, etc.). However, expression data provide a possible explanation for why parasites never recovered following drug pressure with G418 in section 3.5.4. As with GFP, the expression of NeoR is driven by the weak *pfk2* promoter. It is a possibility that insufficient levels of NeoR was produced for the survival of the integrant parasites at the concentration (800 µg/mL) that G418 drug pressure was applied at.

3.5.7. Drug pressure with WR99210 to generate fully transgenic NF54-*pfk2*-GFP-*glmS* or NF54-*pfk2*-GFP-*glmS*-mut lines

The partially integrated NF54-*pfk2*-GFP-*glmS* and NF54-*pfk2*-GFP-*glmS-mut* parasite populations were placed under sole drug pressure with WR99210 (8 nM) instead of G418 to eliminate the WT locus. The hDHFR marker provides parasites with drug resistance against WR99210 and has expression from a promoter on the incorporated plasmid cassette. The partially integrated NF54-*pfk2*-GFP-*glmS* and NF54-*pfk2*-GFP-*glmS*-mut parasite populations were subjected to drug pressure for 10 days and 16 days, respectively, during which the parasitaemia was kept below 2 %. The parasitaemia did not decline to undetectable levels (Figure 3.24), due to the integrated parasites with hDHFR resistance.

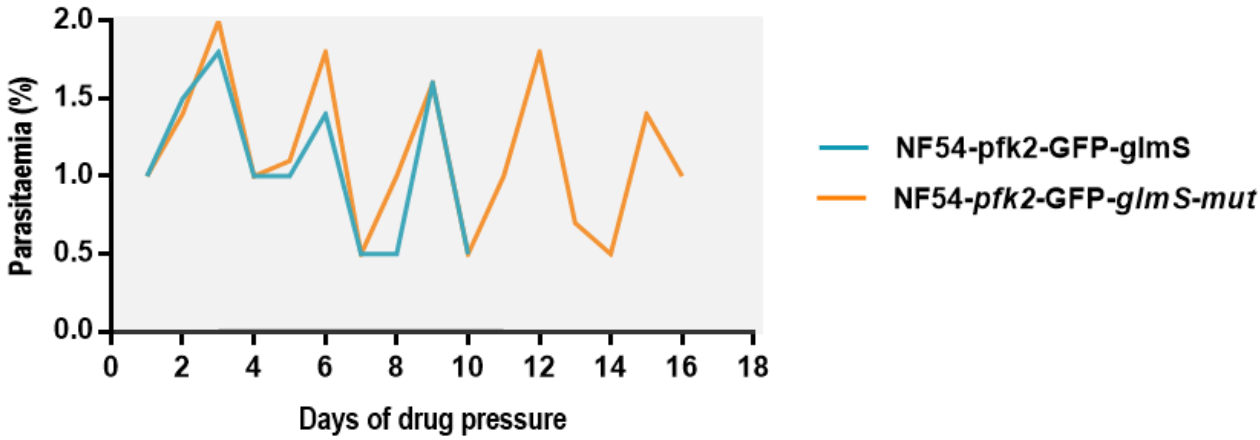

Figure 3.24: Intraerythrocytic *P. falciparum* parasitaemia during pressure with WR99210 on the partially integrated NF54-*pfk2*-GFP-*glmS* and NF54-*pfk2*-GFP-*glmS-mut* parasite populations. The partially integrated NF54-*pfk2*-GFP-*glmS* and NF54-*pfk2*-GFP-*glmS-mut* parasites were subjected to drug pressure with WR99210 (8 nM) for 10 and 16 days, respectively, to eliminate the WT parasites. The parasitaemia was determined from Rapi-Diff-stained thin blood smears with optical microscopy at 1000x magnification. Figure was created with GraphPad Prism version 7.

To investigate whether the WT parasites were eliminated, DNA was isolated from the respective cultures for PCR analysis. For both parasite populations, PCR amplification of 5' (~1368 bp) and 3' (~1259 bp) loci bands confirmed integration (Figure 3.25 A and B) while amplification across the locus indicated that the WT locus was completely eliminated, as seen by the absence of a ~1416 bp band (Figure 3.25 A and B).

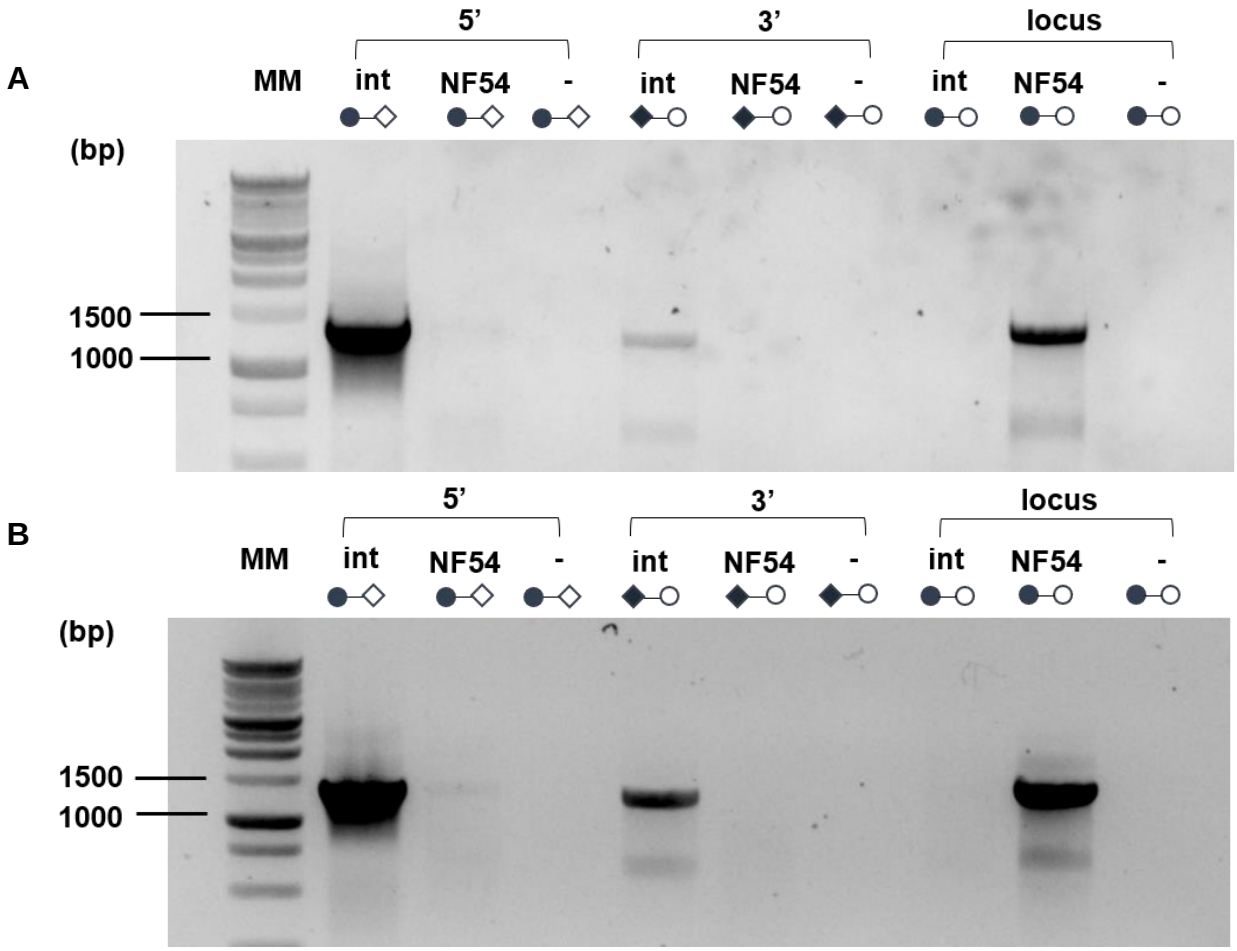

Figure 3.25: PCR analysis of integrated NF54-*pfk2*-GFP-*glmS and* NF54-*pfk2*-GFP-*glmS-mut* lines following drug pressure with WR99210. (PCR analysis for integrated (A) NF54-*pfk2*-GFP-*glmS* and (B) NF54-*pfk2*-GFP-*glmS-mut* parasites following drug pressure with WR99210 for 10 and 16 days, respectively. Integration was confirmed through 5' (1368 bp) and 3' (1259 bp) loci bands. The absence of WT parasites was confirmed through the absence of a ~1416 bp band. The amplified DNA was separated with a 1 % w/v agarose/TAE gel that contained EtBr (1 µg/mL) for visualization under UV light. MM: 1 kb DNA ladder as molecular marker, int: integrated parasite line, NF54: WT parasite control. Negative control (-) with no template DNA was included.

Thus, fully transgenic NF54-*pfk2*-GFP-*glmS* and NF54-*pfk2*-GFP-*glmS-mut* lines were successfully generated. For future studies, it is recommended that the culture be kept under drug pressure with WR99210 to prevent possible loss of the integrated plasmid cassette and/or to eliminate any undetectable WT parasites that possibly remained.

Chapter 4: Discussion

Environmental ionic conditions change drastically as *P. falciparum* parasites progress through a complex life cycle in the human host and the *Anopheles* mosquito vector. It is critical that ion homeostasis is maintained, since multiple biological processes depend on the combined action of various ion transport pathways (50,51,53,55,58,60). Ion homeostasis in asexual *P. falciparum* parasites has been investigated, but not in the transmissible sexual gametocytes. However, inhibition of selected ion transport proteins affects gametocyte development. For instance, a spiroindolone (Cipargamin) that has progressed through Phase I and Phase IIa clinical trials potently inhibits gametocyte development of *P. falciparum* parasites *in vitro*, where it targets the PfATP4 ion transporter that maintains the Na^+ gradient (53,75). This raised the question whether interference with the K^+ gradient may have similar deleterious effects on the *P. falciparum* parasite. Although the effect of K^+ channel inhibitors on gametocyte development is unknown, a K^+ selective ionophore (salinomycin) inhibits gametocyte differentiation of *P. falciparum* parasites by disrupting the K^+ gradient (63).

Two putative K^+ channels (Pfk1 and Pfk2) are encoded in the *P. falciparum* genome, but only PfK2 is expressed during gametocyte development (108,109). Since interference of the K^+ gradient prevents gametocyte differentiation (63), it was postulated that important biological processes depend on PfK2 to maintain the K^+ gradient during gametocytogenesis. The fact that various parasitic organisms are known to be dependent on K^+ channels for survival provided further basis for this postulation. For example, an anthelmintic drug (Profender®) that interferes with K^+ channels is used in cats to treat and control hookworm infections caused by *Ancylostoma tubaeforme*, roundworm infections caused by *Toxocara cati*, and tapeworm infections by *Dipylidium caninum* and *Taenia taeniaeformis* (149).

To investigate the essentiality of the PfK2 K^+ channel in *P. falciparum* parasites, this study aimed to truncate *pfk2* at the 5' terminal using the pSLI-TGD plasmid (112). This will generate a non-functional protein due to a loss of the voltage sensor-, pore-, and Ca^{2+} sensor- domain of the putative BK channel, which was predicted through *in silico* analysis. A recombinant pSLI-TGD-*pfk2* plasmid with a 5' gene fragment of *pfk2* was successfully generated. However, transfection into asexual parasites and subsequent drug pressure to select for episomal uptake was not successful. The transfection efficiency of plasmids into *P. falciparum* parasites was previously estimated to be as low as 0.8×10^{-6} parasites for stable transfections (150). Episomal plasmids have been established to segregate unevenly between daughter merozoites, in which not all of the parasites receive the plasmid during division (147,151). This poor plasmid segregation, along with the fact that only a small number of parasites actually

receive plasmid DNA at the time of transfection likely attributes to the low transfection efficiency (150). An increased number of independent transfections might increase the chances for successful transfection (138) of the pSLI-TGD-*pfk2* plasmid into *P. falciparum* parasites.

A limitation of the TGD system is that functional evaluation cannot be performed for transmissible sexual gametocytes if the targeted gene is essential for the proliferation of asexual parasites. To overcome this limitation, an inducible system is required. Thus, this study additionally aimed to generate transgenic *P. falciparum* parasites in which *pfk2* is modified with a conditional knockdown system (114). Recombinant pSLI-*glmS*-*pfk2* and pSLI-*glmS*-mut-*pfk2* plasmids were previously generated and successfully transfected into asexual parasites to select for episomal uptake [NF54-epi(SLI-*glmS*-*pfk2*) and NF54-epi(SLI-*glmS*-*mut*-*pfk2*)] and subsequently integration (115). However, only partially integrated NF54-*pfk2*-GFP-*glmS* and NF54-*pfk2*-GFP-*glmS*-*mut* lines were generated, in which the original WT locus was still present for both parasite populations (115). In this study, NF54-epi(SLI-*glmS*-pfk2 was selected again for integration over a longer time period than previously (16 versus 14 days). A partially integrated NF54-*pfk2*-GFP-*glmS* line was again obtained.

In this study, it was attempted to obtain clonal isolates of the partially integrated NF54-*pfk2*-GFP-*glmS* and NF54-*pfk2*-GFP-*glmS*-*mut* parasites through limiting dilution. Initial screening indicated that clonal isolates were obtained, but further screening indicated that these populations were still heterogeneous. Theoretically, wells with proliferation should have originated from a single parasite (integrated or WT), but this is dependent on statistical probability. According to the Poisson distribution, approximately one-third of the plated wells will have no parasites deposited, one-third of wells will have a single parasite deposited, while one-third will have multiple parasites deposited per well (152). With this probability it is often required to repeat limiting dilution two or more times to increase the possibility of obtaining clonally-derived lines, but this is time inefficient and resource intensive as the process gets extended by months (152,153). This was furthermore not considered as the proportion of WT parasites in the heterogenous populations did not have a visually significant decrease from before limiting dilution. Increasing the culture volumes from the wells of plates (200 µL to 10 mL) is a time intensive procedure, which either gives ample time for WT parasites below the detection limit to proliferate to larger proportions, or for the integrated parasites to lose the plasmid cassette through another random homologous recombination event.

In another attempt to eliminate the WT locus, the partially integrated NF54-*pfk2*-GFP-*glmS* and NF54-*pfk2*-GFP-*glmS*-*mut* lines were placed under additional drug selection at double the concentration of G418 that was used for initial integration selection. Parasites never recovered following drug pressure, likely due to insufficient expression of the drug resistance marker

under the weak *pfk2* promoter. Placing the partially integrated NF54-*pfk2*-GFP-*glmS* and NF54-*pfk2*-GFP-*glmS-mut* parasites under WR99210 drug pressure instead was successful for eliminating the WT locus from both of the respective parasite populations.

The fully transgenic NF54-*pfk2*-GFP-*glmS* and NF54-*pfk2*-GFP-*glmS-mut* lines generated in this study can be used in future studies to investigate the essentiality of PfK2 for asexual intraerythrocytic *P. falciparum* parasites, and in particular for the transmissible sexual gametocytes through a conditional knockdown approach. The conditional knockdown is based on a *glmS* ribozyme domain, which activates through the addition of glucosamine for self-cleavage of the gene mRNA to regulate the amount of gene product synthesized. The transgenic lines will also allow for localization studies with the attached GFP tag, although a fluorescent detector with superior detection sensitivity might be required due to the weak promoter activity of *pfk2* that drives expression of the GFP fluorescence. Knowing the location of a transporter could be fundamental to understanding its physiological role.

Furthermore, knockdown with the transgenic lines could be used to evaluate and confirm whether PfK2 is involved in maintaining the K^+ gradient during gametocytogenesis of *P. falciparum* parasites. It is postulated that PfK2 maintains the K^+ gradient during gametocytogenesis of *P. falciparum* parasites, which is thought to be essential for important biological processes during these developmental stages. Thus, knockdown of PfK2 with the *glmS* ribozyme system is expected to have detrimental effects for gametocyte development. Alternatively, morphological deformities (i.e., osmotic swelling) might be observed and/or a disruption in stage progression. Although mature gametocytes might still form, it is expected that these will be non-functional, in which gamete formation will not occur.

The detrimental effects are expected to occur due to inhibition of the intracellular influx of K^+ ions via PfK2. These positively charged ions will no longer be available to counter the current associated with the efflux of H^+ ions by the V-type ATPase on the plasma membrane, which is postulated to result in a membrane hyperpolarization. It is thought that the parasite will counteract this through either a decreased efflux of H^+ ions by the V-Type ATPase to give rise to cytosolic acidification, or through an increased influx of Na^+ ions via unknown pathways. An increased Na^+ influx was previously reported upon the removal of extracellular [K^+] along with cytosolic acidification (53). With an increase in intracellular [Na^+], PfATP4 would have increased activity to efflux Na^+ in order to maintain the Na^+ gradient. This would be accompanied with an increased influx of H^+ ions, which results in cytosolic acidification. It is thus postulated that knockdown of PfK2 will result in a decrease in the intracellular [K^+], along with a decrease in cytosolic pH and/or increase in cytosolic [Na^+], which could be measured through fluorescent dyes.

Chapter 5: Conclusion

It is critical for *P. falciparum* parasites to maintain ion homeostasis as environmental conditions change drastically with progression through the life cycle. Ion homeostasis has been studied extensively for the asexual parasites, but limited knowledge is available for the gametocyte stages. Previous research indicates that K^+ homeostasis during gametocytogenesis is maintained by a single K^+ channel (PfK2). For further investigation, this research aimed to develop genetically modified *P. falciparum pfk2* parasite lines for genetic disruption and conditional knockdown studies. With a cloning strategy, a recombinant pSLI-TGD-*pfk2* plasmid was successfully generated and transfected into asexual intraerythrocytic *P. falciparum* parasites to select for episomal uptake. However, for two transfection attempts parasites never recovered following drug pressure for episomal uptake.

Transgenic NF54-*pfk2*-GFP-*glmS* and NF54-*pfk2*-GFP-*glmS-mut* lines were successfully generated. This was achieved from partially integrated lines that were previously generated from the transfection of recombinant pSLI-*glmS-pfk2* and pSLI-*glmS-pfk2*-mut plasmids. The WT locus was successfully eliminated from these partially integrated lines to obtain full integration. In future functional studies, these transgenic lines will allow for investigating the importance of Pfk2 for asexual parasites, and in particular for the transmissible sexual gametocytes through a conditional knockdown approach. The function of PfK2 as a K^+ channel and its involvement in maintaining the K^+ gradient during gametocytogenesis can furthermore be investigated. This could expand and provide fundamental knowledge on the regulation of ion homeostasis during gametocyte development of *P. falciparum* parasites.

References

1. World malaria report 2020: 20 years of global progress and challenges. Geneva: World Health Organization; 2020. Licence: CC BY-NC-SA 3.0 IGO.
2. Cowman, A. F., Healer, J., Marapana, D., and Marsh, K. (2016) Malaria: Biology and Disease. *Cell* **167**, 610-624
3. Guyatt, H. L., and Snow, R. W. (2004) Impact of malaria during pregnancy on low birth weight in sub-Saharan Africa. *Clin Microbiol Rev* **17**, 760-769
4. Griffiths, R. B., and Gordon, R. M. (1952) An apparatus which enables the process of feeding by mosquitoes to be observed in the tissues of a live rodent; together with an account of the ejection of saliva and its significance in Malaria. *Ann Trop Med Parasitol* **46**, 311-319
5. Ta, T. H., Hisam, S., Lanza, M., Jiram, A. I., Ismail, N., and Rubio, J. M. (2014) First case of a naturally acquired human infection with *Plasmodium cynomolgi*. *Malar J* **13**, 68
6. Raja, T. N., Hu, T. H., Kadir, K. A., Mohamad, D. S. A., Rosli, N., Wong, L. L., Hii, K. C., Simon Divis, P. C., and Singh, B. (2020) Naturally Acquired Human *Plasmodium cynomolgi* and *P. knowlesi* Infections, Malaysian Borneo. *Emerg Infect Dis* **26**, 1801-1809
7. Boyd, M. F., and Kitchen, S. F. (1939) The Demonstration of Sporozoites in Human Tissues. *Am J Trop Med Hyg* **s1-19**, 27-31
8. Sidjanski, S., and Vanderberg, J. P. (1997) Delayed migration of *Plasmodium* sporozoites from the mosquito bite site to the blood. *Am J Trop Med Hyg* **57**, 426-429
9. Shortt, H. E., Fairley, N. H., Covell, G., Shute, P. G., and Garnham, P. C. (1951) The pre-erythrocytic stage of *Plasmodium falciparum*. *Trans R Soc Trop Med Hyg* **44**, 405-419
10. Moon, S., Lee, S., Kim, H., Freitas-Junior, L. H., Kang, M., Ayong, L., and Hansen, M. A. (2013) An image analysis algorithm for malaria parasite stage classification and viability quantification. *PLoS One* **8**, e61812
11. Bartoloni, A., and Zammarchi, L. (2012) Clinical aspects of uncomplicated and severe malaria. *Mediterr J Hematol Infect Dis* **4**, e2012026
12. Maccallum, W. G. (1898) On the Haematozoan Infections of Birds. *J Exp Med* **3**, 117-136
13. Field, J. W., and Shute, P. G. (1956) *The microscopic diagnosis of human malaria. II. A Morphological Study of the Erythroeytic Parasites.*, Studies from the Institute for Medical Research, Federated Malay States. Kuala Lumpur: Govt. Pr
14. Joice, R., Nilsson, S. K., Montgomery, J., Dankwa, S., Egan, E., Morahan, B., Seydel, K. B., Bertuccini, L., Alano, P., Williamson, K. C., Duraisingh, M. T., Taylor, T. E., Milner, D. A., and Marti, M. (2014) *Plasmodium falciparum* transmission stages accumulate in the human bone marrow. *Sci Transl Med* **6**, 244re245. 210.1126/scitranslmed.3008882.
15. Janse, C. J., van der Klooster, P. F., van der Kaay, H. J., van der Ploeg, M., and Overdulve, J. P. (1986) DNA synthesis in *Plasmodium berghei* during asexual and sexual development. *Mol Biochem Parasitol* **20**, 173-182
16. Han, Y. S., Thompson, J., Kafatos, F. C., and Barillas-Mury, C. (2000) Molecular interactions between *Anopheles stephensi* midgut cells and *Plasmodium berghei*: the time bomb theory of ookinete invasion of mosquitoes. *EMBO J* **19**, 6030-6040
17. Pimenta, P. F., Touray, M., and Miller, L. (1994) The journey of malaria sporozoites in the mosquito salivary gland. *J Eukaryot Microbiol* **41**, 608-624
18. Okumu, F. O., and Moore, S. J. (2011) Combining indoor residual spraying and insecticide-treated nets for malaria control in Africa: a review of possible outcomes and an outline of suggestions for the future. *Malar J* **10**, 208
19. Lauer, S. A., Rathod, P. K., Ghori, N., and Haldar, K. (1997) A membrane network for nutrient import in red cells infected with the malaria parasite. *Science* **276**, 1122-1125
20. Jagannathan, P., and Kakuru, A. (2022) Malaria in 2022: Increasing challenges, cautious optimism. *Nat Commun* **13**, 2678
21. Reader, J., Botha, M., Theron, A., Lauterbach, S. B., Rossouw, C., Engelbrecht, D., Wepener, M., Smit, A., Leroy, D., Mancama, D., Coetzer, T. L., and Birkholtz, L. M. (2015) Nowhere to hide: interrogating different metabolic parameters of *Plasmodium falciparum* gametocytes in a transmission blocking drug discovery pipeline towards malaria elimination. *Malar J* **14**, 213

22. Scherf, A., Lopez-Rubio, J. J., and Riviere, L. (2008) Antigenic variation in *Plasmodium falciparum*. *Annu Rev Microbiol* **62**, 445-470
23. Recker, M., Buckee, C. O., Serazin, A., Kyes, S., Pinches, R., Christodoulou, Z., Springer, A. L., Gupta, S., and Newbold, C. I. (2011) Antigenic variation in *Plasmodium falciparum* malaria involves a highly structured switching pattern. *PLoS Pathog* **7**, e1001306
24. Praet, N., Asante, K. P., Bozonnat, M. C., Akite, E. J., Ansah, P. O., Baril, L., Boahen, O., Mendoza, Y. G., Haine, V., Kariuki, S., Lamy, M., Maleta, K., Mungwira, R., Ndeketa, L., Oduro, A., Ogutu, B., Olewe, F., Oneko, M., Orsini, M., Roman, F., Bahmanyar, E. R., Rosillon, D., Schuerman, L., Sing'oei, V., Terlouw, D. J., Wery, S., Otieno, W., and Pircon, J. Y. (2022) Assessing the safety, impact and effectiveness of RTS,S/AS01E malaria vaccine following its introduction in three sub-Saharan African countries: methodological approaches and study set-up. *Malar J* **21**, 132
25. Rosenthal, P. J. (2022) Malaria in 2022: Challenges and Progress. *Am J Trop Med Hyg*
26. Mahmoudi, S., and Keshavarz, H. (2017) Efficacy of phase 3 trial of RTS, S/AS01 malaria vaccine: The need for an alternative development plan. *Hum Vaccin Immunother* **13**, 2098-2101
27. Crompton, P. D., Pierce, S. K., and Miller, L. H. (2010) Advances and challenges in malaria vaccine development. *J Clin Invest* **120**, 4168-4178
28. Datoo, M. S., Natama, M. H., Some, A., Traore, O., Rouamba, T., Bellamy, D., Yameogo, P., Valia, D., Tegneri, M., Ouedraogo, F., Soma, R., Sawadogo, S., Sorgho, F., Derra, K., Rouamba, E., Orindi, B., Ramos Lopez, F., Flaxman, A., Cappuccini, F., Kailath, R., Elias, S., Mukhopadhyay, E., Noe, A., Cairns, M., Lawrie, A., Roberts, R., Valea, I., Sorgho, H., Williams, N., Glenn, G., Fries, L., Reimer, J., Ewer, K. J., Shaligram, U., Hill, A. V. S., and Tinto, H. (2021) Efficacy of a low-dose candidate malaria vaccine, R21 in adjuvant Matrix-M, with seasonal administration to children in Burkina Faso: a randomised controlled trial. *Lancet* **397**, 1809-1818
29. Duffy, P. E., and Patrick Gorres, J. (2020) Malaria vaccines since 2000: progress, priorities, products. *NPJ Vaccines* **5**, 48
30. Phillips, M. A., Burrows, J. N., Manyando, C., van Huijsduijnen, R. H., Van Voorhis, W. C., and Wells, T. N. C. (2017) Malaria. *Nat Rev Dis Primers* **3**, 17050
31. Schwartz, E. (2012) Prophylaxis of malaria. *Mediterr J Hematol Infect Dis* **4**, e2012045
32. DeVos, E., and Dunn, N. (2022) Malaria Prophylaxis. in *StatPearls*, Treasure Island (FL). pp
33. Eastman, R. T., and Fidock, D. A. (2009) Artemisinin-based combination therapies: a vital tool in efforts to eliminate malaria. *Nat Rev Microbiol* **7**, 864-874
34. Hott, A., Casandra, D., Sparks, K. N., Morton, L. C., Castanares, G. G., Rutter, A., and Kyle, D. E. (2015) Artemisinin-resistant *Plasmodium falciparum* parasites exhibit altered patterns of development in infected erythrocytes. *Antimicrob Agents Chemother* **59**, 3156-3167
35. Noedl, H., Se, Y., Sriwichai, S., Schaecher, K., Teja-Isavadharm, P., Smith, B., Rutvisuttinunt, W., Bethell, D., Surasri, S., Fukuda, M. M., Socheat, D., and Chan Thap, L. (2010) Artemisinin resistance in Cambodia: a clinical trial designed to address an emerging problem in Southeast Asia. *Clin Infect Dis* **51**, e82-89
36. Tumwebaze, P. K., Conrad, M. D., Okitwi, M., Orena, S., Byaruhanga, O., Katairo, T., Legac, J., Garg, S., Giesbrecht, D., Smith, S. R., Ceja, F. G., Nsobya, S. L., Bailey, J. A., Cooper, R. A., and Rosenthal, P. J. (2022) Decreased susceptibility of *Plasmodium falciparum* to both dihydroartemisinin and lumefantrine in northern Uganda. *Nat Commun* **13**, 6353
37. Alving, A. S., Carson, P. E., Flanagan, C. L., and Ickes, C. E. (1956) Enzymatic deficiency in primaquine-sensitive erythrocytes. *Science* **124**, 484-485
38. White, N. J. (2013) Primaquine to prevent transmission of *falciparum* malaria. *Lancet Infect Dis* **13**, 175-181
39. Howes, R. E., Piel, F. B., Patil, A. P., Nyangiri, O. A., Gething, P. W., Dewi, M., Hogg, M. M., Battle, K. E., Padilla, C. D., Baird, J. K., and Hay, S. I. (2012) G6PD deficiency prevalence and estimates of affected populations in malaria endemic countries: a geostatistical model-based map. *PLoS Med* **9**, e1001339
40. Lee, P., Ye, Z., Van Dyke, K., and Kirk, R. G. (1988) X-ray microanalysis of *Plasmodium falciparum* and infected red blood cells: effects of qinghaosu and chloroquine on potassium, sodium, and phosphorus composition. *Am J Trop Med Hyg* **39**, 157-165
41. Tosteson, D. C., and Hoffman, J. F. (1960) Regulation of cell volume by active cation transport in high and low potassium sheep red cells. *J Gen Physiol* **44**, 169-194

42. Ginsburg, H., Krugliak, M., Eidelman, O., and Cabantchik, Z. I. (1983) New permeability pathways induced in membranes of *Plasmodium falciparum* infected erythrocytes. *Mol Biochem Parasitol* **8**, 177-190
43. Staines, H. M., Rae, C., and Kirk, K. (2000) Increased permeability of the malaria-infected erythrocyte to organic cations. *Biochim Biophys Acta* **1463**, 88-98
44. Staines, H. M., Ellory, J. C., and Kirk, K. (2001) Perturbation of the pump-leak balance for Na^+ and K^+ in malaria-infected erythrocytes. *Am J Physiol Cell Physiol* **280**, C1576-1587
45. De Niz, M., Burda, P. C., Kaiser, G., Del Portillo, H. A., Spielmann, T., Frischknecht, F., and Heussler, V. T. (2017) Progress in imaging methods: insights gained into *Plasmodium* biology. *Nat Rev Microbiol* **15**, 37-54
46. Desai, S. A., Krogstad, D. J., and McCleskey, E. W. (1993) A nutrient-permeable channel on the intraerythrocytic malaria parasite. *Nature* **362**, 643-646
47. Desai, S. A., and Rosenberg, R. L. (1997) Pore size of the malaria parasite's nutrient channel. *Proc Natl Acad Sci U S A* **94**, 2045-2049
48. Ginsburg, H., Handeli, S., Friedman, S., Gorodetsky, R., and Krugliak, M. (1986) Effects of red blood cell potassium and hypertonicity on the growth of *Plasmodium falciparum* in culture. *Z Parasitenkd* **72**, 185-199
49. Mauritz, J. M., Seear, R., Esposito, A., Kaminski, C. F., Skepper, J. N., Warley, A., Lew, V. L., and Tiffert, T. (2011) X-ray microanalysis investigation of the changes in Na^+, K^+, and hemoglobin concentration in *Plasmodium falciparum*-infected red blood cells. *Biophys J* **100**, 1438-1445
50. Allen, R. J., and Kirk, K. (2004) The membrane potential of the intraerythrocytic malaria parasite *Plasmodium falciparum*. *J Biol Chem* **279**, 11264-11272
51. Saliba, K. J., Martin, R. E., Broer, A., Henry, R. I., McCarthy, C. S., Downie, M. J., Allen, R. J., Mullin, K. A., McFadden, G. I., Broer, S., and Kirk, K. (2006) Sodium-dependent uptake of inorganic phosphate by the intracellular malaria parasite. *Nature* **443**, 582-585
52. Martin, R. E., Henry, R. I., Abbey, J. L., Clements, J. D., and Kirk, K. (2005) The 'permeome' of the malaria parasite: an overview of the membrane transport proteins of *Plasmodium falciparum*. *Genome Biol* **6**, R26
53. Spillman, N. J., Allen, R. J., McNamara, C. W., Yeung, B. K., Winzeler, E. A., Diagana, T. T., and Kirk, K. (2013) Na^+ regulation in the malaria parasite *Plasmodium falciparum* involves the cation ATPase PfATP4 and is a target of the spiroindolone antimalarials. *Cell Host Microbe* **13**, 227-237
54. Spillman, N. J., Allen, R. J., and Kirk, K. (2013) Na^+ extrusion imposes an acid load on the intraerythrocytic malaria parasite. *Mol Biochem Parasitol* **189**, 1-4
55. Saliba, K. J., and Kirk, K. (1999) pH regulation in the intracellular malaria parasite, *Plasmodium falciparum*. H^+ extrusion via a V-type H^+-ATPase. *J Biol Chem* **274**, 33213-33219
56. Hayashi, M., Yamada, H., Mitamura, T., Horii, T., Yamamoto, A., and Moriyama, Y. (2000) Vacuolar H^+-ATPase localized in plasma membranes of malaria parasite cells, *Plasmodium falciparum*, is involved in regional acidification of parasitized erythrocytes. *J Biol Chem* **275**, 34353-34358
57. Wunsch, S., Sanchez, C. P., Gekle, M., Grosse-Wortmann, L., Wiesner, J., and Lanzer, M. (1998) Differential stimulation of the Na^+/H^+ exchanger determines chloroquine uptake in *Plasmodium falciparum*. *J Cell Biol* **140**, 335-345
58. Saliba, K. J., and Kirk, K. (2001) H^+-coupled pantothenate transport in the intracellular malaria parasite. *J Biol Chem* **276**, 18115-18121
59. Augagneur, Y., Jaubert, L., Schiavoni, M., Pachikara, N., Garg, A., Usmani-Brown, S., Wesolowski, D., Zeller, S., Ghosal, A., Cornillot, E., Said, H. M., Kumar, P., Altman, S., and Ben Mamoun, C. (2013) Identification and functional analysis of the primary pantothenate transporter, PfPAT, of the human malaria parasite *Plasmodium falciparum*. *J Biol Chem* **288**, 20558-20567
60. Elliott, J. L., Saliba, K. J., and Kirk, K. (2001) Transport of lactate and pyruvate in the intraerythrocytic malaria parasite, *Plasmodium falciparum*. *Biochem J* **355**, 733-739
61. Henry, R. I., Cobbold, S. A., Allen, R. J., Khan, A., Hayward, R., Lehane, A. M., Bray, P. G., Howitt, S. M., Biagini, G. A., Saliba, K. J., and Kirk, K. (2010) An acid-loading chloride transport pathway in the intraerythrocytic malaria parasite, *Plasmodium falciparum*. *J Biol Chem* **285**, 18615-18626
62. Spillman, N. J., and Kirk, K. (2015) The malaria parasite cation ATPase PfATP4 and its role in the mechanism of action of a new arsenal of antimalarial drugs. *Int J Parasitol Drugs Drug Resist* **5**, 149-162

63. D'Alessandro, S., Corbett, Y., Ilboudo, D. P., Misiano, P., Dahiya, N., Abay, S. M., Habluetzel, A., Grande, R., Gismondo, M. R., Dechering, K. J., Koolen, K. M., Sauerwein, R. W., Taramelli, D., Basilico, N., and Parapini, S. (2015) Salinomycin and other ionophores as a new class of antimalarial drugs with transmission-blocking activity. *Antimicrob Agents Chemother* **59**, 5135-5144
64. Rottmann, M., McNamara, C., Yeung, B. K., Lee, M. C., Zou, B., Russell, B., Seitz, P., Plouffe, D. M., Dharia, N. V., Tan, J., Cohen, S. B., Spencer, K. R., Gonzalez-Paez, G. E., Lakshminarayana, S. B., Goh, A., Suwanarusk, R., Jegla, T., Schmitt, E. K., Beck, H. P., Brun, R., Nosten, F., Renia, L., Dartois, V., Keller, T. H., Fidock, D. A., Winzeler, E. A., and Diagana, T. T. (2010) Spiroindolones, a potent compound class for the treatment of malaria. *Science* **329**, 1175-1180
65. Spillman, N. J., Allen, R. J., McNamara, C. W., Yeung, B. K., Winzeler, E. A., Diagana, T. T., and Kirk, K. (2013) Na(+) regulation in the malaria parasite *Plasmodium falciparum* involves the cation ATPase PfATP4 and is a target of the spiroindolone antimalarials. *Cell Host Microbe* **13**, 227-237
66. Flannery, E. L., McNamara, C. W., Kim, S. W., Kato, T. S., Li, F., Teng, C. H., Gagaring, K., Manary, M. J., Barboa, R., Meister, S., Kuhen, K., Vinetz, J. M., Chatterjee, A. K., and Winzeler, E. A. (2015) Mutations in the P-type cation-transporter ATPase 4, PfATP4, mediate resistance to both aminopyrazole and spiroindolone antimalarials. *ACS Chem Biol* **10**, 413-420
67. Vaidya, A. B., Morrisey, J. M., Zhang, Z., Das, S., Daly, T. M., Otto, T. D., Spillman, N. J., Wyvratt, M., Siegl, P., Marfurt, J., Wirjanata, G., Sebayang, B. F., Price, R. N., Chatterjee, A., Nagle, A., Stasiak, M., Charman, S. A., Angulo-Barturen, I., Ferrer, S., Belen Jimenez-Diaz, M., Martinez, M. S., Gamo, F. J., Avery, V. M., Ruecker, A., Delves, M., Kirk, K., Berriman, M., Kortagere, S., Burrows, J., Fan, E., and Bergman, L. W. (2014) Pyrazoleamide compounds are potent antimalarials that target Na^+ homeostasis in intraerythrocytic *Plasmodium falciparum*. *Nat Commun* **5**, 5521
68. Jimenez-Diaz, M. B., Ebert, D., Salinas, Y., Pradhan, A., Lehane, A. M., Myrand-Lapierre, M. E., O'Loughlin, K. G., Shackleford, D. M., Justino de Almeida, M., Carrillo, A. K., Clark, J. A., Dennis, A. S., Diep, J., Deng, X., Duffy, S., Endsley, A. N., Fedewa, G., Guiguemde, W. A., Gomez, M. G., Holbrook, G., Horst, J., Kim, C. C., Liu, J., Lee, M. C., Matheny, A., Martinez, M. S., Miller, G., Rodriguez-Alejandre, A., Sanz, L., Sigal, M., Spillman, N. J., Stein, P. D., Wang, Z., Zhu, F., Waterson, D., Knapp, S., Shelat, A., Avery, V. M., Fidock, D. A., Gamo, F. J., Charman, S. A., Mirsalis, J. C., Ma, H., Ferrer, S., Kirk, K., Angulo-Barturen, I., Kyle, D. E., DeRisi, J. L., Floyd, D. M., and Guy, R. K. (2014) (+)-SJ733, a clinical candidate for malaria that acts through ATP4 to induce rapid host-mediated clearance of *Plasmodium*. *Proc Natl Acad Sci U S A* **111**, E5455-5462
69. Lehane, A. M., Ridgway, M. C., Baker, E., and Kirk, K. (2014) Diverse chemotypes disrupt ion homeostasis in the malaria parasite. *Mol Microbiol* **94**, 327-339
70. Leong, F. J., Zhao, R., Zeng, S., Magnusson, B., Diagana, T. T., and Pertel, P. (2014) A first-in-human randomized, double-blind, placebo-controlled, single- and multiple-ascending oral dose study of novel Imidazolopiperazine KAF156 to assess its safety, tolerability, and pharmacokinetics in healthy adult volunteers. *Antimicrob Agents Chemother* **58**, 6437-6443
71. Stein, D. S., Jain, J. P., Kangas, M., Lefevre, G., Machineni, S., Griffin, P., and Lickliter, J. (2015) Open-label, single-dose, parallel-group study in healthy volunteers to determine the drug-drug interaction potential between KAE609 (cipargamin) and piperaquine. *Antimicrob Agents Chemother* **59**, 3493-3500
72. Huskey, S. E., Zhu, C. Q., Fredenhagen, A., Kuhnol, J., Luneau, A., Jian, Z., Yang, Z., Miao, Z., Yang, F., Jain, J. P., Sunkara, G., Mangold, J. B., and Stein, D. S. (2016) KAE609 (Cipargamin), a New Spiroindolone Agent for the Treatment of Malaria: Evaluation of the Absorption, Distribution, Metabolism, and Excretion of a Single Oral 300-mg Dose of [14^C]KAE609 in Healthy Male Subjects. *Drug Metab Dispos* **44**, 672-682
73. White, N. J., Pukrittayakamee, S., Phyo, A. P., Rueangweerayut, R., Nosten, F., Jittamala, P., Jeeyapant, A., Jain, J. P., Lefevre, G., Li, R., Magnusson, B., Diagana, T. T., and Leong, F. J. (2014) Spiroindolone KAE609 for *falciparum* and *vivax* malaria. *N Engl J Med* **371**, 403-410
74. Hien, T. T., White, N. J., Thuy-Nhien, N. T., Hoa, N. T., Thuan, P. D., Tarning, J., Nosten, F., Magnusson, B., Jain, J. P., and Hamed, K. (2017) Estimation of the *In Vivo* MIC of Cipargamin in Uncomplicated *Plasmodium falciparum* Malaria. *Antimicrob Agents Chemother* **61**
75. van Pelt-Koops, J. C., Pett, H. E., Graumans, W., van der Vegte-Bolmer, M., van Gemert, G. J., Rottmann, M., Yeung, B. K., Diagana, T. T., and Sauerwein, R. W. (2012) The spiroindolone drug candidate NITD609 potently inhibits gametocytogenesis and blocks *Plasmodium falciparum* transmission to *Anopheles* mosquito vector. *Antimicrob Agents Chemother* **56**, 3544-3548

76. Waller, K. L., Kim, K., and McDonald, T. V. (2008) *Plasmodium falciparum*: growth response to potassium channel blocking compounds. *Exp Parasitol* **120**, 280-285
77. Ashton, R., and Steinrauf, L. K. (1970) Thermodynamic consideration of the ion transporting antibiotics. *J Mol Biol* **49**, 547-556
78. Mitani, M., Yamanishi, T., Miyazaki, Y., and Otake, N. (1976) Salinomycin effects on mitochondrial ion translocation and respiration. *Antimicrob Agents Chemother* **9**, 655-660
79. Martin, R. E., Ginsburg, H., and Kirk, K. (2009) Membrane transport proteins of the malaria parasite. *Mol Microbiol* **74**, 519-528
80. Coetzee, W.A. and Rudy, B. (2006). Potassium Channels. In eLS, (Ed.). https://doi.org/10.1038/npg.els.0005670.
81. Prole, D. L., and Marrion, N. V. (2012) Identification of putative potassium channel homologues in pathogenic protozoa. *PLoS One* **7**, e32264
82. Alexander, S. P., Striessnig, J., Kelly, E., Marrion, N. V., Peters, J. A., Faccenda, E., Harding, S. D., Pawson, A. J., Sharman, J. L., Southan, C., Davies, J. A., and Collaborators, C. (2017) THE CONCISE GUIDE TO PHARMACOLOGY 2017/18: Voltage-gated ion channels. *Br J Pharmacol* **174 Suppl 1**, S160-S194
83. Abraham, E. P., and Chain, E. (1988) Mohammad M.A. (2009). Bioelectricity and excitable membranes. In Electrophysiology measurements for studying neural interfaces (pp. 1-23). Academic Press.

.
84. Yellen, G. (2002) The voltage-gated potassium channels and their relatives. *Nature* **419**, 35-42
85. Liman, E. R., Hess, P., Weaver, F., and Koren, G. (1991) Voltage-sensing residues in the S4 region of a mammalian K^+ channel. *Nature* **353**, 752-756
86. Zagotta, W. N., Hoshi, T., and Aldrich, R. W. (1994) Shaker potassium channel gating III: Evaluation of kinetic models for activation. *J Gen Physiol* **103**, 321-362
87. Long, S. B., Campbell, E. B., and Mackinnon, R. (2005) Crystal structure of a mammalian voltage-dependent Shaker family K^+ channel. *Science* **309**, 897-903
88. Heginbotham, L., Lu, Z., Abramson, T., and MacKinnon, R. (1994) Mutations in the K^+ channel signature sequence. *Biophys J* **66**, 1061-1067
89. Heginbotham, L., Abramson, T., and MacKinnon, R. (1992) A functional connection between the pores of distantly related ion channels as revealed by mutant K^+ channels. *Science* **258**, 1152-1155
90. Doyle, D. A., Morais Cabral, J., Pfuetzner, R. A., Kuo, A., Gulbis, J. M., Cohen, S. L., Chait, B. T., and MacKinnon, R. (1998) The structure of the potassium channel: molecular basis of K^+ conduction and selectivity. *Science* **280**, 69-77
91. Kshatri, A. S., Gonzalez-Hernandez, A., and Giraldez, T. (2018) Physiological Roles and Therapeutic Potential of Ca^{2+} Activated Potassium Channels in the Nervous System. *Front Mol Neurosci* **11**, 258
92. Hirschberg, B., Maylie, J., Adelman, J. P., and Marrion, N. V. (1999) Gating properties of single SK channels in hippocampal CA1 pyramidal neurons. *Biophys J* **77**, 1905-1913
93. Fanger, C. M., Ghanshani, S., Logsdon, N. J., Rauer, H., Kalman, K., Zhou, J., Beckingham, K., Chandy, K. G., Cahalan, M. D., and Aiyar, J. (1999) Calmodulin mediates calcium-dependent activation of the intermediate conductance KCa channel, IKCa1. *J Biol Chem* **274**, 5746-5754
94. Adelman, J. P. (2016) SK channels and calmodulin. *Channels (Austin)* **10**, 1-6
95. Schumacher, M. A., Rivard, A. F., Bachinger, H. P., and Adelman, J. P. (2001) Structure of the gating domain of a Ca^{2+}-activated K^+ channel complexed with Ca^{2+}/calmodulin. *Nature* **410**, 1120-1124
96. Lee, C. H., and MacKinnon, R. (2018) Activation mechanism of a human SK-calmodulin channel complex elucidated by cryo-EM structures. *Science* **360**, 508-513
97. Cui, J., and Aldrich, R. W. (2000) Allosteric linkage between voltage and Ca^{2+}-dependent activation of BK-type mslo1 K^+ channels. *Biochemistry* **39**, 15612-15619
98. Barrett, J. N., Magleby, K. L., and Pallotta, B. S. (1982) Properties of single calcium-activated potassium channels in cultured rat muscle. *J Physiol* **331**, 211-230
99. Koval, O. M., Fan, Y., and Rothberg, B. S. (2007) A role for the S0 transmembrane segment in voltage-dependent gating of BK channels. *J Gen Physiol* **129**, 209-220
100. Ma, Z., Lou, X. J., and Horrigan, F. T. (2006) Role of charged residues in the S1-S4 voltage sensor of BK channels. *J Gen Physiol* **127**, 309-328
101. Meera, P., Wallner, M., Song, M., and Toro, L. (1997) Large conductance voltage- and calcium-dependent K^+ channel, a distinct member of voltage-dependent ion channels with seven N-terminal

transmembrane segments (S0-S6), an extracellular N terminus, and an intracellular (S9-S10) C terminus. *Proc Natl Acad Sci U S A* **94**, 14066-14071
102. Xia, X. M., Zeng, X., and Lingle, C. J. (2002) Multiple regulatory sites in large-conductance calcium-activated potassium channels. *Nature* **418**, 880-884
103. Tao, X., Hite, R. K., and MacKinnon, R. (2017) Cryo-EM structure of the open high-conductance Ca^{2+}-activated K^{+} channel. *Nature* **541**, 46-51
104. Jiang, Y., Lee, A., Chen, J., Cadene, M., Chait, B. T., and MacKinnon, R. (2002) Crystal structure and mechanism of a calcium-gated potassium channel. *Nature* **417**, 515-522
105. Shi, J., Krishnamoorthy, G., Yang, Y., Hu, L., Chaturvedi, N., Harilal, D., Qin, J., and Cui, J. (2002) Mechanism of magnesium activation of calcium-activated potassium channels. *Nature* **418**, 876-880
106. Yang, H., Shi, J., Zhang, G., Yang, J., Delaloye, K., and Cui, J. (2008) Activation of Slo1 BK channels by Mg^{2+} coordinated between the voltage sensor and RCK1 domains. *Nat Struct Mol Biol* **15**, 1152-1159
107. Waller, K. L., McBride, S. M., Kim, K., and McDonald, T. V. (2008) Characterization of two putative potassium channels in *Plasmodium falciparum*. *Malar J* **7**, 19
108. Naude, M. (2018) Dynamic bioinformatics and isotopic evaluation of the permeome of intraerythrocytic *Plasmodium falciparum* parasites, University of Pretoria. *Lancet* **386**, 31-45
109. Painter, H. J., Carrasquilla, M., and Llinas, M. (2017) Capturing in vivo RNA transcriptional dynamics from the malaria parasite *Plasmodium falciparum*. *Genome Res* **27**, 1074-1086
110. Zhang, M., Wang, C., Otto, T. D., Oberstaller, J., Liao, X., Adapa, S. R., Udenze, K., Bronner, I. F., Casandra, D., Mayho, M., Brown, J., Li, S., Swanson, J., Rayner, J. C., Jiang, R. H. Y., and Adams, J. H. (2018) Uncovering the essential genes of the human malaria parasite *Plasmodium falciparum* by saturation mutagenesis. *Science* **360**, eaap7847. doi: 7810.1126/science.aap7847
111. van Biljon, R., van Wyk, R., Painter, H. J., Orchard, L., Reader, J., Niemand, J., Llinas, M., and Birkholtz, L. M. (2019) Hierarchical transcriptional control regulates *Plasmodium falciparum* sexual differentiation. *BMC Genomics* **20**, 920
112. Birnbaum, J., Flemming, S., Reichard, N., Soares, A. B., Mesen-Ramirez, P., Jonscher, E., Bergmann, B., and Spielmann, T. (2017) A genetic system to study *Plasmodium falciparum* protein function. *Nat Methods* **14**, 450-456
113. Donnelly, M. L. L., Luke, G., Mehrotra, A., Li, X., Hughes, L. E., Gani, D., and Ryan, M. D. (2001) Analysis of the aphthovirus 2A/2B polyprotein 'cleavage' mechanism indicates not a proteolytic reaction, but a novel translational effect: a putative ribosomal 'skip'. *J Gen Virol* **82**, 1013-1025
114. Prommana, P., Uthaipibull, C., Wongsombat, C., Kamchonwongpaisan, S., Yuthavong, Y., Knuepfer, E., Holder, A. A., and Shaw, P. J. (2013) Inducible knockdown of *Plasmodium* gene expression using the *glmS* ribozyme. *PLoS One* **8**, e73783. 73710.71371/journal.pone.0073783
115. Els, F. (2021) Genetic manipulation of *Plasmodium falciparum* for conditional knockdown of potassium channels, University of Pretoria.
116. Hallgren, J., Tsirigos, K. D., Pedersen, M. D., Almagro Armenteros, J. J., Marcatili, P., Nielsen, H., Krogh, A., and Winther, O. (2022) DeepTMHMM predicts alpha and beta transmembrane proteins using deep neural networks. *bioRxiv*, 2022.2004.2008.487609
117. McGuffin, L. J., Bryson, K., and Jones, D. T. (2000) The PSIPRED protein structure prediction server. *Bioinformatics* **16**, 404-405
118. Tsirigos, K. D., Peters, C., Shu, N., Kall, L., and Elofsson, A. (2015) The TOPCONS web server for consensus prediction of membrane protein topology and signal peptides. *Nucleic Acids Res* **43**, W401-407
119. Krogh, A., Larsson, B., von Heijne, G., and Sonnhammer, E. L. (2001) Predicting transmembrane protein topology with a hidden Markov model: application to complete genomes. *J Mol Biol* **305**, 567-580
120. Reynolds, S. M., Kall, L., Riffle, M. E., Bilmes, J. A., and Noble, W. S. (2008) Transmembrane topology and signal peptide prediction using dynamic bayesian networks. *PLoS Comput Biol* **4**, e1000213
121. Kall, L., Krogh, A., and Sonnhammer, E. L. (2005) An HMM posterior decoder for sequence feature prediction that includes homology information. *Bioinformatics* **21 Suppl 1**, i251-257
122. Bernsel, A., Viklund, H., Falk, J., Lindahl, E., von Heijne, G., and Elofsson, A. (2008) Prediction of membrane-protein topology from first principles. *Proc Natl Acad Sci U S A* **105**, 7177-7181
123. Viklund, H., and Elofsson, A. (2008) OCTOPUS: improving topology prediction by two-track ANN-based preference scores and an extended topological grammar. *Bioinformatics* **24**, 1662-1668

124. Viklund, H., Bernsel, A., Skwark, M., and Elofsson, A. (2008) SPOCTOPUS: a combined predictor of signal peptides and membrane protein topology. *Bioinformatics* **24**, 2928-2929
125. Tsirigos, K. D., Govindarajan, S., Bassot, C., Vastermark, A., Lamb, J., Shu, N., and Elofsson, A. (2018) Topology of membrane proteins-predictions, limitations and variations. *Curr Opin Struct Biol* **50**, 9-17
126. Kyte, J., and Doolittle, R. F. (1982) A simple method for displaying the hydropathic character of a protein. *J Mol Biol* **157**, 105-132
127. Madeira, F., Pearce, M., Tivey, A. R. N., Basutkar, P., Lee, J., Edbali, O., Madhusoodanan, N., Kolesnikov, A., and Lopez, R. (2022) Search and sequence analysis tools services from EMBL-EBI in 2022. *Nucleic Acids Res*
128. McWilliam, H., Li, W., Uludag, M., Squizzato, S., Park, Y. M., Buso, N., Cowley, A. P., and Lopez, R. (2013) Analysis Tool Web Services from the EMBL-EBI. *Nucleic Acids Res* **41**, W597-600
129. Jumper, J., Evans, R., Pritzel, A., Green, T., Figurnov, M., Ronneberger, O., Tunyasuvunakool, K., Bates, R., Zidek, A., Potapenko, A., Bridgland, A., Meyer, C., Kohl, S. A. A., Ballard, A. J., Cowie, A., Romera-Paredes, B., Nikolov, S., Jain, R., Adler, J., Back, T., Petersen, S., Reiman, D., Clancy, E., Zielinski, M., Steinegger, M., Pacholska, M., Berghammer, T., Bodenstein, S., Silver, D., Vinyals, O., Senior, A. W., Kavukcuoglu, K., Kohli, P., and Hassabis, D. (2021) Highly accurate protein structure prediction with AlphaFold. *Nature* **596**, 583-589
130. Varadi, M., Anyango, S., Deshpande, M., Nair, S., Natassia, C., Yordanova, G., Yuan, D., Stroe, O., Wood, G., Laydon, A., Zidek, A., Green, T., Tunyasuvunakool, K., Petersen, S., Jumper, J., Clancy, E., Green, R., Vora, A., Lutfi, M., Figurnov, M., Cowie, A., Hobbs, N., Kohli, P., Kleywegt, G., Birney, E., Hassabis, D., and Velankar, S. (2022) AlphaFold Protein Structure Database: massively expanding the structural coverage of protein-sequence space with high-accuracy models. *Nucleic Acids Res* **50**, D439-D444
131. Mariani, V., Biasini, M., Barbato, A., and Schwede, T. (2013) lDDT: a local superposition-free score for comparing protein structures and models using distance difference tests. *Bioinformatics* **29**, 2722-2728
132. Pettersen, E. F., Goddard, T. D., Huang, C. C., Couch, G. S., Greenblatt, D. M., Meng, E. C., and Ferrin, T. E. (2004) UCSF Chimera-a visualization system for exploratory research and analysis. *J Comput Chem* **25**, 1605-1612
133. Baek, M., Park, T., Heo, L., Park, C., and Seok, C. (2017) GalaxyHomomer: a web server for protein homo-oligomer structure prediction from a monomer sequence or structure. *Nucleic Acids Res* **45**, W320-W324
134. Blum, M., Chang, H. Y., Chuguransky, S., Grego, T., Kandasaamy, S., Mitchell, A., Nuka, G., Paysan-Lafosse, T., Qureshi, M., Raj, S., Richardson, L., Salazar, G. A., Williams, L., Bork, P., Bridge, A., Gough, J., Haft, D. H., Letunic, I., Marchler-Bauer, A., Mi, H., Natale, D. A., Necci, M., Orengo, C. A., Pandurangan, A. P., Rivoire, C., Sigrist, C. J. A., Sillitoe, I., Thanki, N., Thomas, P. D., Tosatto, S. C. E., Wu, C. H., Bateman, A., and Finn, R. D. (2021) The InterPro protein families and domains database: 20 years on. *Nucleic Acids Res* **49**, D344-D354
135. Trager, W., and Jensen, J. B. (1976) Human malaria parasites in continuous culture. *Science* **193**, 673-675
136. Rug, M. and Maier, A. G. (2013) Transfection of *Plasmodium falciparum*. Methods in Molecular Biology. 923, 75-98.
137. Oyelade, J., Isewon, I., Rotimi, S., and Okunoren, I. (2016) Modeling of the Glycolysis Pathway in *Plasmodium falciparum* using Petri Nets. *Bioinform Biol Insights* **10**, 49-57
138. Caro, F., Miller, M. G., and DeRisi, J. L. (2012) Plate-based transfection and culturing technique for genetic manipulation of *Plasmodium falciparum*. *Malar J* **11**, 22
139. Sheffield, J. (2007). ImageJ, A Useful Tool for Biological Image Processing and Analysis. Microscopy and Microanalysis, 13(S02), 200-201. doi:10.1017/S1431927607076611.
140. Alballa, M., and Butler, G. (2020) Integrative approach for detecting membrane proteins. *BMC Bioinformatics* **21**, 575
141. Gajewski, C., Dagcan, A., Roux, B., and Deutsch, C. (2011) Biogenesis of the pore architecture of a voltage-gated potassium channel. *Proc Natl Acad Sci U S A* **108**, 3240-3245
142. Molbaek, K., Tejada, M., Ricke, C. H., Scharff-Poulsen, P., Ellekvist, P., Helix-Nielsen, C., Kumar, N., Klaerke, D. A., and Pedersen, P. A. (2020) Purification and initial characterization of *Plasmodium falciparum* K^+ channels, PfKch1 and PfKch2 produced in *Saccharomyces cerevisiae*. *Microb Cell Fact* **19**, 183

143. Kelley, L. A., Mezulis, S., Yates, C. M., Wass, M. N., and Sternberg, M. J. (2015) The Phyre2 web portal for protein modeling, prediction and analysis. *Nat Protoc* **10**, 845-858
144. Yuan, P., Leonetti, M. D., Pico, A. R., Hsiung, Y., and MacKinnon, R. (2010) Structure of the human BK channel Ca^{2+}-activation apparatus at 3.0 A resolution. *Science* **329**, 182-186
145. Wu, Y., Yang, Y., Ye, S., and Jiang, Y. (2010) Structure of the gating ring from the human large-conductance Ca^{2+}-gated K^+ channel. *Nature* **466**, 393-397
146. van der Watt, M. E., Reader, J., and Birkholtz, L. M. (2022) Adapt or Die: Targeting Unique Transmission-Stage Biology for Malaria Elimination. *Front Cell Infect Microbiol* **12**, 901971
147. O'Donnell, R. A., Preiser, P. R., Williamson, D. H., Moore, P. W., Cowman, A. F., and Crabb, B. S. (2001) An alteration in concatameric structure is associated with efficient segregation of plasmids in transfected *Plasmodium falciparum* parasites. *Nucleic Acids Res* **29**, 716-724
148. Wang, B., Chen, Q.H., Brenner, R., Health, T., Antonio, S., Antonio, S. (2009). Proepileptic effects of BK channel gene mutations. In Encyclopedia of basic epilepsy research (pp. 662–669). Cambridge: Academic Press.
149. Martin, R. J., Buxton, S. K., Neveu, C., Charvet, C. L., and Robertson, A. P. (2012) Emodepside and SL0-1 potassium channels: a review. *Exp Parasitol* **132**, 40-46
150. O'Donnell, R. A., Freitas-Junior, L. H., Preiser, P. R., Williamson, D. H., Duraisingh, M., McElwain, T. F., Scherf, A., Cowman, A. F., and Crabb, B. S. (2002) A genetic screen for improved plasmid segregation reveals a role for Rep20 in the interaction of *Plasmodium falciparum* chromosomes. *EMBO J* **21**, 1231-1239
151. van Dijk, M. R., Vinkenoog, R., Ramesar, J., Vervenne, R. A., Waters, A. P., and Janse, C. J. (1997) Replication, expression and segregation of plasmid-borne DNA in genetically transformed malaria parasites. *Mol Biochem Parasitol* **86**, 155-162
152. Coller HA, Coller BS. Poisson statistical analysis of repetitive subcloning by the limiting dilution technique as a way of assessing hybridoma monoclonality. Methods Enzymol. 1986;121:412–417.
153. Coller HA, Coller BS. Statistical analysis of repetitive subcloning by the limiting dilution technique with a view toward ensuring hybridoma monoclonality. Hybridoma. 1983;2:91–96.

Supplementary information

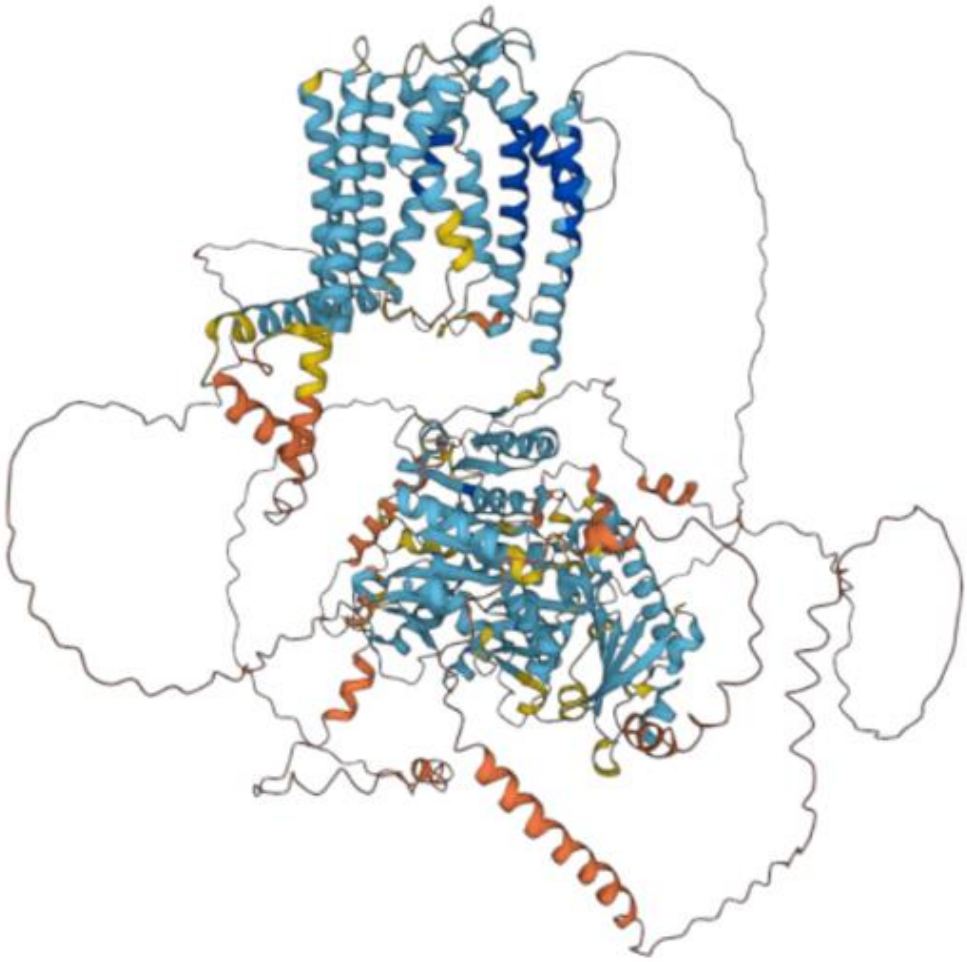

Figure S1: AlphaFold predicted three-dimensional structure of a single subunit of PfK2 in *P. falciparum* parasites. Predicted structure of PfK2 from AlphaFold (https://alphafold.ebi.ac.uk/) with colour schemes corresponding to a per-residue confidence score (pLDDT) on a scale from 0 to 100. Dark blue residues have very high confidence (pLDDT > 90), light blue residues have confidence (90 > pLDDT > 70), yellow residues have low confidence (70 > pLDDT > 50), and red residues have very low confidence (pLDDT < 50).